

Title of thesis

Design, Simulation and Modeling of a Micromachined High Temperature Microhotplate for Application in Trace Gas Detection

I ABDELAZIZ YOUSIF AHMED ALMAHI

hereby allow my thesis to be placed at the Information Resources Center (IRC) of Universiti Teknologi PETRONAS (UTP) with the following conditions:

1. The thesis becomes the property of UTP
2. The IRC of UTP may make copies of the thesis for academic purposes only.
3. This thesis is classified as

Confidential

Non-confidential

If this thesis is confidential, please state the reason:

---

The contents of the thesis will remain confidential for \_\_\_\_\_ years.

Remarks on disclosure:

---

Endorsed by

ABDELAZIZ YOUSIF AHMED ALMAHI

JOHN OJUR DENNIS

Signature of Author

Signature of Supervisor

Permanent Address of Author

Permanent Address of Supervisor

Date: \_\_\_\_\_

Date: \_\_\_\_\_

UNIVERSITI TEKNOLOGI PETRONAS

Approval by Supervisor (s)

The undersigned certify that they have read, and recommend to the Postgraduate Studies Programme for acceptance, a thesis entitled “Design, Simulation and Modeling of a Micromachined High Temperature Microhotplate for Application in Trace Gas Detection.” submitted by (Abdelaziz Yousif Ahmed Almahi) for the fulfillment of the requirements for the degree of Master of Science in Electrical and Electronics Engineering.

.....

Date

Main Supervisor : Dr. John Ojur Dennis .....

Signature : .....

Date : .....

Co- Supervisor : Dr. Mohamad Naufal Mohamad Saad .....

Signature : .....

Date : .....

UNIVERSITI TEKNOLOGI PETRONAS

Design, Simulation and Modeling of a Micromachined High Temperature  
Microhotplate for Application in Trace Gas Detection

By

Abdelaziz Yousif Ahmed Almahi

A THESIS

SUBMITTED TO THE POSTGRADUATE STUDIES PROGRAMME AS  
A REQUIREMENT FOR THE  
DEGREE OF MASTER OF SCIENCE  
IN ELECTRICAL AND ELECTRONICS ENGINEERING

BANDAR SERI ISKANDAR,  
PERAK

July 2009

## DECLARATION

I hereby declare that the thesis is based on my original work except for the quotations and citations which have been duly acknowledged. I also declare that it has not been previously or concurrently submitted for any other degree at UTP or other institutions.

Signature: \_\_\_\_\_

Name : ABDELAZIZ YOUSIF AHMED ALMAHI

Date : \_\_\_\_\_

## ACKNOWLEDGEMENTS

First of all, I would like to express my greatest thankful to Allah *for his uncountable* blessings and for giving me the strength to success and finish my research.

I would like to express my gratitude to my supervisor, Dr. John Ojur Dennis, whose support, encouragement, expertise, understanding, and patience, added considerably to my graduate experience during my research. Since the first day I started until the moment I finished my final version of the dissertation.

This appreciation also goes to my co-supervisor, Dr. Mohamad Naufal Mohamad Saad for his valuable assistant, encouragement and helpfulness during my research. His assistance always there at the moment I really needed one.

I would also like to thank my parents and family members (Mom and Dad, Brothers, Sisters, Fiancé and Friends) for always supporting me and believing in me, not just for this work, but everything in my life and provided me through my entire life and in particular.

I must also acknowledge the members of postgraduate office for helpfulness, all the lecturers of electrical and electronic engineering department for their advices and all my friends in Universiti Teknologi PETRONAS for sharing experiences

In conclusion, I recognize that this research would not have been possible without the financial assistance of Universiti Teknologi PETRONAS (UTP), the Department of Electrical and Electronics Engineering.

Abdelaziz Yousif Ahmed Almahi

Universiti Teknologi PETRONAS July 2009

## ABSTRACT

A microhotplate (MHP) is a basic Microelectromechanical System (MEMS) structure that is used in many applications such as a platform for metal oxide gas sensors, microfluidics and infrared emission. Semiconductor gas sensors usually require high power because of their elevated operating temperatures. The uniformity of the temperature distribution over the sensing area is an important factor in gas detection. There are several silicon micromachined MHP that can easily withstand temperatures between 200°C and 500°C for long periods. However there is no systematic study on the effect of the thickness of the various layers of the MHP on its characteristics at high operating temperatures of up to 700°C with lower power dissipation, lower mechanical displacement and good uniformity of the temperature distribution on the MHP. The MHP for the present study consists of a 100  $\mu\text{m}$   $\times$  100  $\mu\text{m}$  membrane supported by four microbridges of length 113  $\mu\text{m}$  and width 20  $\mu\text{m}$  designed and simulated using CoventorWare. Tetrahedron mesh with 80 $\mu\text{m}$  element size is applied to the solid model, while the membrane area is meshed with 5 $\mu\text{m}$  element size to obtain accurate FEM simulation results. In the characterization of the MHP, the length and width of the various layers (membrane, heat distributor and sensing film) are fixed while their thicknesses are varied from 0.3  $\mu\text{m}$  to 3  $\mu\text{m}$  to investigate the effect of thickness on the MHP characteristics. At the fixed operation temperature of 700°C, it is shown that as membrane thickness increases, power dissipation, current density, time constant and heat transfer to the silicon substrate increases, while mechanical displacement of the membrane remains constant. When the SiC heat distributor thickness increases, a small increase in power dissipation is observed while the displacement decreases. The temperature gradient on the MHP is found to decrease with increasing thickness of the SiC and is a minimum with a value of 0.005°C/ $\mu\text{m}$  for a thickness of 2  $\mu\text{m}$  and above. An optimized MHP device at an operating temperature of 700°C was found to have a low power dissipation of about 9.25 mW, maximum mechanical displacement of 1.2  $\mu\text{m}$ , a temperature gradient of 0.005°C/ $\mu\text{m}$  and a short time constant of 0.17 ms.

## Abstrak

Bekas Panas Mikro (MHP) adalah satu struktur Sistem Mikroelektromekanikal (MEMS) asas yang digunakan di dalam pelbagai aplikasi seperti di platform untuk sensor gas metal oksida, cecair mikro dan pancaran infra merah. Sensor gas semikonduktor selalunya memerlukan kuasa yang tinggi disebabkan oleh suhu operasional yang tinggi. Penyebaran suhu secara sekata di sekitar kawasan yang dipantau adalah sangat penting dalam pengesanan gas. Terdapat beberapa silikon mesin mikro MHP yang boleh menahan suhu di antara 200°C dan 500°C untuk jangka masa yang panjang. Bagaimanapun, tiada terdapat cara yang sistematik ke atas kesan ketebalan pelbagai lapisan MHP ke atas pelbagai karekteristik bahan tersebut bagi suhu sehingga 700°C dengan penyerapan kuasa yang rendah, pergerakan mekanikal yang rendah dan penyebaran haba di atas MHP yang sekata. MHP untuk kajian ini terdiri daripada 100  $\mu\text{m}$   $\times$  100  $\mu\text{m}$  membrane disokong oleh empat jambatan-mikro dengan panjang 113  $\mu\text{m}$  dan lebar 20  $\mu\text{m}$  dilukis dan disimulasikan dengan CoventorWare. Rangkaian Tetrahedron dengan elemen bersaiz 80 $\mu\text{m}$  diaplikasikan ke setiap model solid, sementara kawasan membran dirangkaikan dengan elemen bersaiz 5 $\mu\text{m}$  untuk memperolehi keputusan simulasi FEM yang tepat. Bagi mengkarakteristikkan MHP, panjang dan lebar untuk pelbagai lapisan (membran, penyebar haba dan filem pengesan) ditetapkan sementara ketebalan berubah dari 0.3 $\mu\text{m}$  kepada 3 $\mu\text{m}$  untuk mengkaji pengaruh ketebalan ke atas MHP. Di suhu operasi tetap 700°C, ia telah ditunjukkan bahawa apabila ketebalan membran meningkat, penyerapan kuasa, densiti arus, konstan masa terma dan pengalihan haba ke substrat silikon juga akan meningkat sementara pengalihan mekanikal membran tidak berubah. Apabila ketebalan penyebar haba SiC naik, sedikit kenaikan dalam penyerapan kuasa haba dilihat dan pergerakan menurun. Gradian suhu pada MHP menurun apabila ketebalan bahagian penyebaran suhu SiC meningkat dan minima dengan 0.005°C/ $\mu\text{m}$  bagi ketebalan bahagian dari 2 $\mu\text{m}$  dan ke atas. Bahan MHP optimum di bawah suhu operasi 700°C dilihat mempunyai penyerapan haba yang rendah di sekitar 9.25 mW, pergerakan mekanikal maxima sebanyak 1.2 $\mu\text{m}$ , gradian suhu sebanyak 0.005°C/ $\mu\text{m}$  dan masa konstan yang pendek iaitu 0.17 ms.

## TABLE OF CONTENTS

ACKNOWLEDGEMENT .....	v
A BSTRACT .....	vi
A BSTRAK .....	vii
LIST OF TABLES .....	xi
LIST OF FIGURES .....	xii
CHAPTER 1 .....	1
1.1 Background of Study .....	1
1.2 Problem Statement.....	2
1.3 Objectives of Study .....	5
1.4 Scope of Study.....	5
1.5 Thesis Overview .....	5
CHAPTER 2 .....	7
2.1 Overview of the microhotplate (MHP).....	7
2.2 Micromachining techniques for MHP .....	13
2.2.1 Bulk Micromachining.....	13
2.2.2 Surface micromachining.....	15
2.3 Theory of Heat Transfer .....	16
2.3.1 Conduction Heat Transfer .....	16
2.3.2 Convection Heat Transfer.....	17
2.3.3 Radiation Heat Transfer.....	18
2.3.4 Thermoresistors .....	19
2.4 Summary.....	19
CHAPTER 3 .....	21
3.1 Design of MHP.....	21
3.1.1 Materials properties and selection .....	26
3.2 Description of the Simulation Procedure.....	28
3.3 CoventorWare Components .....	31
3.3.1 Material Properties Database.....	31

3.3.2	Process Editor .....	32
3.3.3	Designer.....	34
3.3.4	Analyzer.....	39
3.4	Modelling of MHP.....	41
3.4.1	Heat Conduction through the membrane and air .....	42
3.4.2	Heat convection through air .....	44
3.4.3	Radiation.....	44
3.4.4	Transient response .....	46
3.5	Summary.....	47
CHAPTER 4	.....	48
4.1	Typical 3-D FEM Simulations on the MHP devices.....	48
4.1.1	Front and back side etching .....	48
4.1.2	Potential distribution and current density .....	50
4.1.3	Heat distribution and mechanical displacement .....	51
4.2	Effect of Si <sub>3</sub> N <sub>4</sub> membrane thickness on MHP characteristics .....	52
4.2.1	Temperature and displacement.....	52
4.2.2	Power dissipation and displacement.....	54
4.2.3	Comparison between simulated and calculated values of power dissipation .....	56
4.2.4	Comparison between simulated and calculated values of current density .....	57
4.2.5	Time constant .....	58
4.2.6	Heat losses to Si substrate layer .....	59
4.3	Effect of Pt heater thickness on MHP characteristics.....	61
4.3.1	Temperature and displacement.....	61
4.3.2	Applied voltage, displacement, current density and mises stress.....	64
4.4	Effect of the thickness of the SiC heat distributor layer on the MHP characteristics.....	66
4.4.1	Heat distribution on the MHP surface .....	66
4.4.2	Temperature and displacement.....	69
4.4.3	Power dissipation and displacement.....	70
4.4.4	Comparison between simulated and calculated values of power dissipation .....	72
4.5	Effect of SnO <sub>2</sub> sensing film thickness on the MHP characteristics...	72

4.5.1 Displacement and mises stress .....	73
4.5.2 Applied voltage and temperature.....	74
4.5.3 Applied voltage, displacement and misses stress .....	75
4.5.4 Comparison between simulated and calculated values of power dissipation .....	76
4.6 Final design and simulation of a MHP with selected parameters for optimum operation at the elevated temperature of 700°C.....	77
4.7 Summary.....	80
CHAPTER 5 .....	81
5.1 Conclusion.....	81
5.2 Recommendation .....	82
LIST OF PUBLICATION .....	83
REFERENCES.....	84
APPENDIX A .....	91

## LIST OF TABLES

Table 2.1: Micro hotplate specifications.....	12
Table 3.1: Material properties of layers used in the MEMS microhotplate structure.	24
Table 4.1: The values for the thicknesses of the various MHP layers.....	78
Table A1: Thermal conductivity calculation of membrane, heater, plate and sensing film layers used in the MEMS microhotplate.....	94
Table A2: Summary of results for membrane characterization.....	94

## LIST OF FIGURES

Figure 2.1: (a) Isotropic and (b, c) anisotropic etching of the silicon substrate.....	14
Figure 2.2: Surface micromachining [43].....	16
Figure 3.1: Flowchart of the MHP Design and Characterization.....	23
Figure 3.2: Layers in the micro-hotplate (MHP) design.....	24
Figure 3.3: Cross-sectional Schematic view of Silicon MHP Gas Sensor with Front side Etch .....	25
Figure 3.4: Cross-sectional Schematic view of Silicon MHP Gas Sensor with Backside Etch .....	25
Figure 3.5: Top View of MHP with front side etch.....	26
Figure 3.6: Heater Structure.....	27
Figure 3.7: Interdigitated Electrodes Structure .....	27
Figure 3.8: The Function Manager .....	29
Figure 3.9: Block Diagram of CoventorWare Process.....	30
Figure 3.10: Materials Editor Windows for platinum.....	32
Figure 3.11: Elements of Process Editor.....	34
Figure 3.12: 2-D layout of a MHP design.....	35
Figure 3.13: Preprocessor rendering of the 3-D MHP model .....	36
Figure 3.14: Properties of the platinum heater.....	37
Figure 3.15: 3D solid model with a mesh of 80 $\mu\text{m}$ element size on the.....	38
Figure 3.16: 3D solid model of the MHP showing (a) more refined mesh and (b) magnified view showing details of the finer element size.....	38
Figure 3.17: Temperature and displacement on the MHP vs. Mesh size at an applied voltage of 0.7 V.....	39
Figure 3.18: Boundary Condition window of the design.....	40
Figure 3.19: Heat pathways of a microhotplate .....	41
Figure 3.20: Theoretical determination of power losses through air [48].....	43
Figure 4.1: Temperature distribution for an MHP etched from (a) back side and (b) front side.....	49
Figure 4.2: Mechanical deflection of the MHP etched from (a) back side and (b) front side.....	50
Figure 4.3: Atypical FEM simulation result of the (a) potential distribution and (b) current density profile in the Pt heater of the MHP for an applied voltage of 7.0 V .....	51

Figure 4.4: Typical FEM simulation of (a) temperature distribution and (b) mechanical displacement on the MHP for an applied voltage 0.7 V ...	52
Figure 4.5: Maximum operating temperature on the MHP vs. thickness of Si <sub>3</sub> N <sub>4</sub> membrane at an applied voltage 0.7 V .....	53
Figure 4.6: Maximum displacement on the MHP vs. thickness of Si <sub>3</sub> N <sub>4</sub> membrane at an applied voltage 0.7 V .....	54
Figure 4.7: Power dissipation of the MHP vs. thickness of Si <sub>3</sub> N <sub>4</sub> membrane at an operating temperature of 700°C.....	55
Figure 4.8: Displacement of the MHP vs. thickness of Si <sub>3</sub> N <sub>4</sub> membrane at an operating temperature of 700°C .....	55
Figure 4.9: Simulated and calculated results of power dissipation vs. Si <sub>3</sub> N <sub>4</sub> membrane thickness at an operating temperature of 700°C .....	57
Figure 4.10: Simulated and calculated values of current densities vs. Si <sub>3</sub> N <sub>4</sub> membrane thickness at the operating temperature of 700°C.....	58
Figure 4.11: Theoretically calculated thermal time constant of the MHP vs. thickness of the Si <sub>3</sub> N <sub>4</sub> membrane at an operating temperature of 700°C.....	59
Figure 4.12: Heat dissipation to the Si substrate for Si <sub>3</sub> N <sub>4</sub> membrane thickness of (a) 0.3 μm, (b) 1 μm, (c) 2 μm and (d) 3 μm at the MHP operating temperature of 700°C .....	60
Figure 4.13: Maximum temperature on the Si substrate as a function of the Si <sub>3</sub> N <sub>4</sub> membrane thickness .....	61
Figure 4.14: MHP operating temperature vs. thickness of the heater at an applied voltage of 0.7 V .....	62
Figure 4.15: Maximum displacement on MHP vs. thickness of the heater at an applied voltage of 0.7 V .....	62
Figure 4.16: Current Density on the MHP vs. thickness of the heater at an applied voltage of 0.7 V .....	63
Figure 4.17: Misses Stress on the MHP vs. thickness of the heater at 0.7 V.....	63
Figure 4.18: Voltage of the MHP vs. thickness of the heater at a constant membrane temperature of 700°C .....	64
Figure 4.19: Displacement of the MHP vs. thickness of the heater at a constant membrane temperature of 700°C.....	65
Figure 4.20: Current density of the MHP vs. thickness of the heater at an operating temperature of 700°C.....	65
Figure 4.21: Mises Stress of the MHP vs. thickness of the heater at an operating temperature of 700°C.....	66
Figure 4.22: Heat distribution on the MHP surface with SiC layer of various thicknesses at an operating temperature of 700°C.....	68

Figure 4.23: Temperature gradient on the MHP surface vs. thickness of SiC heat distributor layer at an operating temperature of 700°C .....	68
Figure 4.24: Maximum temperature on the MHP surface vs. thickness of the SiC heat distributor layer at the applied voltage of 0.7 V .....	69
Figure 4.25: Maximum displacement of the MHP vs. thickness of the SiC heat distributor at an applied voltage 0.7 V .....	70
Figure 4.26: Power dissipation of the MHP vs. thickness of the SiC heat distributor layer at an operating temperature of 700°C .....	71
Figure 4.27: Maximum displacement of the MHP vs. thickness of the SiC heat distributor at an operating temperature of 700°C .....	71
Figure 4.28: Simulated and calculated MHP Power dissipation vs. thickness of the SiC heat distributor layer at an operating temperature of 700°C.....	72
Figure 4.29: Displacement on the MHP vs. thickness of the SnO <sub>2</sub> sensing film at an operating temperature of 700°C.....	73
Figure 4.30: Mises stress vs. thickness of the SnO <sub>2</sub> at the operating temperature of 700°C .....	74
Figure 4.31: Temperature on MHP surface vs. applied voltage at a constant SnO <sub>2</sub> sensing film thickness of 0.5 μm .....	74
Figure 4.32: Mechanical displacement of the MHP vs. applied voltage at a constant SnO <sub>2</sub> sensing film thickness of 0.5 μm.....	75
Figure 4.33: Mises stress on the MHP vs. applied voltage at a constant SnO <sub>2</sub> sensing film thickness of 0.5 μm .....	76
Figure 4.34: Simulated and calculated power dissipation on the MHP vs. thickness of the SnO <sub>2</sub> sensing film at an operating temperature of 700°C.....	77
Figure 4.35: (a) applied voltage to the heater element, (b) temperature profile on the MHP, (c) mechanical displacement of the MHP and (d) current density in the Pt heating element .....	79

## List of symbols

Symbol	Description	Unit
$\alpha$	Thermal expansion coefficient	1/K
$\varepsilon$	Emissivity	---
$\kappa$	Thermal diffusivity	m <sup>2</sup> /s
K	Thermal conductivity	W/(m K)
$\nu$	Kinematic viscosity	m <sup>2</sup> /s
$\rho$	Density	Kg/m <sup>3</sup>
$\sigma$	Stefan-Boltzmann constant	W/(m <sup>2</sup> K <sup>4</sup> )
$\Pi$	3.14159265	---
$K_{\text{Si}_3\text{N}_4}$	Thermal conductivity of Si <sub>3</sub> N <sub>4</sub>	W/ (m K)
U	Energy	J
h	Convection coefficient	W/m <sup>2</sup>
d	Thickness	$\mu\text{m}$
w	width	$\mu\text{m}$
$\tau$	Time constant	s
$K_{\text{Pt}}$	Thermal conductivity of Pt	W/(m K)
A	Area	m <sup>2</sup>
$A_{\text{bridge}}$	Cross sectional area of micro bridge	m <sup>2</sup>
c	Specific heat capacity	J/Kg.K
Nu	Nusselt Number	---
Nu <sub>l</sub>	Longitudinal Nusselt Number	---
Nu <sub>t</sub>	Transversal Nusselt Number	---
$P_{\text{cond}}$	Power conduction	W
$P_{\text{conv}}$	Power convection	W

$P_{radi}$	Power radiation	W
$P_{air}$	Power conduction through air	W
$P_{in}$	Input power	W
$P_{diss}$	Power dissipation	W
Pr	Prandtl Number	---
$C_1$	Longitudinal coefficient	---
$r_o$	Radius	m
Ra	Rayleigh Number	---
$T_{hot}$	hot temperature	K
$T_{amb}$	room temperature	K
V	Voltage	V
v	Volume	$m^3$
X	Length	m
J	Current density	$A/m^2$
g	Gravitational acceleration constant (9, 81 $m/s^2$ )	$m/s^2$
$\lambda$	Thermal conductivity of air	W/(m K)

## List of acronyms

BEM	Boundary Element Meshes
CMOS	Complementary Metal Oxide Semiconductor
2D	Two Dimensional
3D	Three Dimensional
FEM	Finite Element Method
FETs	Field Effect Transistors
IDE	Interdigitated Electrodes
KOH	Potassium Hydroxide
MEMS	Micro Electro-Mechanical Systems
MHP	Microhotplate
MOSFET	Metal Oxide Semiconductor Field-Effect Transistor
MOSIS	Metal Oxide Semiconductor Implementation Service
MPD	Material Properties Database
PS	Porous Silicon
SCS	Single Crystal Silicon
TCR	temperature Coefficient of Resistance
TMAH	Tetramethylammonium Hydroxide

## CHAPTER 1

### INTRODUCTION

#### 1.1 Background of Study

A microhotplate (MHP) is a thermally isolated stage designed using microtechnological processes. The layers of the MHP consist of substrate, membrane, heating element, heat distributor, and temperature sensor to measure the MHP temperature. On the top layer, two or more electrodes are used to perform resistance or impedance measurements of the sensing material. There are several good reviews on micromachined metal oxide sensors [1, 2]. Microhotplates are not only used for metal oxide based gas sensor applications but can also be used with different materials [3] such as polymer based capacitive sensors [4], pellistors [5, 6], Gas Field Effect Transistors (FETs) [7, 8] and sensors based on changes in thermal conductivity [9].

Future sensors are expected to have some advantages such as very small dimensions, low weight, low power consumption, high operating temperature, low manufacturing cost and pulsed or modulated mode of operation of the heater element. In order to satisfy these specifications there is need to improve and optimize the MHP. Microhotplates have tremendous importance in the field of high temperature gas sensing devices (e.g. metal oxide) since they allow the reduction of the sensor power consumption and the use of new modes of operation such as temperature cycling due to their low thermal mass [10-15].

SnO<sub>2</sub> based nanocrystalline thick films deposited on micromachined hotplates have been investigated during the past years as a combination of thick and thin film technology for gas detection [15, 16]. Thick film technology is well established in the field of the gas sensitive materials. Moreover, the use of microhotplates as substrate makes this technology suitable for markets where low power consumption, low cost and reliable devices are needed, such as in the production of portable instruments and in the automotive industry.

The applications of microhotplates, although many and varied, share the same key design requirements:

- Fast response time.
- Low power consumption.
- Uniform plate temperature.
- Scalability.

Fast response time is essential for applications where the plate is operated dynamically. Low power consumption is a ubiquitous requirement, and is particularly important to fabricate battery operated sensors. A uniform MHP temperature is a necessary requirement as it often enhances the operation of the sensor in question, as the film overlying the MHP should be maintained at a uniform temperature for maximum sensitivity and stability.

## **1.2 Problem Statement**

Semiconductor gas sensors usually require high power consumption because of their elevated operating temperature. In recent applications, including portable sensors and wireless sensor networks, low power consumption is very important. The high power consumption problem of these sensors can be reduced by employing MHP designed using bulk micromachining techniques to locally confine the temperature in small isolated area with minimal heat conduction to the surrounding substrate [17].

MHP's is basic microelectromechanical systems (MEMS) structures that are used in many applications such as a platform for metal oxide gas sensors, microfluidics and infrared emission. There are several silicon micromachined MHP that can easily withstand temperatures between 350°C and 500°C for long periods [16, 18-21], but there are no commercial sensors to date with structures that can withstand up to 700°C with lower power consumption. High temperature operation capability of MHP is important for two reasons. First, as the MHP is a platform on which to

deposit the active metal oxide based sensing material, it will facilitate the annealing or sintering of the metal oxide sensor on the MHP itself by raising the temperature to over 700°C. Secondly it possible use the MHP to remove the residual gas molecules on the surface of the sensing material after use in detecting gases by firing it to high temperatures. There are many papers that focus on different designs of the geometry of the dielectric membrane of the MHP. For example, Semancik et al [22] presented an array of suspended MHP that are based on a SiO<sub>2</sub> insulating plate with four arms and can operate to temperatures up to 500°C due to the Al metallization. Solzbacher et al [23] propose a SiC MHP, which consists of a square membrane suspended by six arms and achieves 400°C with a power of 35 mW. Lee et al. [24] reported an MHP which is totally suspended in air by Pt bonding wires and with a power consumption of 100 mW at 400°C [25].

The uniformity of the temperature distribution over the sensing area is also an important factor in gas detection. Using coated membrane on the front side with a thin diamond or silicon carbide film and on the backside coated with high reflective gold film can achieve extremely good temperature distribution over the whole membrane area without exceptional heater geometry [26]. The temperature distribution has also been improved by adding silicon island under the membrane using simple meander and double mender heater and at an operation temperature of 400°C the temperature gradient between the centre and the edge of the sensing area is 23°C and 10°C [27] . Recent research showed that a polysilicon plate can be placed in the membrane centre instead of a silicon island underneath the membrane layer. Temperature gradient on the MHP using silicon island at 300°C is about 0.3C/µm while it is 0.07C/µm when polysilicon plate is used [28, 29]. These observations indicate that the temperature gradient at elevated temperatures will be higher still and needs to be homogenized. The conductive heat distribution plate can be made from any metal or compounds. In this study silicon carbide (SiC) is used as a material for conductive heat distribution plate for high temperature application in MHP.

The micro-sensor must be compatible with low cost electronics. Electronics are used to control the hotplate's temperature and heating characteristics, as well as sense the changes in conductivity of the sensing film. It is very important to keep the cost of electronic device low, lower power consumption, low voltage hotplates that are simple to operate and improve the uniformity of the temperature distribution over the sensing area. Fast response time is important factor for quick sensor cycling, minimizing power requirements, and real time sensing capabilities. Response time is an important area for chemical sensor development in general, allowing for virtual real time information processing [30].

CoventorWare simulation software is the most comprehensive suite of MEMS design tools in the industry [31]. It acts as a seamless integrated design environment that reduces design risk, speeds time to market and lowers development costs. Various parameters of a MEMS device can be investigated and optimized in this simulation environment before actual device fabrication is undertaken. In CoventorWare, the Electrothermalmechanical solver (EthermMech) module is used to simulate the temperature and displacement distribution of a high temperature MEMS MHP. This solver computes the electrical potential field, thermal, displacement distributions and current density resulting from an applied voltage through a resistive heater made of platinum. CoventorWare simulations are used to optimize the MHP for temperature uniformity, fast response time, low power consumption, good mechanical stability under high temperature operation. These requirements are used as guideline for the designs described in this research.

The aim of this study is therefore to use CoventorWare electro-thermal simulator to optimize the design of MHP for tin dioxide ( $\text{SnO}_2$ ) based gas sensor, with respect to some technological and functional rules. In an effort to dramatically shorten the development time and reduce prototyping costs, 3D simulations is used to optimize

micro-heater geometry. The advantages of using simulation in improving the performance of the MHP device are to save the cost and time.

### **1.3 Objectives of Study**

The main objective of this research is to optimize the design of a MHP for low power dissipation, uniformity of temperature distribution and mechanical stability. Specific objectives include:

- To design and simulate the MHP using finite element method (FEM).
- To optimize a high temperature MHP for applications in trace gas detection.
- To analyze and validate the simulation results with appropriate mathematical modeling.

### **1.4 Scope of Study**

The MHP is designed to achieve temperatures of up to about 700°C with low power consumption, to have good mechanical stability and fast response time as well as improving the uniformity of the temperature distribution on the MHP. This research therefore focuses on the problem of high power consumption, uniformity of temperature distribution and minimization of mechanical deflection of the MHP. To analyze and resolve these issues CoventorWare is used to simulate the MHP using the conventional methods of bulk micromachining and thin film technologies.

### **1.5 Thesis Overview**

This thesis is organized in a manner that follows the analysis steps taken during the design of the MHP and consists of 5 chapters. Chapter 1 outlines the basic introduction, a general view of the MHP design and operations, problem statement, objectives and scope of the study. From the general introductory background in chapter 1, chapter 2 focuses on an extensive literature review on the MHP (overview of the MHP, micromachining techniques, modelling of MHP, applications of MHP

and Review of previous studies on MHP). Chapter 3 will cover the methodology for the design and modeling of the MHP. Chapter 4 analyzes and discusses the results of the simulation and modeling of the MHP obtained using CoventorWare software 2006 and also comparison between simulation and calculation results. Finally, Chapter 5 presents the conclusions and recommendations of the study.

## CHAPTER 2

### MICROHOTPLATE

#### 2.1 Overview of the microhotplate (MHP)

The MHP is basic MEMS device. It consists of a Si substrate, a supporting membrane with microbridges, various layers that include the heating element, temperature sensor, insulating layers and a set of contact electrodes for sensitive layer. Many researchers have focused on different designs of the geometry of the dielectric membrane. S. Wessel [12] have presented the suspended membrane that is generally released by anisotropic etching of the silicon substrate.

J.S. Suehle [13] Reported a monolithic tin oxide ( $\text{SnO}_2$ ) gas sensor realized by commercial CMOS foundry fabrication Metal Oxide Semiconductor Implementation Service (MOSIS) and fabrication processing techniques. Thermal response time of 0.6 ms to raise the temperature of the MHP from ambient to  $500^\circ\text{C}$  has been achieved with a power consumption 68 mW. The gas sensor responses of pure  $\text{SnO}_2$  films to  $\text{H}_2$  and  $\text{O}_2$  at an operating temperature of  $350^\circ\text{C}$  are reported. The fabrication methodology allows integration of an array of gas sensors of various films with separate temperature control for each element in the array and circuits for a low-cost CMOS-based gas sensor system.

Fabrication of a high temperature resistive sensor has been presented in [32]. The sensor has been fabricated using silicon micro technology that lies on a sub-micron thick membrane. A platinum resistance heater has been embedded. At  $500^\circ\text{C}$ , it has been mentioned that the micro sensor has a low d.c. power consumption of 250 mW, and can be operated up to  $600^\circ\text{C}$ . The thermal time constant was found to be 4 ms or less to reaching a temperature of  $400^\circ\text{C}$  from ambient.

A CMOS compatible integrated gas sensor has been described in [33]. As mentioned, the sensor has been designed as the front-end fabrication compatible with the standard CMOS process. The consistency of the temperature was improved by

adopting a polysilicon ring heater that surrounds the MHP. An operating temperature of 300°C (that considered as a high in the study) was achieved using only 12 mW. The thermal time constant at the same temperature (300°C) was 3ms. On the entire MHP the unsteady temperature was less than 35°C, while the maximum one was 407°C.

In [34], an approach that aims to reduce power consumption of an integrated tin oxide gas sensor using a silicon oxynitride membrane has been introduced. Low thermal conductivity and high mechanical strength are some of results obtained. The results had been obtained using both silicon and silicon oxynitride. At 500°C, the power consumption was 220 mW and 75 mW for the silicon and silicon oxynitride respectively.

In [7], a characterization of the low-power consumption Metal Oxide Semiconductor Field-Effect Transistor (MOSFET) gas sensor has been reported. The design was fabricated using anisotropic bulk silicon micromachining. The design combined a heater resistor, a temperature sensor diode, in addition to four MOSFET; all are located at a silicon island that is suspended by dielectric membrane. The designed device allows -as cited- the reduction of power consumption to 90 mW for an array MOSFET at 170°C. Applying 6V to the heater, it has been found that the power consumption was 70 mW, while the rising time constant was about 65ms and the cooling time constant 100ms.

A modular system of MHP based on SiC and Hafnium Diboride ( $\text{HfB}_2$ ) has been presented in [23]. The design consists of a basic heater membrane area of about  $100 \mu\text{m} \times 100 \mu\text{m}$  structure suspended by six micro bridges and can be adjusted to battery powered and automotive application that either uses  $\text{HfB}_2$  thin film heater or doping and directly contacting SiC heater area. At 380°C, the power consumption was found to be about 35 mW for the membrane with 20  $\mu\text{m}$  bridge widths.

Another way to fabricate the membrane is through a combination of anisotropic etching from both back and front side etching that leads to bridge membrane

suspended by six arms [23, 35]. The etching that had been done from the front side removed some parts of the membrane. It is observed that when more MHP arms (bridges) are used, more heat will be transferred to the substrate.

A low-power Si-based micro-machined micro-heater array has been developed by F. Solzbacher, [36]. In this design, the same Pt/Ti layer has been used as a micro heater and temperature detector. At 400°C, with 80  $\mu\text{m} \times 80 \mu\text{m}$  membrane area, the power consumption was about 9 mW, while the thermal time constant is 1ms.

Danick Briand, [27] focused on the optimization of an MHP power consumption based on finite element method (FEM). To improve the temperature distribution on a drop-coated metal-oxide, a 10  $\mu\text{m}$  thick silicon island was added under the membrane. Two heater geometries such as simple meander and double meander were studied. A size of 1 mm  $\times$  1 mm and 1.5 mm  $\times$  1.5 mm area of the membrane has been presented. The temperature gradient between the centre and the edge of the sensing area is found to be 100°C for the simple meander and 23°C for the double mender at an operating of 400°C.

In [37] the suspended microhotplates characteristics made of porous silicon (PS) used as thermal sensor has been reported. The PS was designed with 100  $\mu\text{m} \times 100 \mu\text{m}$  membrane area with four supporting beams. At an operating temperature 600°C the power consumption obtained is 35 mW.

In [38] the design of a polysilicon loop-shaped microheater on 1-  $\mu\text{m}$  thin dielectric membrane was presented. The power consumption was found to be about 38 mW, 50 mW and 67mw for three different of square membrane 840  $\mu\text{m} \times 840 \mu\text{m}$ , 640  $\mu\text{m} \times 640 \mu\text{m}$  and 440  $\mu\text{m} \times 440 \mu\text{m}$  at operating temperature of about 600°C.

A design of doped single crystal silicon (SCS) micro-hotplates for gas sensor was described and proposed in [39]. The shapes of both membrane and heater have been chosen to be circular with a radius of 282  $\mu\text{m}$  for the membrane and 75  $\mu\text{m}$  for the

heater. An operating temperature of about 500°C was obtained at a drive voltage of about 5 V and the power consumption is found to be less than 100 mW.

Inderjit Singh and S. Mohan [17] proposed five different micro-heater designs. These are (a) Plane plate with central whole (b) double spiral (c) S-shape (d) fan shape (e) honeycomb. They used heaters with different shapes in order to investigate the effect of heater geometry on the uniformity of the temperature distribution on the hotplate. The S-shape and double spiral design give only 15°C difference between maximum temperature and average sensor temperature. A power consumption of between 50-100 mW has been obtained at operation temperature in the range of 400°C to 500°C. The S-shape design was selected as having the better characteristic and designed with a final membrane area of 1800  $\mu\text{m} \times 1800 \mu\text{m}$  and a microheater area 900  $\mu\text{m} \times 400 \mu\text{m}$ .

In [40] a new MEMS MHP design for gas sensing application has been presented. A low cost process that includes physical vapor deposition, photolithography, electroplating, and photoresist-sacrificed process was used to fabricate the structure on a glass substrate. CoventorWare simulation has been used to design the new MEMS micro-hotplate. The effects of the thickness of the NiCr heater layer on the operating temperature, mechanical deflection, stresses, and power consumption has been studied. The power consumption and Mises stress are reduced from 126 mW to 7 mW and 1280 MPa to 472 MPa, respectively, when the thickness of the heater was reduced from 5  $\mu\text{m}$  to 0.25  $\mu\text{m}$  at the operation temperature of 400°C.

In [41] the fabrication steps and the implementation of a suspended micro-hotplate device for high temperature gas sensing applications have been described. The BaSnO<sub>3</sub> gas sensing layer has been deposited over interdigitated platinum electrodes, a SiO<sub>2</sub> layer as an insulating layer, a platinum heater with a double spiral shape and a Si<sub>3</sub>N<sub>4</sub> dielectric layer suspended by four bridges. At an operating temperature 700°C and without the gas sensitive layer a mechanical stress of more than 712 MPa and a vertical displacement of more than 7  $\mu\text{m}$  had been obtained. The power

consumption of this device was found to be 50 mW at an operating temperature of about 400°C.

A novel convex micro-hotplate structure using surface micromachining technology has been Fabricated [42]. An integrated  $4 \times 4$  tin oxide gas sensor array was designed and heating this array to an operation temperature 300°C required 23 mW of power.

Table 2.1 gives an overview of recently presented micro heaters and micro hotplates for gas sensor applications. The table presents the size of the active membrane (Mem), materials used for the membrane and heater, the process technology. It is also indicated in the table whether the device was only simulated (S) or fabricated (F) or both, the maximum operating temperature to which the device was heated (Op. tem.), the power dissipation at maximum operating temperature, the thermal time constant ( $\tau$ ) and References (Ref.).

**Table 2.1:** Micro hotplate specifications

Mem. size ( $\mu\text{m}^2$ )	Mem. type	Heater type	Process	S or F	Op. Te ( $^{\circ}\text{C}$ )	Power (mW)	$\tau$ ms	Ref.
N/A	$\text{SiO}_2 / \text{Si}_3\text{N}_4$	Poly Si	bulk	F	500	68	0.6	[13]
$324 \times 111$	$\text{Si}_3\text{N}_4$	Pt	bulk	S/F	500	250	N/A	[32]
$150 \times 150$	$\text{SiO}_2$	Poly Si.	bulk	F	300	12	3	[33]
$150 \times 150$ $100 \times 100$	$\text{Si}_2\text{N}_2\text{O}$	Poly Si.	bulk	F	500	220 And 75	N/A	[34]
$180 \times 180$	$\text{Si}_3\text{N}_4$	Pt	bulk	F	170	75	65	[7]
$100 \times 100$	SiC	$\text{HfB}_2$	bulk	F	380	35	N/A	[23]
$100 \times 100$	SiC	$\text{HfB}_2$	Bulk/SiC	F	250	20	50	[35]
$80 \times 80$	$\text{SiO}_2$	Pt/Ti	bulk	F	400	9	1	[36]
$150 \times 150$ $100 \times 100$	$\text{Si}_3\text{N}_4$	Pt	bulk	F	300	50 75	10 25	[27]
$100 \times 100$	PS	Pt	bulk	F	600	35	N/A	[37]
$840 \times 840$ $640 \times 640$ $440 \times 440$	$\text{Si}_3\text{N}_4$	Poly Si.	bulk	F	600	38 50 67	N/A	[38]
Radius $282 \mu\text{m}$	$\text{Si}_3\text{N}_4 / \text{SiO}_2$	SCS	N/A	S	500	100	N/A	[39]
$1800 \times 1800$	$\text{Si}_3\text{N}_4$	Pt	bulk	S	400- 500	50-100	N/A	[17]
N/A	Glass	NiCr	N/A	S	400	7	N/A	[40]
$100 \times 100$	$\text{Si}_3\text{N}_4$	Ti/Pt	bulk	F	400	50	40	[41]
$190 \times 190$	O/N/O	Pt	Surface	F	300	23	N/A	[52]

## 2.2 Micromachining techniques for MHP

The micromachining techniques are categorized into bulk micromachining and surface micromachining processes [43].

### 2.2.1 Bulk Micromachining

Bulk micromachining is a process used to produce MEMS. It defines structures on silicon substrate by selectively etching inside the substrate. Membranes, cavities, bridges and cantilevers are fabricated using etching of silicon. In order to form a functional MEMS structure on a substrate, it is necessary to etch the thin films previously deposited and/or the substrate itself. There are two basic categories of etching processes [44]:

- i. Wet etching where the material is dissolved when immersed in a chemical solution.
- ii. Dry etching where the material is sputtered or dissolved using reactive ions or a vapor phase etchant.

Wet etching is a process in which chemical solutions, or etchants, are used to dissolve areas of a silicon substrate that are unprotected by an etching mask. Due to the chemical nature of this etching process good selectivity can often be obtained, which means that the etching rate of the target material is considerably higher than that of the mask material if selected carefully. There are two different types of wet etching; isotropic and anisotropic wet etch [44]. Isotropic wet etch etches in all directions at the same rate (non-directional etchants are used to remove exposed areas of a substrate) while anisotropic etch etches the substrate faster in one direction than another [45]. Anisotropic wet etching of silicon is the most common micromachining technique as shown in fig 2.1(a) isotropic and (b, c) anisotropic etching of the silicon substrate [43].

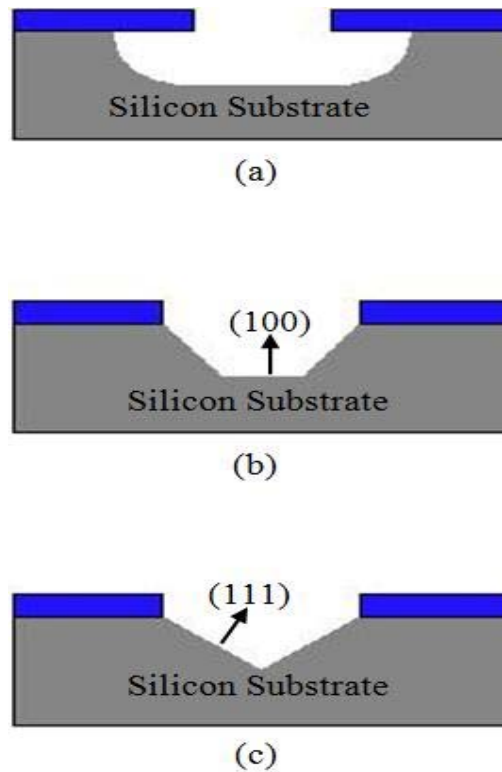


**Figure 2.1:** (a) Isotropic and (b, c) anisotropic etching of the silicon substrate

There are two types of the wet etching; front side and backside. The sidewall angle is pre-defined with  $-35.3^\circ$  to represent a characteristic etch angle for crystal silicon. Despite the high anisotropy of Potassium Hydroxide (KOH) wet etching, usually the mask is still undercut by a few percentage of the total etch depth. The most common anisotropic silicon etching uses KOH, KOH etching provides the best selectivity for  $\{111\}$  planes versus  $\{100\}$  planes to produce well defined and controlled cavities and very smooth etched surfaces [44].

Anisotropic wet etch, using KOH or tetramethyl ammonium hydroxide (TMAH), is a bulk silicon etch whose etch rate is very dependent on the orientation of the silicon's crystal planes. For example,  $\{111\}$  crystal silicon planes etch significantly slower than  $\{100\}$  planes [46, 47]. This makes it possible to create specific geometries difficult to produce with other micromachining techniques. The most characteristic

feature of anisotropic ally etched structures on (100) silicon wafers are cavities or V-grooves (fig 2.1: c) that are bounded by {111} planes, which intersect under an angle of  $54.7^\circ$  ( $90^\circ - 35.3^\circ$ ) with the {100} plane of the top surface. This process modeling step doesn't count for all possible geometries, but emulates the etching result of rectangular mask aligned parallel to the  $\langle 100 \rangle$  direction, which is a cavity bounded by inclined crystal silicon {111} planes. Some common examples of anisotropic wet etching are KOH, TMAH and ethylene diamine.

### **2.2.2 Surface micromachining**

Surface micromachining uses layers deposited on the surface of a substrate as the structural materials, rather than using the substrate itself. As the structures are built on top of the substrate and not inside it, the substrate's properties are not as important as in bulk micromachining, and the expensive silicon wafers can be replaced by cheaper substrates, such as glass or plastic. The original surface micromachining concept was based on thin polycrystalline silicon layers patterned as movable mechanical structures and released by sacrificial etching of the under laying oxide layer. Fabrication process of the surface micromachining starts with a silicon wafer or other substrate and grows layers on top. These layers are selectively etched by photolithography and either a wet etch involving an acid or a dry etch involving an ionized gas, or plasma. Dry etching can combine chemical etching with physical etching, or ion bombardment of the material. Fig 2.2 shows the example of surface micromachining [43]. A sacrificial layer is deposited and patterned on a substrate. After that, a structural thin film, in most cases polysilicon, is deposited and patterned, which will perform the mechanical or electrical functions in the final device. A selective etchant then removes exclusively the sacrificial layer material. The thickness of the sacrificial layer determines the distance of the structural parts from the substrate surface. Common sacrificial layer materials include silicon oxide etched by hydrogen fluoride and aluminum etched by a mixture of phosphoric, nitric and acetic acid.

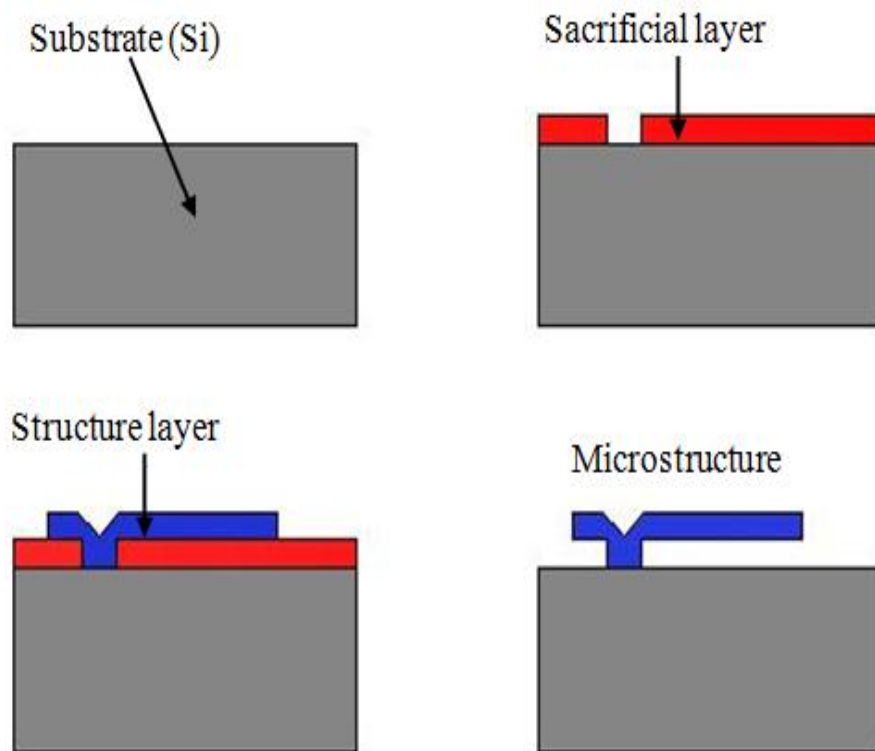


**Figure 2.2:** Surface micromachining [43]

## 2.3 Theory of Heat Transfer

Heat transfer occurs due to conduction, convection and radiation.

### 2.3.1 Conduction Heat Transfer

Conduction is the transfer of thermal energy from a point of higher temperature to a point of lower temperature. The equation for power dissipated via conduction,  $P_{condu}$ , is given by

$$P_{condu} = 4kA \frac{dT}{dx} \quad (2.1)$$

where  $K$  is thermal conductivity of the material in W/m.K,  $A$  is cross sectional area normal to the direction of heat flow, in  $m^2$ ,  $\frac{dT}{dx}$  is temperature gradient at the section [39].

### 2.3.2 Convection Heat Transfer

Convection is the transfer of heat in fluid (liquid or gas) or air caused by the movement of the heated air or fluid. There are two types of convection; natural convection and forced convection. Natural convection means that the reason for the particle flow is a temperature gradient only. Forced convection implies another source of particle flow. The heat transfer between a fluid at a point of higher temperature  $T_{hot}$  to a point of lower temperature  $T_{amb}$  can be expressed by the equation:

$$P_{conv} = Ah(T_{hot} - T_{amb}) \quad (2.2)$$

where  $P$  is the power in W,  $A$  it the area in  $m^2$  and  $h$  is the emperitical convection coefficient in  $W/m^2.K$  and the heat transfer coefficient is given by

$$h = \frac{Nu\lambda}{l} \quad (2.3)$$

where

$$Nu \text{ (Nusselt number)} = [(Nu_1)^{10} + (Nu_t)^{10}]^{1/10} \quad (2.4)$$

With

$$Nu_1 = \frac{1.4}{\ln\left(1 + \frac{1.677}{(C_1 Ra^{1/4})}\right)} \quad (2.5)$$

$$\text{Nu}_t = 0.14\text{Ra}^{1/3} \quad (2.6)$$

And

$$C_1 = \frac{0.671}{\left[1 + \left(\frac{0.492}{\text{Pr}}\right)^{9/16}\right]^{4/9}} \quad (2.7)$$

$$\text{Pr(Prandtl number)} = \frac{\text{Kinematic viscosity}(\nu)}{\text{Thermal diffusivity}(\kappa)} \quad (2.8)$$

$$\text{Ra(Rayleigh number)} = \frac{\gamma g l^3 \Delta T}{\nu \kappa} \quad (2.9)$$

$\gamma$  is air coefficient of thermal expansion,  $g$  is gravitational constant and  $l$  is length of the plate (membrane) [48].

### 2.3.3 Radiation Heat Transfer

Radiation is energy that comes from a source and travels through some material or through space. Light, heat and sound are types of radiation. Power losses by radiation can be obtained by Stefan-Boltzmann Law:

$$P_{air} = \sigma \varepsilon A (T_{hot}^4 - T_{amb}^4) \quad (2.10)$$

Where  $\sigma$  is stefan boltmann constant =  $5.67 \times 10^{-8} \text{ Wm}^{-2}\text{K}^{-4}$  and  $\varepsilon$  is emissivity it has a value between 0 and 1, depending on the composition of the surface. A surface with the maximum emissivity of 1 is said to be a blackbody radiator.

### 2.3.4 Thermoresistors

Thermoresistors are devices for temperature measurement that use the temperature sensitivity of electrical conductive materials like metals or semiconductors. The dependence of the resistivity of these materials on temperature has been intensively investigated, so that by measuring the resistance, the temperature can be deduced directly from tables or curves. Platinum has a positive temperature coefficient. The resistance as a function of temperatures between 0 and 600°C can be written as:

$$R = R_0[1 + \alpha(T - T_0)] \quad (2.11)$$

where  $R_0$  is the resistance at the reference temperature  $T_0$  and  $\alpha$  is the temperature coefficient of the resistance, for the Platinum,  $\alpha \approx 3.927 \times 10^{-3}/K$  [49]. But for the temperatures between 73K and 1123K, the resistance of a standard platinum temperature can be represented by the equation:

$$R\{T\} = R_0\{1 + AT + BT^2 + CT^3(T - 100^\circ C)\} \quad (2.12)$$

with  $A = 3.908 \times 10^{-3}K^{-1}$ ,  $B = -5.802 \times 10^{-7}K^{-2}$  and  $C = -4.273 \times 10^{-12}K^{-4}$ , all the temperature in °C [50].

Platinum (Pt) is used as the heater element and temperature sensor when the MHP is operated at elevated temperatures ( $\geq 700^\circ C$ ) because it does not oxidize and there is close to linear relationship between platinum resistance and temperature. (i.e a constant temperature coefficient) [49].

## 2.4 Summary

This chapter presented a review of previous works on the MHP. Some researchers have designed and characterized the MHP by simulation, others by fabrication, third groups using both simulation and fabrication. The area of focus by the previous researchers differs from one study to the other. Some group focused on the size of the active membrane area and others on different materials for the membrane and heater. The parameters investigated included operating

temperature, power consumption, time constant, mechanical displacement and the uniformity of temperature distribution on the MHP. This chapter also discusses the various micromachining techniques such as bulk and surface micromachining technology used in MEMS designs. Finally, the general theories of heat transfer including (conduction, convection and radiation) were presented.

## CHAPTER 3

### DESIGN & SIMULATION OF MHP

#### 3.1 Design of MHP

The MHP is a basic component of sensors and lab-on-chip devices. It consists of thermally isolated stage with membrane, heater structure, a heat distributor, a temperature sensor, and contact electrodes for the sensitive layer and silicon based micromachined substrate. The MHP becomes a metal oxide based gas sensor after the gas sensitive layer is deposited on it. There are numerous papers on micromachined metal-oxide sensors [1, 22-25, 27, 28, 48].

The present study focuses on simulation and optimization of a micromachined MHP for high-temperature gas sensing application. The most important parameters to be considered in the MHP design are:

- i. High thermal uniformity of heated sensing layers to increase the sensitivity and selectivity of the active element.
- ii. Low power consumption for portable applications.
- iii. Low mechanical deflection of supporting membrane to reduce stress on the MHP.
- iv. Minimize residual stress in the applied layers in order to select the optimum functionality of the device.

The general design shape, dimensions, geometry and layers are developed using CoventorWare simulation environment. Suitable materials and layer thickness for high temperature ( $\geq 700^{\circ}\text{C}$ ) application, low mechanical deflection of structure, heater metallization and uniformity of heat distribution are presented, compared and selected. The micro sensor detection principle depends on changes in electrical conductivity of metal oxide thin films.

The MEMS MHP was designed on single side p-type [100] silicon wafer as substrate. The thickness of the silicon substrate used is 300  $\mu\text{m}$  and has an area of 400  $\mu\text{m} \times 400 \mu\text{m}$ . Silicon nitride ( $\text{Si}_3\text{N}_4$ ) is selected as the membrane layer because of its high melting point, high mechanical strength, low thermal conductivity and ability to operate at high temperature [48]. The  $\text{Si}_3\text{N}_4$  membrane layer has an area of 100  $\mu\text{m} \times 100 \mu\text{m}$  and is supported by four micro bridges of length 113  $\mu\text{m}$  and width 20  $\mu\text{m}$ . The basic steps for the design of the MHP are:

- Deposition of a thermal oxide ( $\text{SiO}_2$ ) insulating layer on the  $\text{Si}_3\text{N}_4$  membrane.
- Deposition and patterning of the platinum metal layer that forms the meandering heating element with an area of 85  $\mu\text{m} \times 85 \mu\text{m}$ , length of 1195  $\mu\text{m}$  and width of 5  $\mu\text{m}$ .
- Deposition of  $\text{SiO}_2$  insulating layer on top of the platinum heating element followed by silicon carbide ( $\text{SiC}$ ) layer with an area of 80  $\mu\text{m} \times 80 \mu\text{m}$  that acts as a heat distributor to improve the homogeneity of the temperature distribution on the MHP.
- A  $\text{SiO}_2$  insulating layer is again deposited on top of the  $\text{SiC}$  layer followed by a platinum temperature sensor deposited diagonally to the membrane with length of 360  $\mu\text{m}$  and width of 5  $\mu\text{m}$ .
- Next a  $\text{SiO}_2$  insulating layer is deposited on the temperature sensor to prevent leakage current and short circuit between the temperature sensor followed by an interdigitated electrodes made of Gold ( $\text{Au}$ ) with an area of 75  $\mu\text{m} \times 75 \mu\text{m}$  and width of 5  $\mu\text{m}$ .
- On the interdigitated  $\text{Au}$  electrode is deposited the active Tin oxide ( $\text{SnO}_2$ ) thin film sensing layer with an area of 80  $\mu\text{m} \times 80 \mu\text{m}$ .
- Finally as post processing step,  $\text{KOH}$  anisotropic etching of the front-side or backside of the wafer is carried out to isolate the membrane area from the silicon substrate and thus minimize heat dissipation to the substrate.

In a metal oxide gas sensor, a microhotplate is necessary to heat the gas sensitive metal oxide. Fig. 3.1 shows a flowchart of the design and characterization process of the MHP.

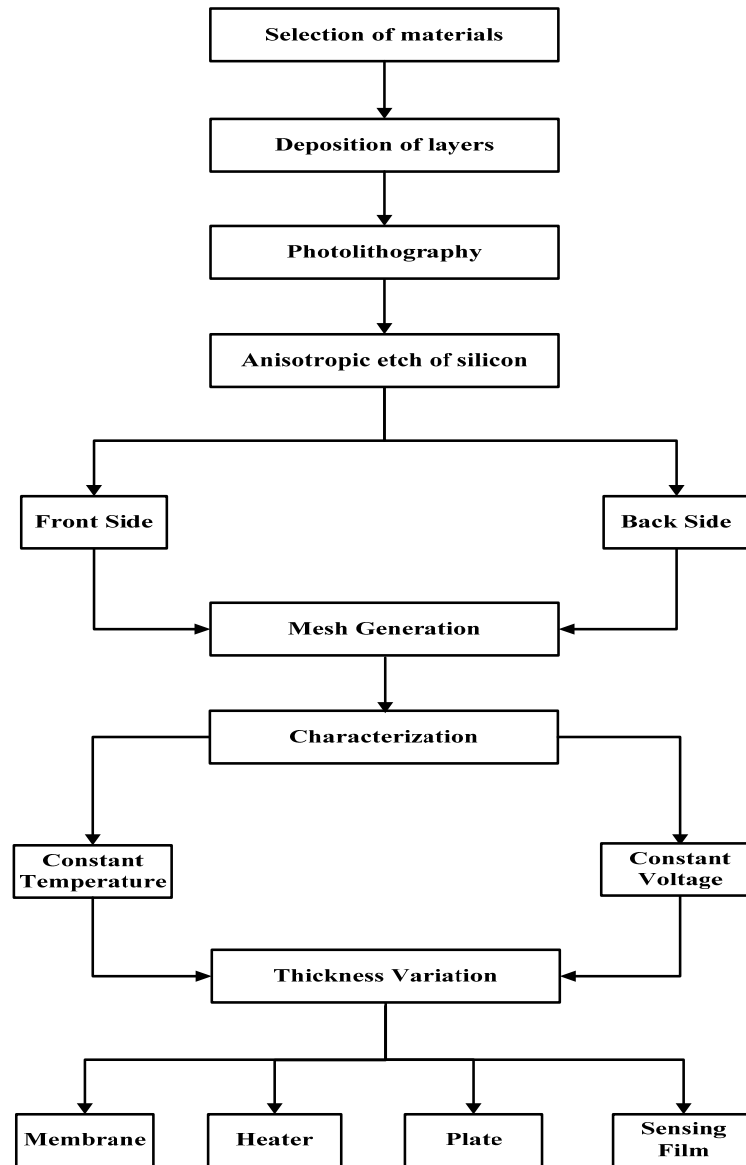


**Figure 3.1:** Flowchart of the MHP Design and Characterization

Fig. 3.2 shows a schematic block diagram of the various layers of the designed MHP structure excluding the substrate (Si) and table 3.1 shows a summary of the material properties of all the layers which have been used in the simulations. The values shown in the table are measured at the temperature of 27°C.

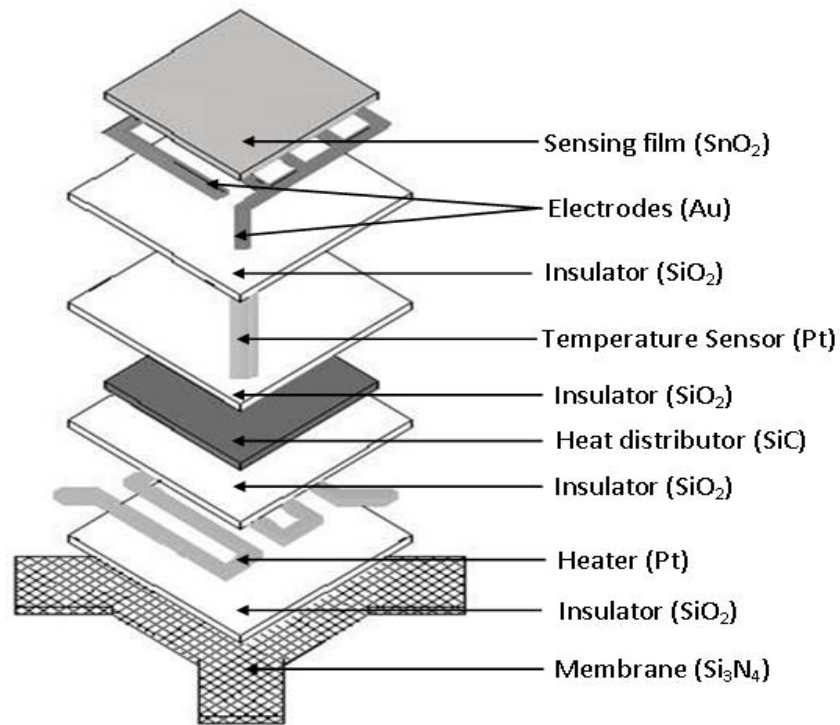


**Figure 3.2:** Layers in the micro-hotplate (MHP) design

**Table 3.1:** Material properties of layers used in the MEMS microhotplate structure

Material	(Si)	(Si <sub>3</sub> N <sub>4</sub> )	(SiO <sub>2</sub> )	(Pt)	(SiC)	(SnO <sub>2</sub> )	Au
Young's Modulus (Mpa)	1.5E+5	2.9 E +5	0.7 E +5	1.7 E +5	4.1 E +5	5 E +5	78 E +3
Poisson's Ratio	0.17	0.27	0.2	0.38	0.14	0.36	0.44
Density (kg/μm <sup>3</sup> )	2.3 E - 15	2.9 E - 15	2.3 E - 15	2.1 E - 14	3.1 E - 15	7.3 E - 15	1.9 E - 14
Thermal Conductivity (pW/μm.K)	150 E +6	22 E +6	1.4 E +6	72 E +6	12 E +7	67 E +6	32 E +6
Dielectric Constant	1.2e+1	8.0	3.9	-----	10.8	-----	-----
Specific Heat (pJ/Kg.k)	7.1 E +14	17 E +13	1E +15	1.3 E +14	15 E +13	1 E +13	1.3 E +14
Electrical Conductivity (ps/μm)	-----	-----	-----	9.6 E +12	1 E +6	2.1 E +5	4.4 E +13
Melting Point (°C)	1414	1480	1600	1768	2730	1127	1064

The suspended membrane is formed by anisotropic etch of p-type {100} Si planes from the front or back side as shown in fig. 3.3 and fig. 3.4. Fig. 3.5 shows the top view of MHP that has been etched from the front side.

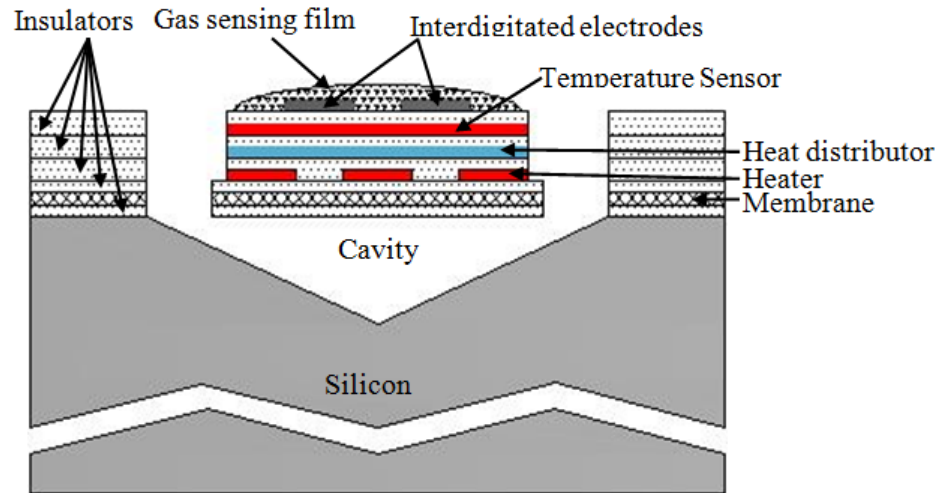


**Figure 3.3:** Cross-sectional Schematic view of Silicon MHP Gas Sensor with Front side Etch

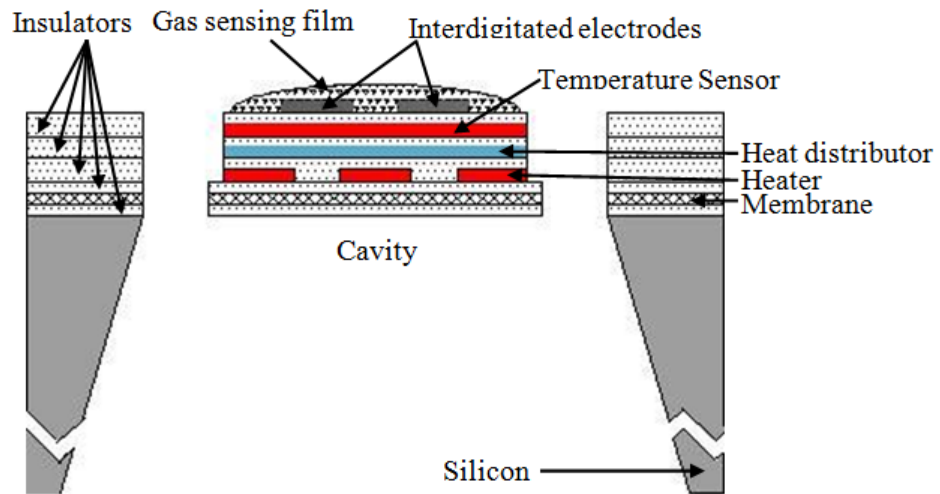


**Figure 3.4:** Cross-sectional Schematic view of Silicon MHP Gas Sensor with Backside Etch

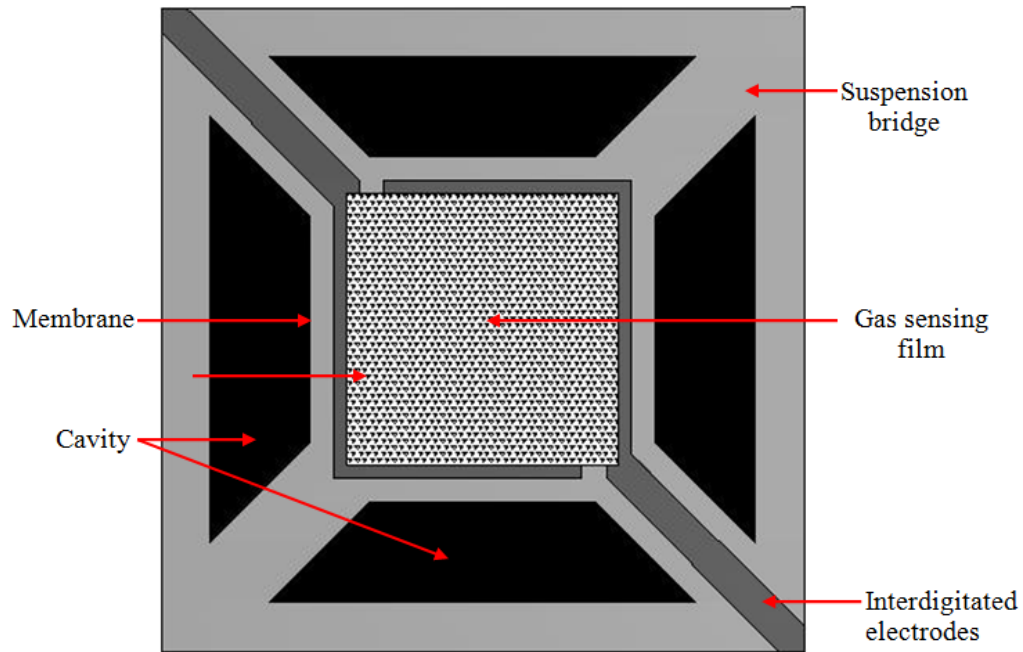


**Figure 3.5:** Top View of MHP with front side etch

### 3.1.1 Materials properties and selection

The material chosen as membrane of the MHP is silicon nitride ( $\text{Si}_3\text{N}_4$ ) and combines low thermal conductivity to avoid high thermal losses with high mechanical strength and low displacement. Platinum (Pt) was selected as the heater element and temperature sensor because it does not oxidize at elevated temperatures and the temperature has a close to linear relationship with the platinum resistance heater (i.e. a constant temperature coefficient). The design chosen for the platinum (Pt) is a loop-shape (meandering) with an area of  $85 \mu\text{m} \times 85 \mu\text{m}$ , a length of  $1195 \mu\text{m}$  and a width of  $5 \mu\text{m}$  as shown in fig. 3.6. Silicon carbide (SiC) is an excellent semiconductor for high temperature because of its good thermal conductivity, good electrical conductivity, and wide energy band gap. This wide gap allows SiC to be operated at high temperature without suffering from intrinsic conduction effects. The MHP is designed with a silicon carbide (SiC) heat distributing layer above the silicon oxide ( $\text{SiO}_2$ ) insulating layer on top of the heater. Tin Dioxide ( $\text{SnO}_2$ ) is an n-type semiconductor with attractive characteristics for gas sensor application. Recently,

$\text{SnO}_2$  thin films have drawn much interest because of their potential application in microsensor devices [51]. Interdigitated electrodes with an area of  $75 \mu\text{m} \times 75 \mu\text{m}$  and width of  $5 \mu\text{m}$  is design using Gold (Au) as shown in fig. 3.7.

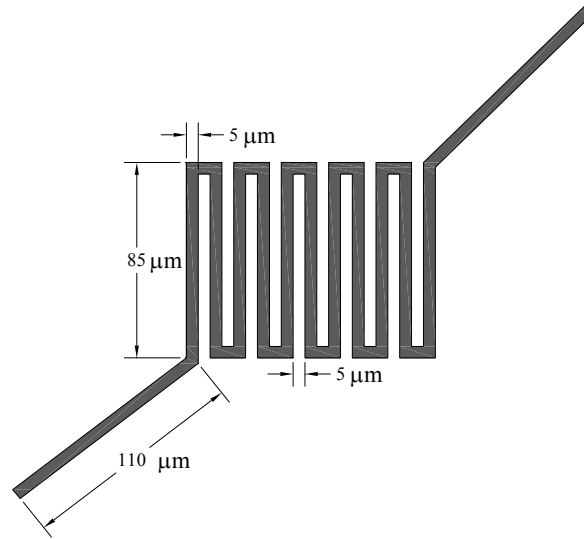


**Figure 3.6:** Heater Structure

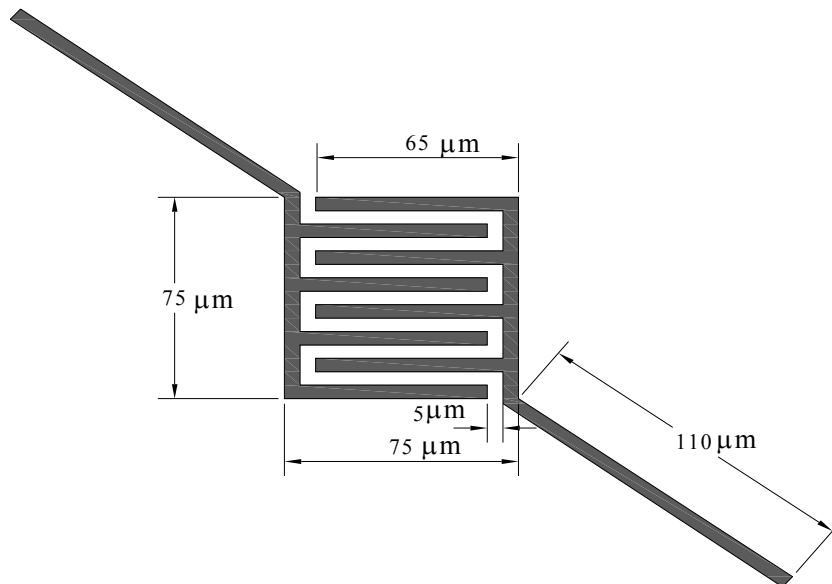


**Figure 3.7:** Interdigitated Electrodes Structure

In the simulation characterization, the thickness of the various layers (membrane, heater, heat distributor and sensing film) are varied from 0.3  $\mu\text{m}$  to 3  $\mu\text{m}$  and meshed with 5  $\mu\text{m}$  element size to obtain accurate FEM simulation results at constant temperature of 727°C. This is done to investigate the effect of the thickness of these layers on power consumption and mechanical deflection of the MHP at elevated temperatures and also to improve the uniformity of heat distribution on the MHP membrane.

On the other hand, a constant voltage of 0.7 V is applied to the terminals of the platinum heater and the thickness of the various layers (membrane, heater, heat distributor and sensing film) are increased from 0.3  $\mu\text{m}$  to 3  $\mu\text{m}$  to investigate the influence of these layers at constant voltage on the MHP characteristics.

### **3.2 Description of the Simulation Procedure**

CoventorWare is one of the most comprehensive suites of MEMS and micro fluidics design and simulation tools in the industry [31]. It acts as a design environment that reduces design risk, reduces manufacturing time and lowers development costs. In order to work with CoventorWare the necessary settings is created in the Function Manage as shown in fig. 3.8.

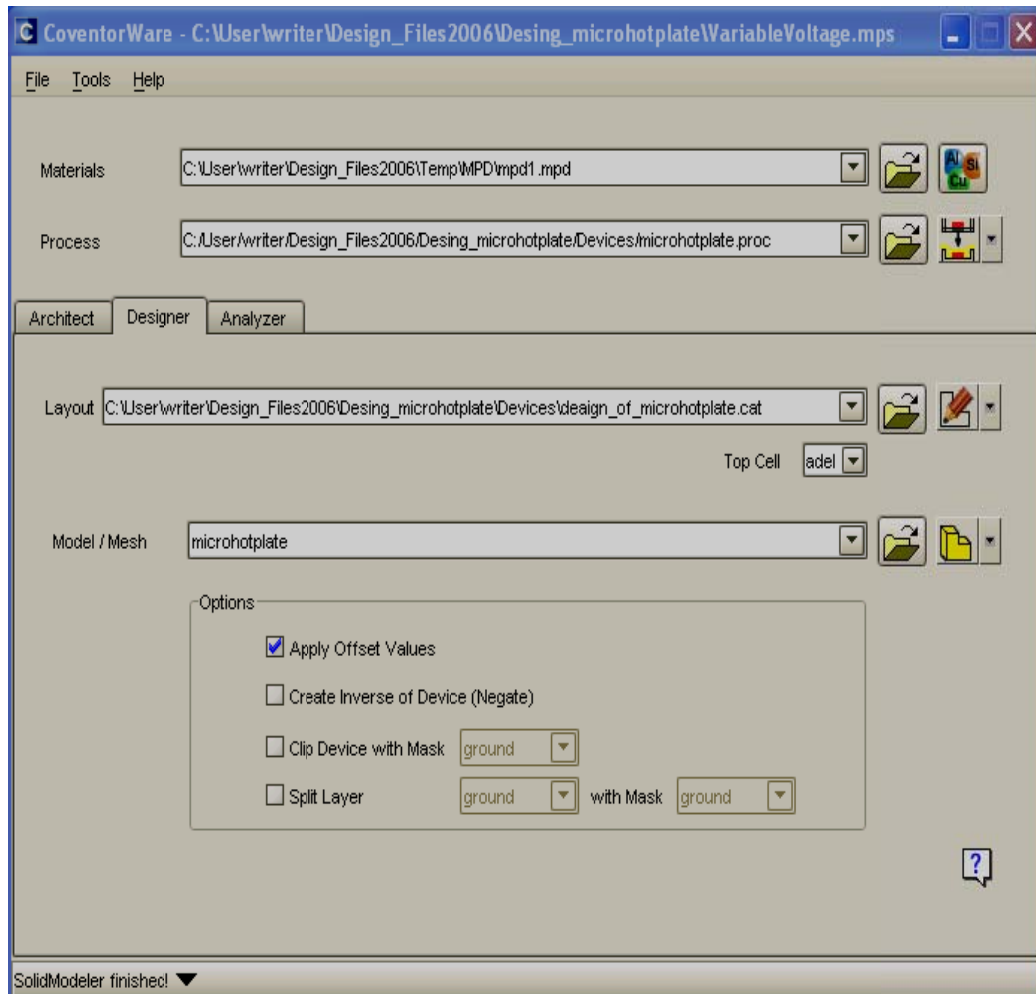


**Figure 3.8:** The Function Manager

CoventorWare supports both system level and physical design approaches. The system level approach involves use of behavioral model libraries with a high-speed system simulator. The system level MEMS design can be used to generate a 2-D layout and involves building a 3-D model, generating a mesh, and simulating using Finite Element Method (FEM) or Boundary Element Meshes (BEM) solvers. Fig. 3.9 shows a simple schematic block diagram of CoventorWare process.

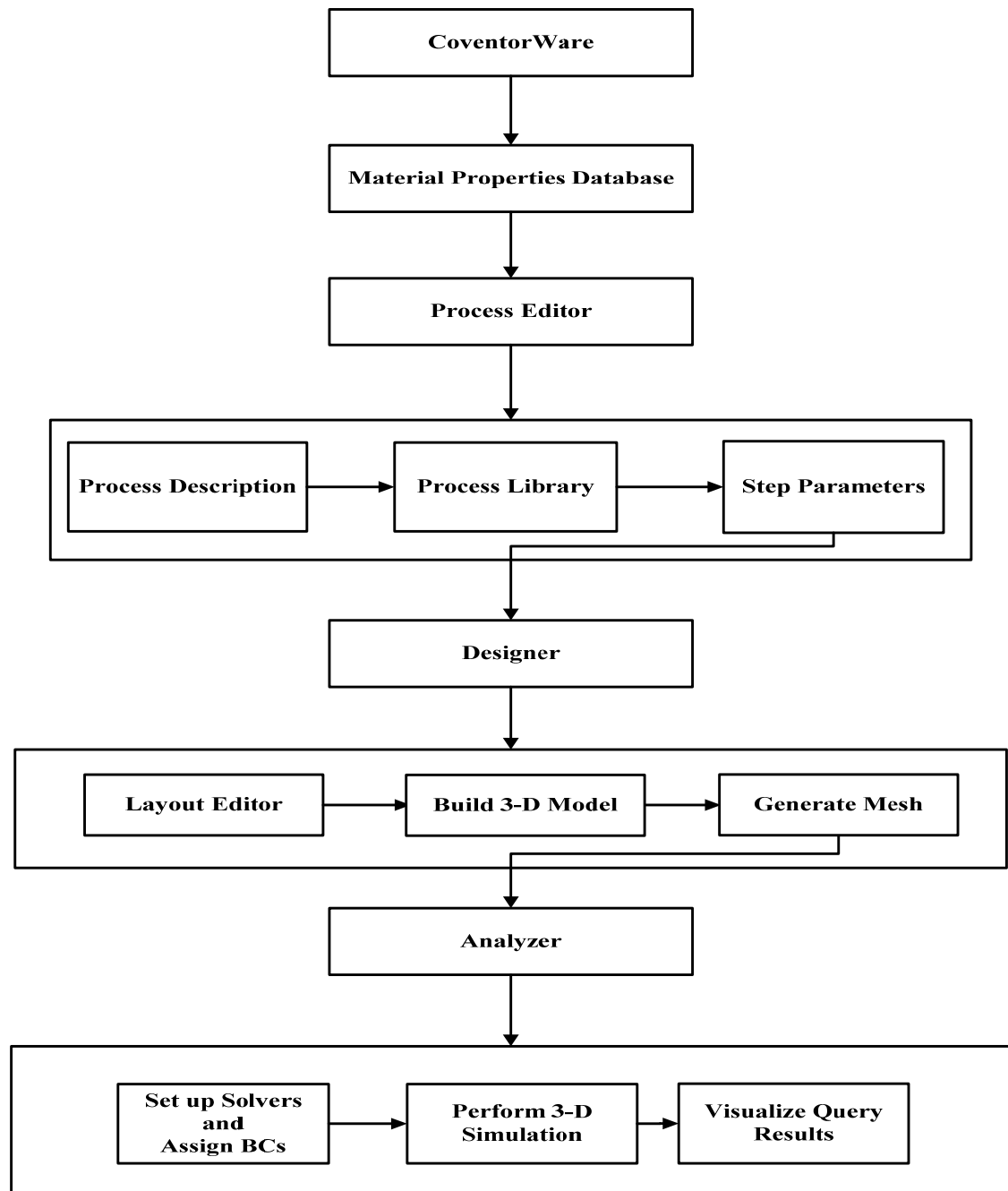


**Figure 3.9:** Block Diagram of CoventorWare Process

### **3.3 CoventorWare Components**

The major components of CoventorWare are the Material Properties Database, Process Editor, Designer and Analyzer.

#### **3.3.1 Material Properties Database**

The Material Properties Database (MPD) Editor allows you to add, delete and modify material properties. This database stores characteristics of the materials used in the fabrication process. The properties of the material include density, thermal conductivity, electrical conductivity, specific heat, strength and dielectric constant. A material has to be selected for each of the deposit steps in the process, and only those materials in the MPD can be selected. The MPD is the basic foundation for the design. It stores properties for materials used for MEMS design. Fig. 3.10 shows the Material Editor Window for platinum as an example. For other materials, the properties will be changed accordingly in the Editor Window (Refer to table 3.1).

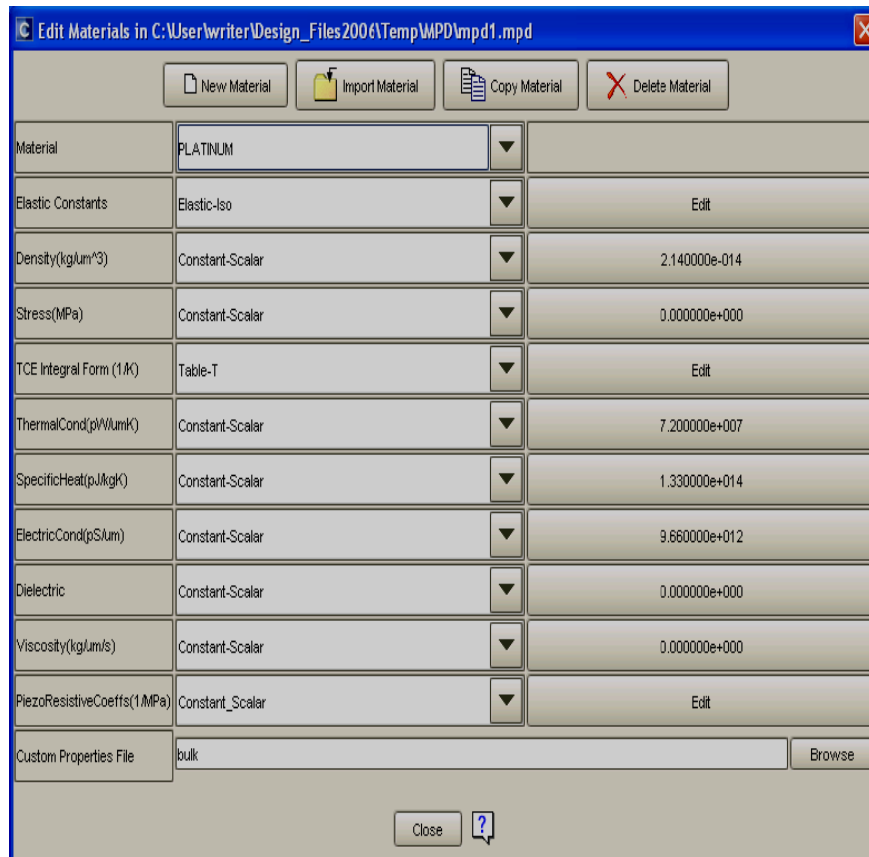


**Figure 3.10:** Materials Editor Windows for platinum

### 3.3.2 Process Editor

The Process Editor supplies the information needed to construct the 3-D solid model of the MHP from the 2-D masks viewed in the Layout Editor. Material layers are constructed in a deposit and etch sequence that emulates the Process Editor which allows building or editing a simulated process flow that models the fabrication process to be used by the foundry. The Process Editor includes three elements:

- i. Process description.
- ii. Process library.
- iii. Step parameters.

The Process Description identifies all the steps used in creating the MHP design and displays each step in its own row in a spreadsheet format. Each row lists settings or parameters that are used in creating step, and when a process step is selected, the step parameters window become active and the step parameters such as materials used, materials thickness, types of deposition, and etch techniques can be changed. The Process Library provides the modelling step options (planar fill, stack material, straight cut, conformal shell, anisotropic KOH wet Etch from the front or backside). The materials selected from the database in the process flow are used throughout the simulation process. For each step, a mask name can be selected or created. These masks will become active masks in the 2-D Layout Editor. CoventorWare is designed to be process-independent; this allows the software to accurately model many different types of MEMS processes, even if they run on different fabrication lines. In fact, the software can accommodate a design that is transferred to a new or different process line by recharacterizing the mask set flow. Fig. 3.11 shows the three elements of Process Editor.

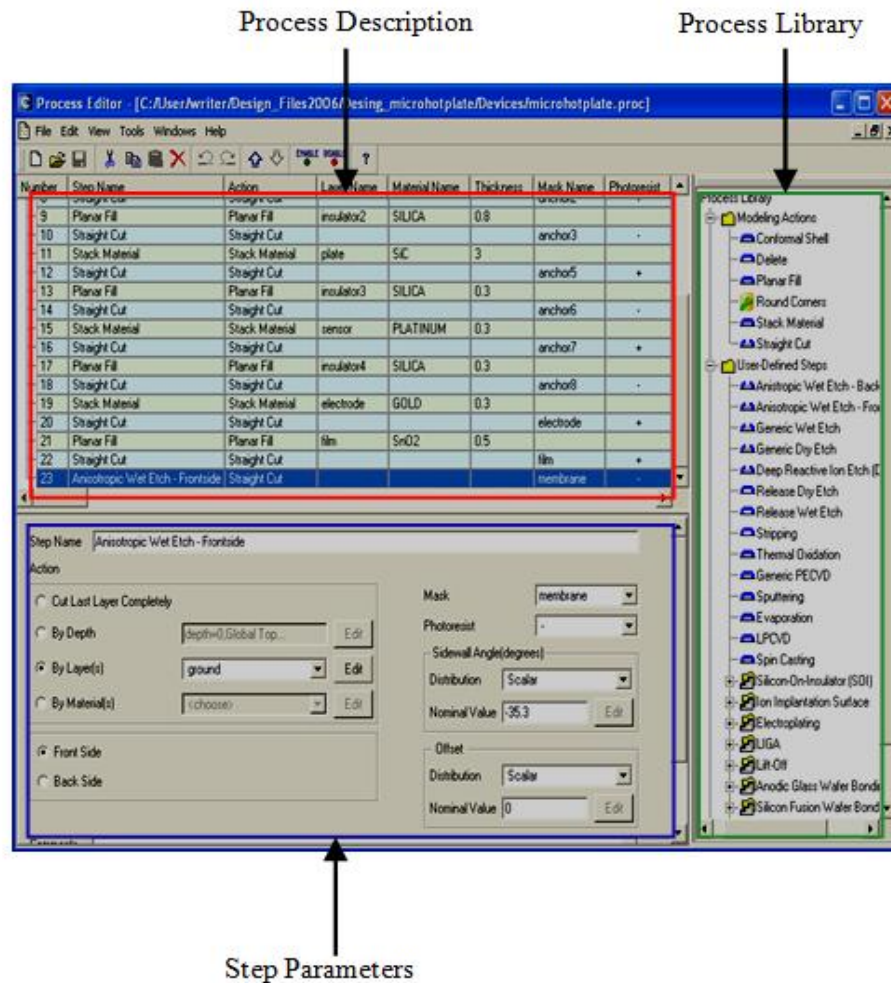


**Figure 3.11:** Elements of Process Editor

### 3.3.3 Designer

After defining material properties, the deposit and etch sequence, the next step is creating the 2-D layout. The 2-D layout information is used to create 3-D model for meshing and solving. It also shows how to customize the Layout Editor window to explain how to create basic objects using the mouse or with commands entered in the Layout Editor terminal window to design all the layers of MHP. Fig. 3.12 shows the 2-D Layout Editor with a microhotplate design displayed.

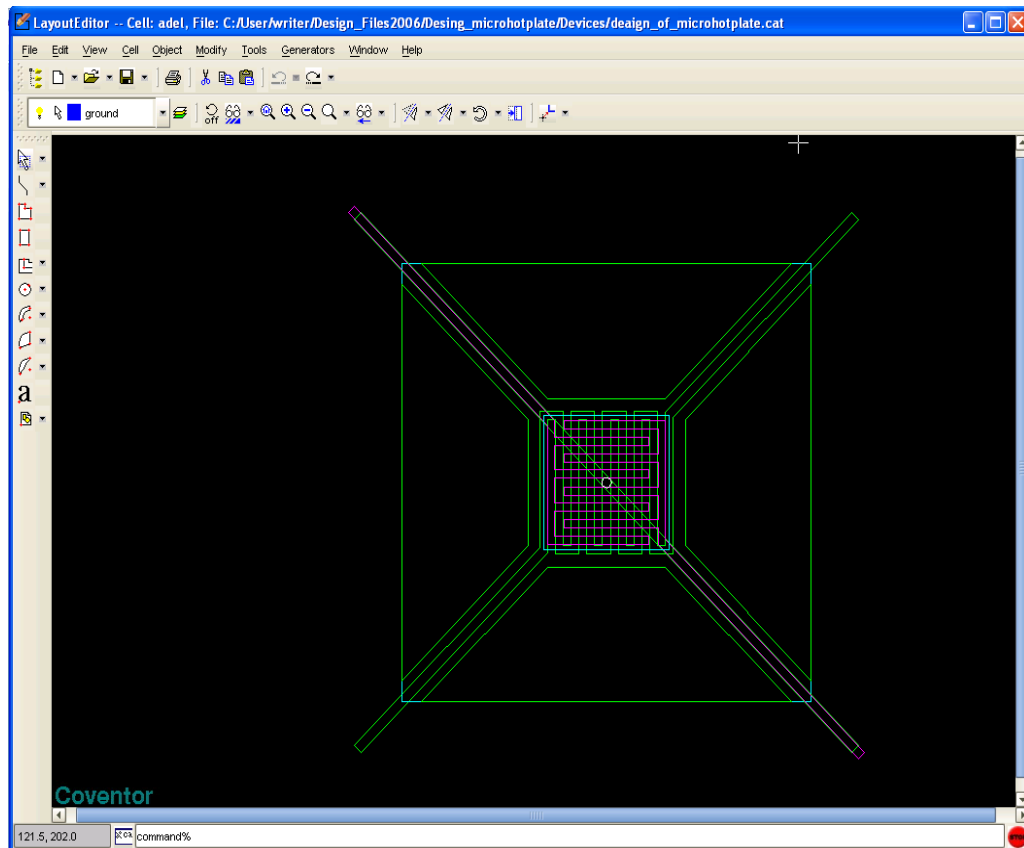


**Figure 3.12:** 2-D layout of a MHP design

After the process and layout are complete, the 3-D model of the MHP is generated and typically appears as shown in the example in fig. 3.13. The layers are then added to mesh setting, the properties are applied for each layer, the layers and the input, and output voltages of the heater layer, temperature sensor and sensing film are named. Fig. 3.14 shows the properties of platinum as an example and for other layers the properties will be changed accordingly in the Editor Window (Refer to table 3.1).

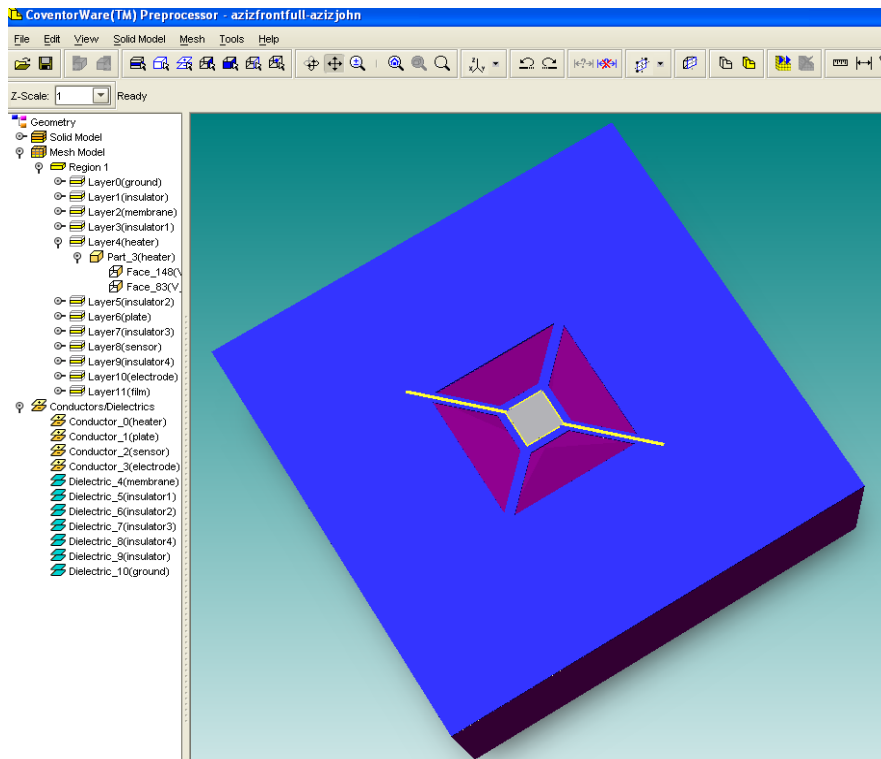


**Figure 3.13:** Preprocessor rendering of the 3-D MHP model

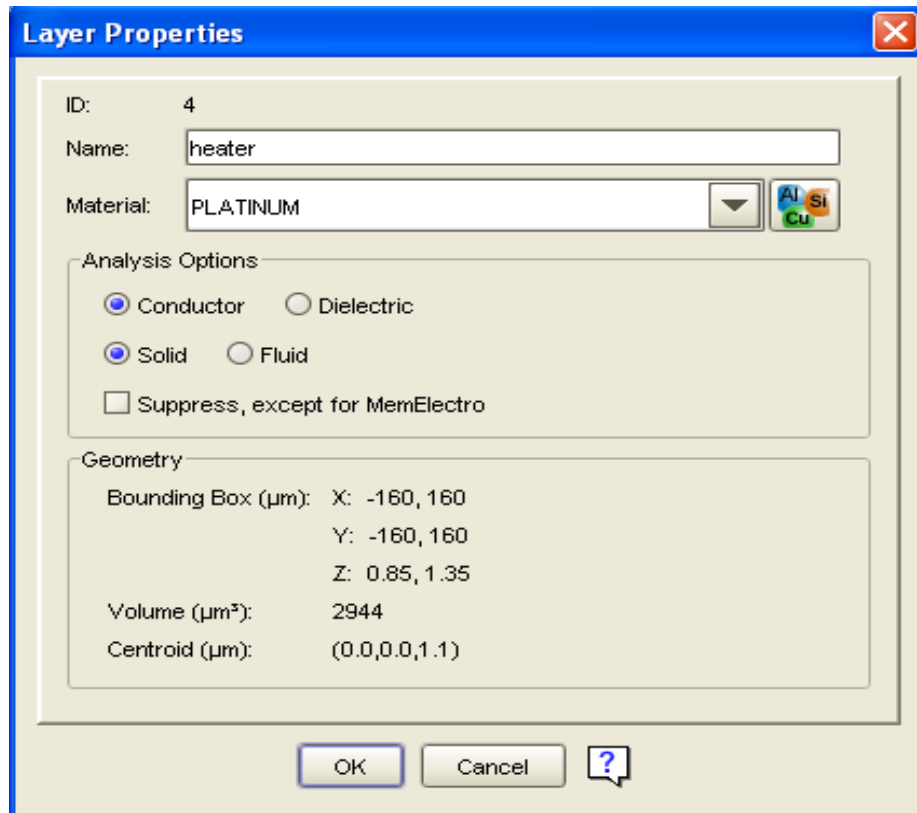


**Figure 3.14:** Properties of the platinum heater

The next step in the design process is meshing. The 3-D model must be meshed so the geometry of the structure can be reduced to a group of simpler finite elements and presented to the solver for finite element method (FEM) analysis. CoventorWare has several meshing options including surface, tetrahedral, extruded, and brick meshing. The meshing method will be selected, and then a mesh for the MHP will be created. A Tetrahedron  $80\ \mu\text{m}$  element mesh size is applied to the Si substrate of the solid model as shown in fig. 3.15. It is very important to optimize the mesh for the MHP so that acceptable results can be obtained in an acceptable amount of time. The element size of the meshed for the MHP is, therefore, varied from  $20\ \mu\text{m}$  to  $3\ \mu\text{m}$  (with  $0.5\ \mu\text{m}$  thickness to the membrane and heater) as shown in fig 3.16 (a) with a magnified view showing details in (b).

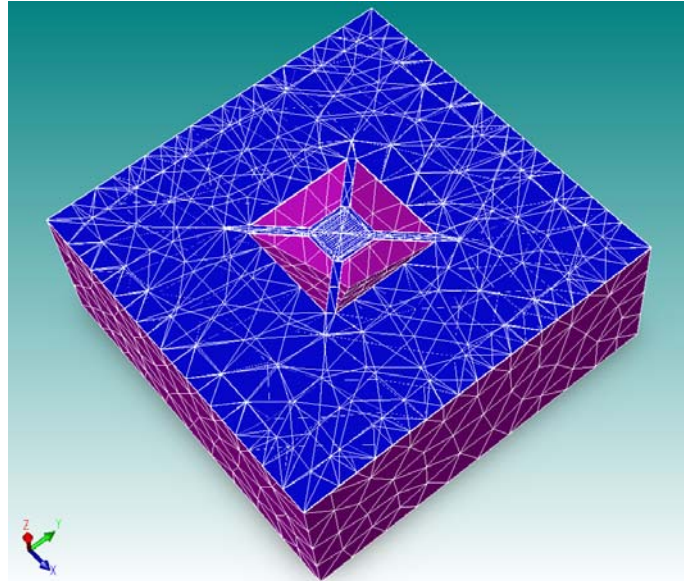


**Figure 3.15:** 3D solid model with a mesh of  $80\ \mu\text{m}$  element size on the substrate and a finer mesh on the MHP membrane

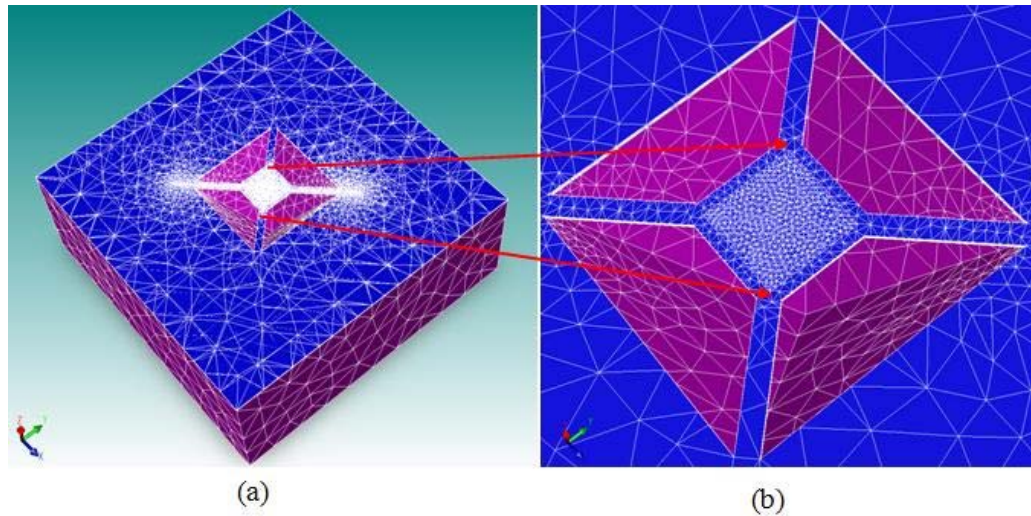


**Figure 3.16:** 3D solid model of the MHP showing (a) more refined mesh and (b) magnified view showing details of the finer element size

When a constant voltage of  $0.7\ \text{V}$  is applied to the terminals of the platinum heater, increasing the meshing of the MHP from  $3\ \mu\text{m}$  to  $20\ \mu\text{m}$  results in a decrease of the temperature of the MHP from  $727^\circ\text{C}$  to  $677^\circ\text{C}$ , while the mechanical displacement of

the membrane at mesh 3 and 5 is  $5.4 \mu\text{m}$  after that it decreases to  $5.3 \mu\text{m}$  as shown in fig 3.17. It is observed that the temperature and displacement values become comparable at the mesh sizes of  $0.5$  and  $0.3 \mu\text{m}$ . The mesh size of  $0.5 \mu\text{m}$  is therefore selected for the simulations performed in this study.

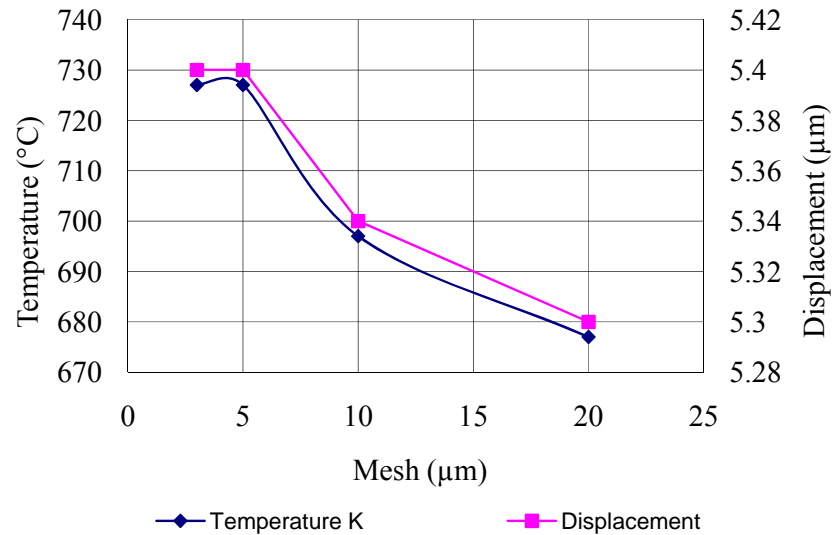


**Figure 3.17:** Temperature and displacement on the MHP vs. Mesh size at an applied voltage of  $0.7 \text{ V}$

### 3.3.4 Analyzer

The analyzer sets boundary conditions and chooses one or more solvers to perform FEM or BEM analysis. Fig. 3.18 shows the Boundary Condition window of the design.



**Figure 3.18:** Boundary Condition window of the design

The simulation results can also be viewed in 3-D and the Query function used to extract additional data from solver results. Output for most MEMS models includes a significant amount of data for analysis and post processing. The solvers include tables of primary result values, along with graphing capabilities where appropriate. The Visualizer tool supplements this capability by enabling users to map these results graphically onto the original model and visually analyze the solution. The Visualizer enables viewing of electrostatic fields, mechanical deformations, stresses, thermal variations, temperature gradients, pressures, current densities, and many other parameters. Selected parameters are colour-mapped onto the 3-D model, allowing a complete surface analysis of the model after the solution is complete. An adjustable slice plane and selected probing of interior bricks allow the entire volume to be visualized. The Query probe extends the analysis capability for more detailed results. The Analysis Results window of each solver allows access to a Query capability.

### 3.4 Modelling of MHP

The main goals of modelling the MHP designs of micromachined gas sensors include

- i. Reducing power consumption.
- ii. Increasing the hotplate temperature homogeneity.
- iii. Improve uniformity of heat distribution on the MHP surface.
- iv. Reduce response time.

Thermo-mechanical static as well as electrical simulations were performed to optimize the MHP design for low power losses, improved uniformity of heat distribution and minimizing the mechanical deflection and stresses. The power dissipation in the MHP structure occurs due to conduction, convection and radiation. The different pathways heat transfer of a MHP is indicated in fig. 3.19.

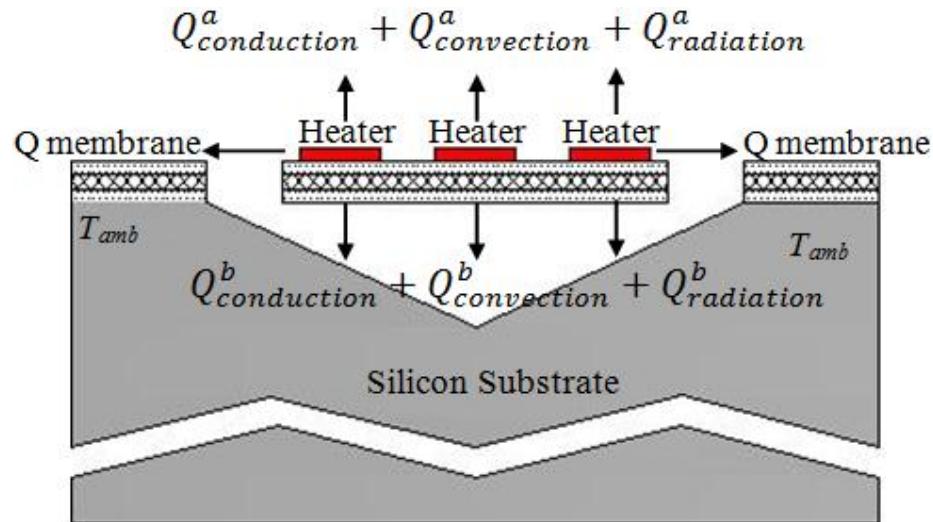


**Figure 3.19:** Heat pathways of a microhotplate

The heat losses from the heated sensing area are due to:

- i. Heat conduction through the membrane microbridges to the substrate.
- ii. Heat conduction and convection to the surrounding atmosphere.
- iii. Heat losses due to radiation that may also be taken into account depending on the application.

As a result of the different multiple pathways of heat transfer, the determination of the total heat loss and temperature distribution is not an easy task.

### 3.4.1 Heat Conduction through the membrane and air

Conduction is the transfer of thermal energy from a point of higher temperature to a point of lower temperature. Conduction losses appear through the supporting material ( $\text{Si}_3\text{N}_4$  microbridges). The total power transfer by conduction through the MHP can be determining by

$$P_{conduction} = 4kA \frac{dT}{dx} \quad (3.1)$$

where  $\kappa$  is thermal conductivity in W/mK [37] can be calculated using

$$K = (4d_{\text{SiO}_2} k_{\text{SiO}_2} + d_{\text{Si}_3\text{N}_4} k_{\text{Si}_3\text{N}_4} + 2d_{\text{Pt}} k_{\text{Pt}} + d_{\text{SiC}} k_{\text{SiC}} + d_{\text{Au}} k_{\text{Au}} + d_{\text{SnO}_2} k_{\text{SnO}_2}) / b \times c \quad (3.2)$$

where  $d$  is the thickness of each layer,  $b$  and  $c$  are factors that are determined as follows

$$b = (4d_{\text{SiO}_2} + d_{\text{Si}_3\text{N}_4} + 2d_{\text{Pt}} + d_{\text{SiC}} + d_{\text{Au}} + d_{\text{SnO}_2}) \quad (3.3)$$

$$c = \frac{(4d_{\text{SiO}_2} + d_{\text{Si}_3\text{N}_4} + 2d_{\text{Pt}} + d_{\text{SiC}} + d_{\text{Au}} + d_{\text{SnO}_2})}{(d_{\text{SiO}_2} + d_{\text{SnO}_2})} \quad (3.4)$$

The microbridges of the membrane have a different cross-sectional area depending on the thickness of the supporting membrane that is varied from  $0.3 \mu\text{m}$  to  $3 \mu\text{m}$  and has a length of  $113 \mu\text{m}$ .

The power losses through air thermal conduction can be obtained by simplifying the model of the microheater as a spherical heat source in a spherical coordinate system as shown in fig 3.20 [48] from which the following equation is obtained

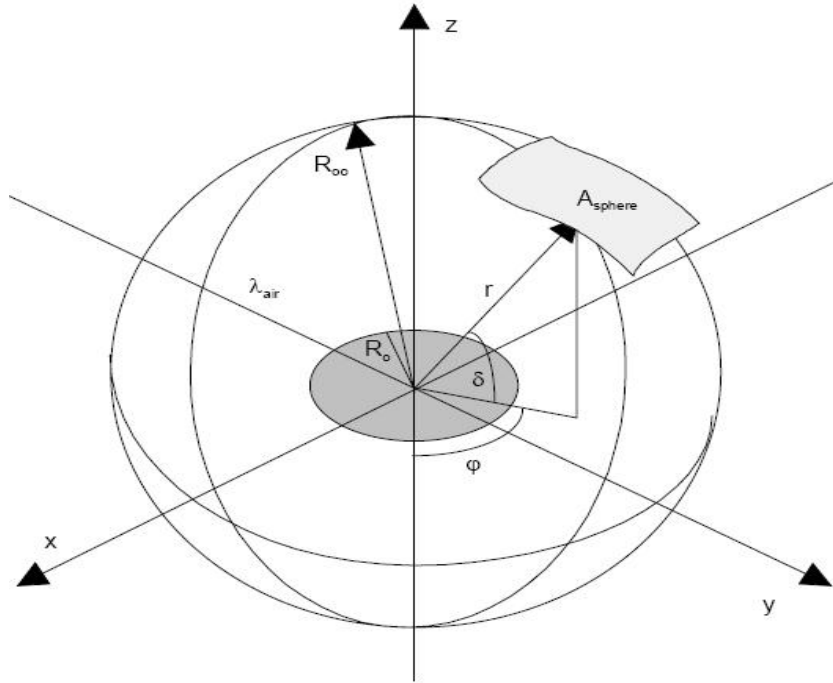


**Figure 3.20:** Theoretical determination of power losses through air [48]

$$P = \int_{r_0}^{r_\infty} \lambda A(r) \frac{dT}{dr} \quad (3.5)$$

$$\Leftrightarrow P = \int_{r_0}^{r_\infty} \lambda 4\pi r^2 \frac{dT}{dr} \quad (3.6)$$

$$\Leftrightarrow \int_{r_o}^{r_\infty} \frac{P}{\lambda 4\pi r^2} dr = \int_{T_{r_o}}^{T_{r_\infty}} dT \quad (3.7)$$

$$\Leftrightarrow P_{r_o r_\infty} = 4\pi\lambda r_o (T_{r_o} - T_{r_\infty}) \quad (3.8)$$

where  $\lambda$  is thermal conductivity of air in W/mK and  $r_o$  is radius of the heater in m.

### 3.4.2 Heat convection through air

Convection is the transfer of heat in fluid (liquid or gas) or air caused by the movement of the heated air or fluid. Heat losses to the surrounding air can occur through two different mechanisms, i.e. fluid motion and conduction. The heat transfer by convection is neglected because there is no fluid motion and also it is assumed that there is no significant contribution of convective fluid motion because of the small size of the heated structures [52-54].

### 3.4.3 Radiation

Radiation refers to heat transfer via the emission of electromagnetic waves. An object may exchange heat by emitting or absorbing thermal radiation [44]. Power losses by radiation can be obtained by using Stefan-Boltzmann Law

$$P_{radi} = \sigma \varepsilon A (T_{hot}^4 - T_{amb}^4) \quad (3.9)$$

where  $\sigma (= 5.67 \times 10^{-8} \text{ Wm}^{-2}\text{K}^{-4})$  is Stefan-Boltzmann constant and  $\varepsilon$  (emissivity) that has a value between 0 and 1, depending on the composition of the surface. From equations (3.1), (3.8) and (3.9), we obtained the total power dissipation ( $P_{disp}$ ):

$$P_{disp} = P_{conduction\ bridges} + P_{conduction\ air} + P_{radiation} \quad (3.10)$$

The power supplied to the terminals of the platinum heater of the MHP in order to make it reach the desired operating temperature should be equal to the maximum power dissipation (the power loss when the MHP reaches the operating temperature). This way, upon reaching the operating temperature, the power supplied and dissipated will be equal and the MHP will reach a steady state.

In order to operate the heater it is necessary to know the voltage required to increase the temperature until the desired value. The voltage can be calculated by using

$$V = \sqrt{P_{in} \times R} \quad (3.11)$$

where  $V$  is the input voltage,  $R$  is the resistance of the heater and  $P_{in}$  is the power supplied to the heater. The resistance for the heater is given by

$$R = \frac{\rho \times L}{A} \quad (3.12)$$

Where  $\rho$  is the resistivity,  $L$  is the length and  $A$  is the cross sectional area of the heater element. Once the equivalent resistant for the heater is known and the voltage applied is defined, the current through the sensor can be calculated using Ohms law. The current density of the microheater can be calculated using

$$J = \frac{V/R}{d \times W} \quad (3.13)$$

Where  $J$  is the current density,  $V$  is the applied voltage,  $d$  and  $W$  are the thickness and width, respectively, of the Pt heater layer, respectively [42].

### 3.4.4 Transient response

For the operation of the sensors in a pulse mode, short response times are very important. In order to calculate the transient time response needed for the MHP to reach the desired operating temperature, a dynamic energy balance of the system is considered. The difference between the rate of energy input into a system and rate of energy output from the system is equal to the rate of energy accumulation [55]. This relation may be expressed as

$$P_{in} - P_{diss} = \frac{d(\rho v c T)}{dt} \quad (3.14)$$

where  $\rho$  is the density,  $v$  is the volume,  $c$  is the specific heat capacity and  $T$  is operating temperature. The power dissipated is given by

$$P_{diss} = k_{total} \Delta T \quad (3.15)$$

where,  $k_{total}$  represents the total conductivity of heat transfers by conduction convection and radiation. Therefore equation (3.14) may be written as

$$P_{in} - k_{total} \Delta T = \frac{d(\rho v c T)}{dt} \quad (3.16)$$

which gives after rearranging

$$\frac{\rho v c}{k_{total}} \frac{dT}{dt} + \Delta T = \frac{1}{k_{total}} P_{in} \quad (3.17)$$

from which after substituting  $\tau = \frac{\rho v c}{K_{total}}$ , we obtain

$$\tau \frac{dT}{dt} + \Delta T = \frac{1}{k_{total}} P_{in} \quad (3.18)$$

where,  $\tau = \frac{\rho v c}{K_{total}}$

Equation (3.17) can be solved [55] to give the following equation

$$T_{(t)} = \frac{P_{in}}{K_{total}} \left(1 - e^{-\frac{t}{\tau}}\right) \quad (3.19)$$

here,  $\tau$  represents the system's time constant and the transient time (the time needed for the system to reach 99.3% of its total change) is equal to  $5\tau$  [55].

The thermal time constant,  $\tau$ , obtained by this equation

$$\tau = \frac{U}{P} = \frac{\rho v c (T_{hot} - T_{amb})}{P} \quad (3.20)$$

where  $U$  the energy required for heating the active area of the MHP.

### 3.5 Summary

The methodology chapter covers the design of the MHP which consists of a suspended  $\text{Si}_3\text{N}_4$  membrane that can withstand high temperatures for application in trace gas detection. The MHP has been designed and simulated using CoventorWare software. The description of the components of Coventorware software used in this study is given and includes material properties database, process editor, designer and analyzer. Finally, in the modeling part the heat conduction through the membrane microbridges to the substrate, heat conduction and convection to the surrounding atmosphere, heat losses due to radiation and transient response is presented.

## CHAPTER 4

### RESULTS AND DISCUSSION

#### 4.1 Typical 3-D FEM Simulations on the MHP devices

This chapter consists of results based on the simulation analysis when various parameters of the MHP are varied while others are held constant. It also involves the comparison of simulation results with results obtained by utilizing theoretical modeling of the MHP. CoventorWare simulations were performed to optimize the membrane thickness, to achieve uniform heat distribution over the whole active area and to achieve low power consumption and low mechanical deflection of the MHP. After designing the MHP in CoventorWare simulation environment, 3-D Layouts were generated. Using these 3-D layouts, the potential distribution, current density, heat distribution and the vertical mechanical deflections were displayed and analyzed.

##### 4.1.1 Front and back side etching

In designing an MHP using CMOS technology and bulk micromachining, two methods for post process etching of the substrate may be used; front side and back side etching. In standard foundry fabrication process, it is easier to implement front side etching than back side etching. In this section the results of simulation studies on the two methods is presented. A comparison between the performances of the MHP etched from the front side and that from the back side in terms of operating temperature achieved at a given voltage, mechanical displacement, current density, and mises stress is presented. Fig. 4.1 shows the temperature distribution profile for (a) etched from the backside and (b) etched from the front side. The maximum operating temperature attained at the centre of the MHP is 900°C in both cases when the applied voltage is 0.7 V at Si<sub>3</sub>N<sub>4</sub> membrane thickness of 0.5 μm. Fig. 4.2 shows the mechanical displacement profile on the MHP at the operating temperature of 900°C when the device is etched from (a) back side and (b) front side. It is observed that a maximum temperature of 900°C is achieved at the centre of the

MHP in both cases. Furthermore, fig 4.1 and fig 4.2 indicates that there is no difference in the temperature distribution and mechanical displacement in both cases. It is therefore concluded from the simulation results in this section that there is no significant difference in the observed properties of the MHP when it is etched from the back side as compared to that etched from the front side. Front side etching method was therefore adopted in the following sections as it will make the subsequent actual fabrication of the device utilizing CMOS technological processes and post processing utilizing bulk micromachining easier to implement.

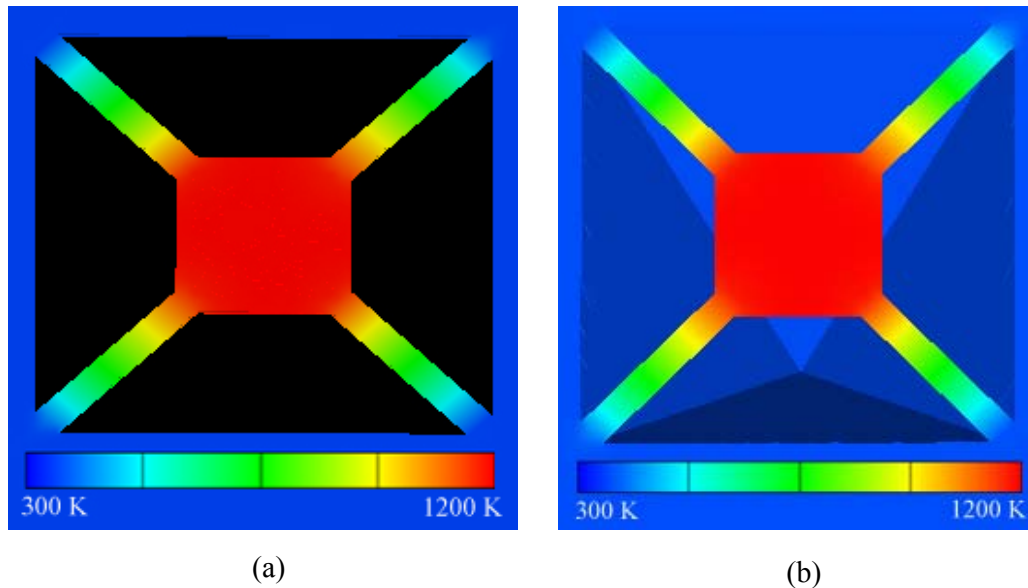
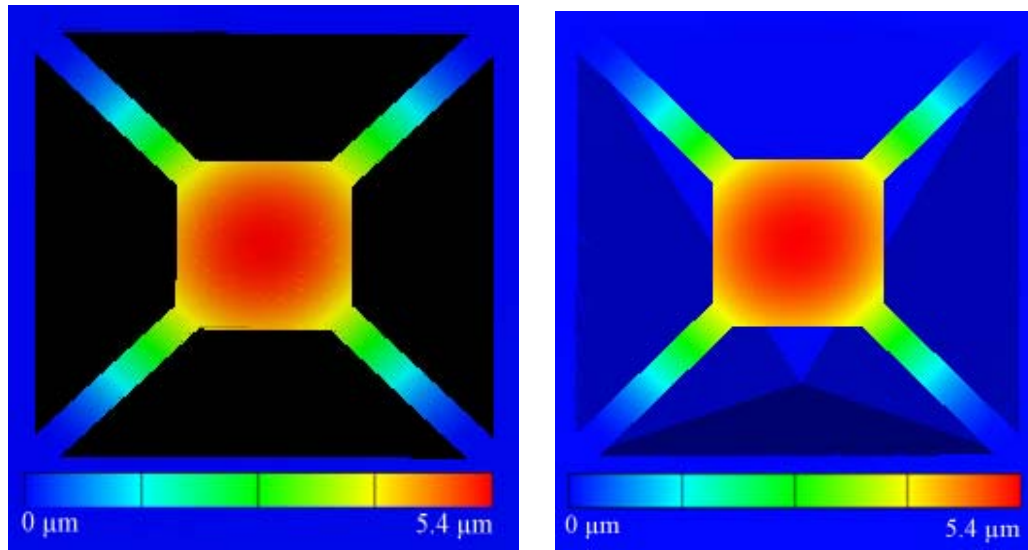


**Figure 4.1:** Temperature distribution for an MHP etched from (a) back side and (b) front side



(a)

**Figure 4.2:** Mechanical deflection of the MHP etched from (a) back side and (b) front side

#### 4.1.2 Potential distribution and current density

Fig. 4.3(a and b) and fig. 4.4(a and b) show typical simulation results of 3-D MHPs for a  $\text{Si}_3\text{N}_4$  membrane thickness of  $0.5 \mu\text{m}$  and a constant applied voltage to the platinum microheater of  $0.7 \text{ V}$ . Fig. 4.3 (a) shows typical distribution profile of the electric potential on the platinum heater element resulting from the application of a potential difference of  $0.7 \text{ V}$ . The red end ( $V_{\text{in}}$ ) indicates the point of application of the maximum potential of  $0.7 \text{ V}$  while the other end ( $V_{\text{out}}$ ) is at ground potential. It is observed, as expected, that the voltage drop over the Pt meander heater element decrease from the maximum value of  $0.7 \text{ V}$  to  $0 \text{ V}$  at the other hand.

Fig 4.3 (b) shows typical current density distribution on the Pt heater for the same device with the same applied voltage of  $7.0 \text{ V}$ . The heater current density is generally uniform except at the inner corners of the turning points of the wire where it reaches a maximum value of  $6.3 \times 10^{10} \text{ pA}/\mu\text{m}^2$  because of decrease in the cross-sectional area at the corners.

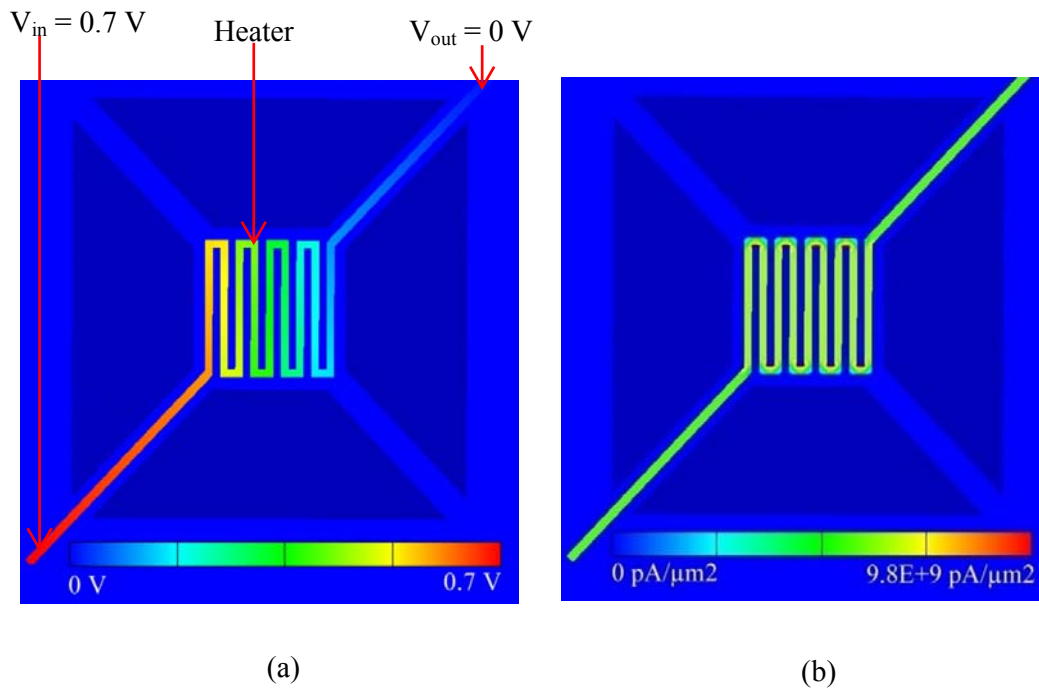


**Figure 4.3:** Atypical FEM simulation result of the (a) potential distribution and (b) current density profile in the Pt heater of the MHP for an applied voltage of 7.0 V

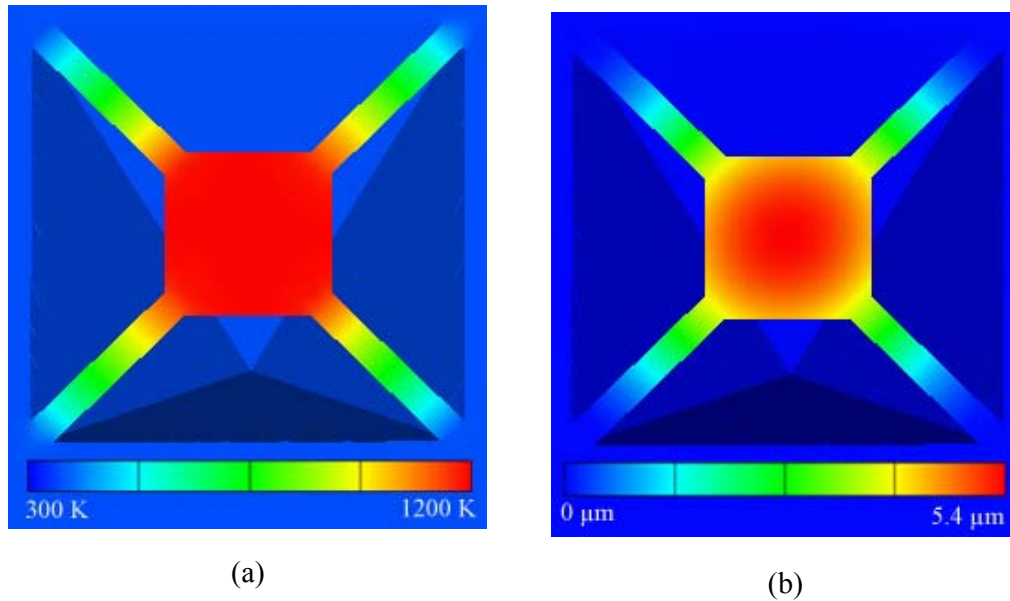
#### 4.1.3 Heat distribution and mechanical displacement

Fig. 4.4 (a) shows typical temperature distribution profile on the MHP due to an applied voltage to the Pt heating element of 7.0 V about 900°C at the center of the MHP membrane. This shows that the heat has been effectively confined to the MHP.

Fig. 4.4 (b) shows the FEM simulation results of the thermally induced vertical displacement on the MHP at the high operating temperature of about 900°C. It can be observed that the displacement is non-uniform with a maximum vertical displacement of about 7.2 μm at the centre of the MHP and dropping to zero level on the silicon substrate. It was confirmed that the displacement is in the negative z direction as expected.

Variations in the thickness of the various MHP layers is investigated to study the effect of these layers on its operating temperature, mechanical displacement, power

dissipation, current density and misses stress. These layers include the  $\text{Si}_3\text{N}_4$  membrane layer, the Pt heater element, the SiC heat distributor layer and the  $\text{SnO}_2$  thin film sensing layer.



**Figure 4.4:** Typical FEM simulation of (a) temperature distribution and (b) mechanical displacement on the MHP for an applied voltage 0.7 V

## 4.2 Effect of $\text{Si}_3\text{N}_4$ membrane thickness on MHP characteristics

The effect of the variation in the thickness of the  $\text{Si}_3\text{N}_4$  layer from 0.3  $\mu\text{m}$  to 3  $\mu\text{m}$  on the operating temperature, mechanical deflection, power dissipation, current density, time constant and heat dissipation to the substrate of the MHP is investigated in this section.

### 4.2.1 Temperature and displacement

When a constant voltage of 0.7 V is applied to the terminals of the Pt heater, increasing the thickness of the  $\text{Si}_3\text{N}_4$  membrane from 0.3  $\mu\text{m}$  to 3  $\mu\text{m}$  resulted in the

exponential decrease of the maximum operating temperature of the MHP from 1100°C to 290°C as shown in fig. 4.5, while the mechanical displacement of the membrane decreased from 8  $\mu\text{m}$  to 0.9  $\mu\text{m}$  as shown in fig. 4.6. In order to maintain a high operating temperature of about 700°C, therefore, it is required to apply a higher voltage as the membrane thickness is increased. This implies an increase in the power consumption of the MHP as a result of increasing membrane thickness. This effect is now examined more closely in the next section.

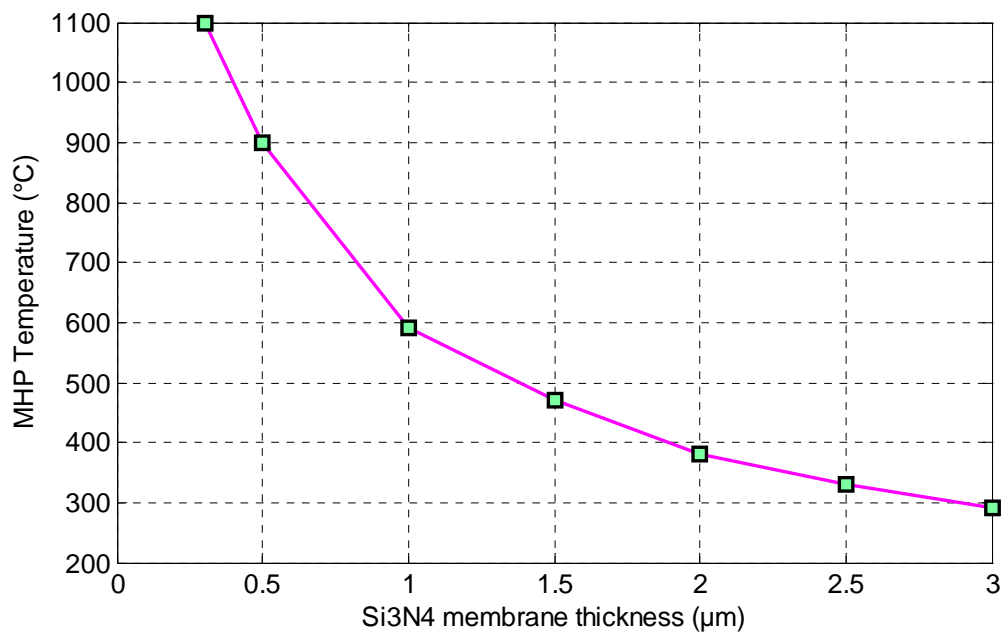


**Figure 4.5:** Maximum operating temperature on the MHP vs. thickness of Si<sub>3</sub>N<sub>4</sub> membrane at an applied voltage 0.7 V

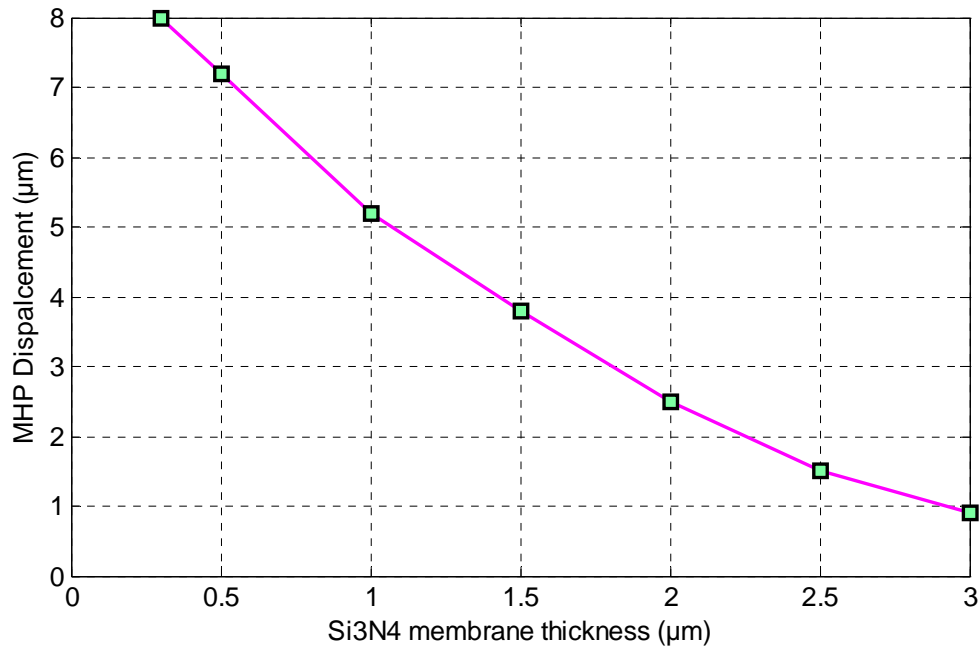


**Figure 4.6:** Maximum displacement on the MHP vs. thickness of Si<sub>3</sub>N<sub>4</sub> membrane at an applied voltage 0.7 V

#### 4.2.2 Power dissipation and displacement

In order to maintain the operating temperature at the nominal high value of 700°C, the applied voltage had to be increased from 0.75 V to 0.92 V while the thickness is increased from 0.3 μm to 3 μm. This increase in voltage to maintain the constant temperature at 700°C implies an increase in the power dissipation on the MHP from 11.25 mW to about 16.92 mW as the membrane thickness is increased as shown in fig. 4.7, while the mechanical displacement of the membrane was observed to remain constant at about 6 μm as shown in fig. 4.8. The increase in power as the membrane thickness increases can be explained by the fact that a thicker membrane requires a higher voltage than a thinner one to raise it to the same temperature. The displacement, however, remains the same because the materials coefficient of expansion remains the same at the constant operating temperature.

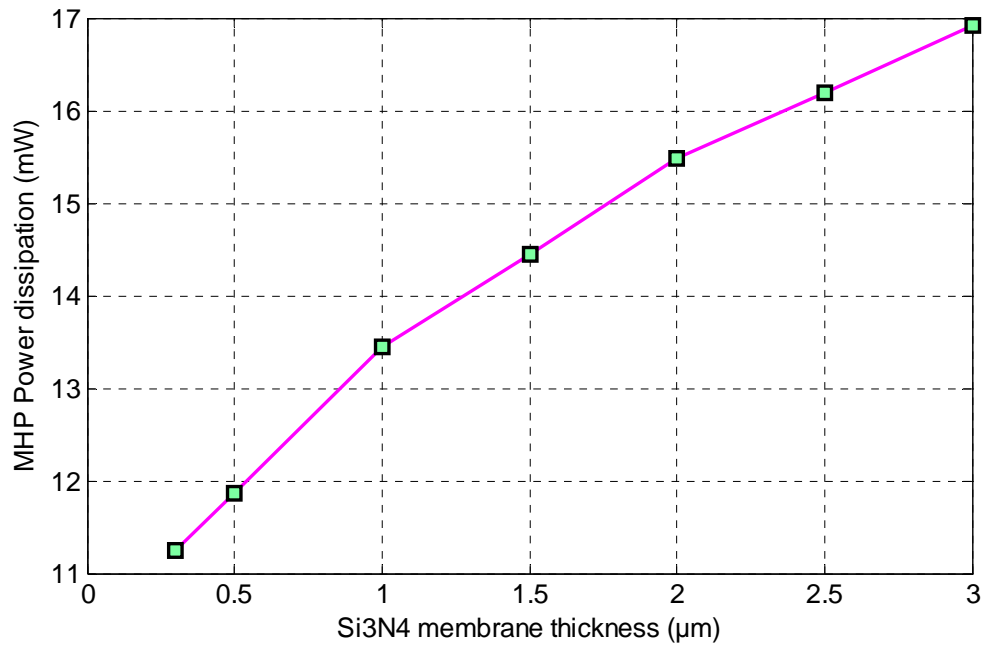


**Figure 4.7:** Power dissipation of the MHP vs. thickness of Si<sub>3</sub>N<sub>4</sub> membrane at an operating temperature of 700°C

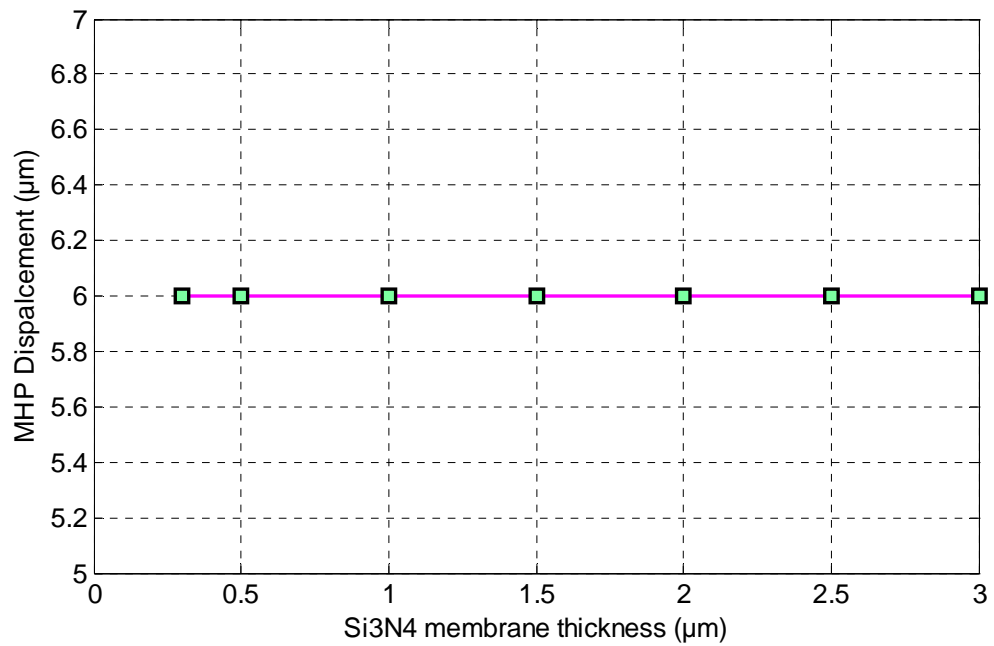


**Figure 4.8:** Displacement of the MHP vs. thickness of Si<sub>3</sub>N<sub>4</sub> membrane at an operating temperature of 700°C

### **4.2.3 Comparison between simulated and calculated values of power dissipation**

Equations (3.1) through (3.4) are used to obtain the heat conduction through the membrane. The thermal conductivity of the various MHP layers are taken from table 1.1 (chapter one). The overall thermal conductivity of the MHP when the thickness of the  $\text{Si}_3\text{N}_4$  membrane layer is varied from  $0.3 \mu\text{m}$  to  $3 \mu\text{m}$  is then obtained. The heat conduction through the surrounding air is calculated by using equation (3.8) while equation (3.9) is used to determine heat loss through radiation. Finally, the total power dissipation by the MHP as the thickness of the  $\text{Si}_3\text{N}_4$  membrane layer is varied from  $0.3 \mu\text{m}$  to  $3 \mu\text{m}$  is computed using equation (3.10).

Fig. 4.9 shows the graph of the calculated and simulated total power dissipation by the MHP as a function of the  $\text{Si}_3\text{N}_4$  membrane thickness at the operating temperature of  $700^\circ\text{C}$ . The power dissipation increases hyperbolically with the increase in the thickness of the membrane. The variation in membrane thickness results in variation in membrane cross-sectional area. Simulation and calculation values indicate a good agreement which increases our confidence in the values obtained.

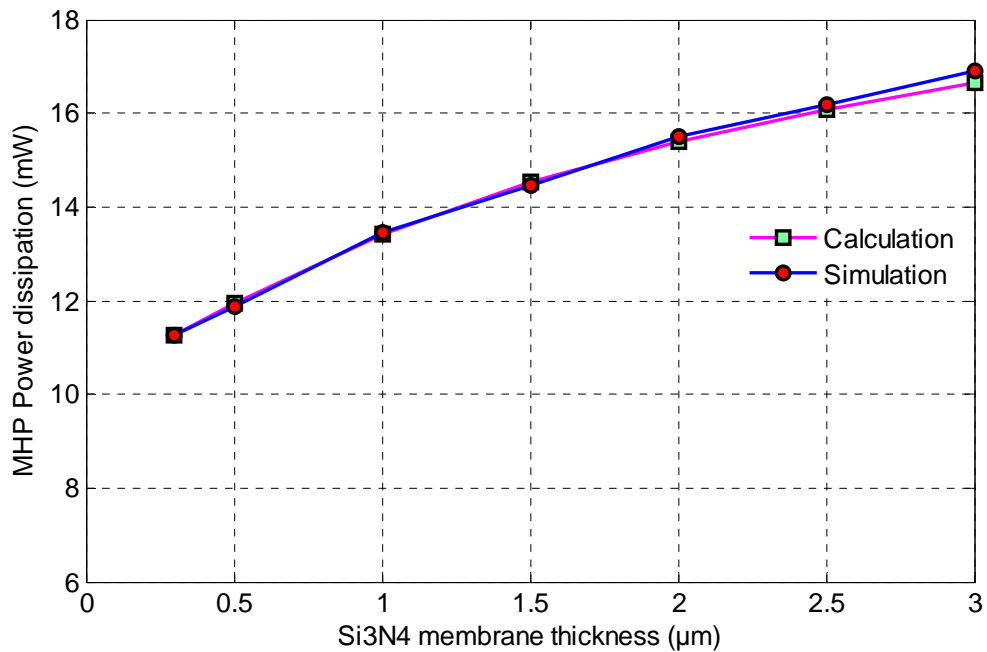


**Figure 4.9:** Simulated and calculated results of power dissipation vs. Si<sub>3</sub>N<sub>4</sub> membrane thickness at an operating temperature of 700°C

#### 4.2.4 Comparison between simulated and calculated values of current density

Equations (3.10) through (3.13) are used to calculate the theoretical current density that is following in the Pt microheater. This is done under the simulated current density obtained from the simulation. In the calculation, the thickness of Si<sub>3</sub>N<sub>4</sub> membrane was varied while the dimension of the Pt microheater is kept constant.

Fig. 4.10 shows a plot of calculated and simulated current densities as a function of Si<sub>3</sub>N<sub>4</sub> membrane thickness of the MHP. The graph indicates an increase in current density when the Si<sub>3</sub>N<sub>4</sub> membrane thickness of the MHP is increased from 0.3 µm to 3 µm. Good agreement between simulation and calculation results is obtained.

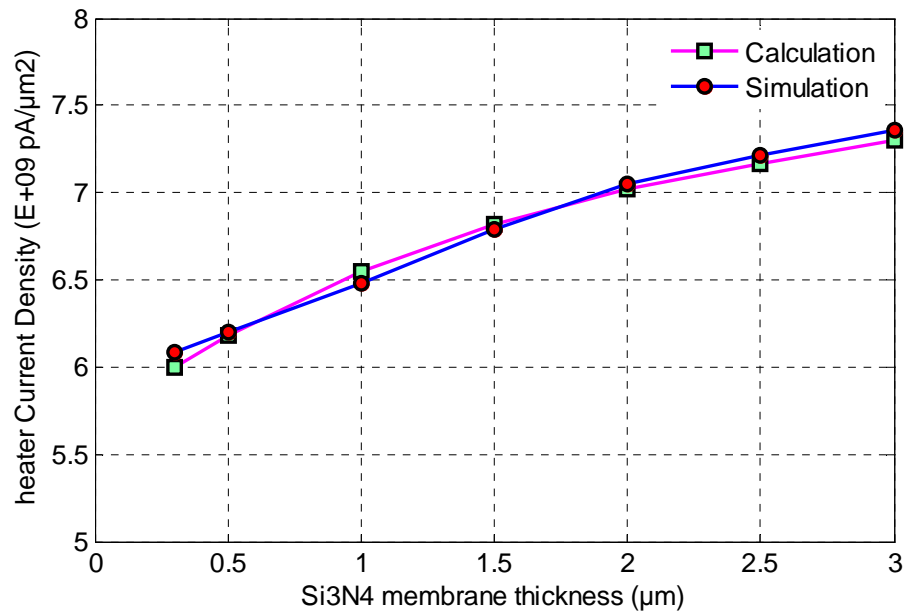


**Figure 4.10:** Simulated and calculated values of current densities vs. Si<sub>3</sub>N<sub>4</sub> membrane thickness at the operating temperature of 700°C

#### 4.2.5 Time constant

The time constant has been described in 3.4.4. It is essentially the time requested for the system to reach the designated temperature. However, to maintain the MHP at operation temperature of 700°C as well as the thickness of the Si<sub>3</sub>N<sub>4</sub> membrane, the applied voltage had to be increased as shown in 4.2.2. The increase in the thickness of the Si<sub>3</sub>N<sub>4</sub> membrane from 0.3 μm to 3 μm implies an increase in the thermal time constant of the MHP which is calculated to vary from 0.5 ms to 3.1 ms according to equation (3.20).

Fig. 3.11 shows the calculated thermal time constant of the MHP as a function of the Si<sub>3</sub>N<sub>4</sub> membrane thickness. It is observed that the time constant increases linearly in this range as a function of the membrane thickness. From the graph, it can be concluded that to design MHP with small time constant of 0.5 ms the thickness of the Si<sub>3</sub>N<sub>4</sub> membrane should be less than 0.5 μm.

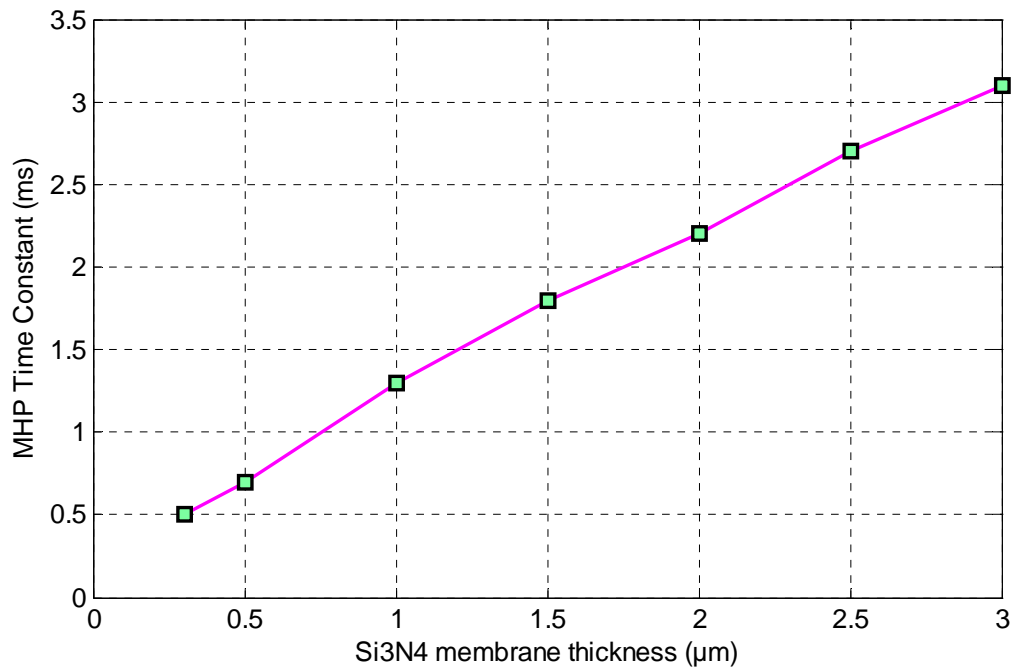
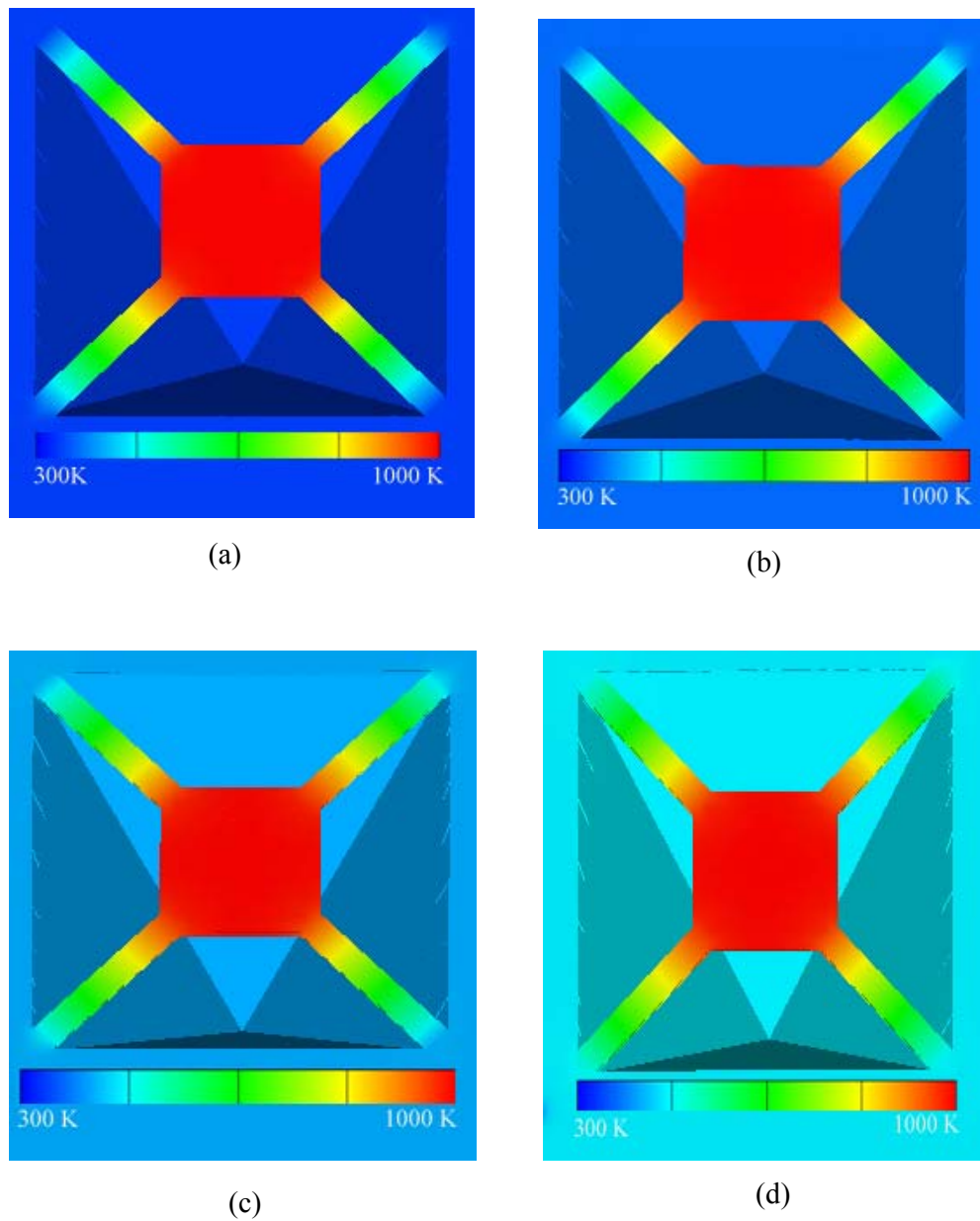


**Figure 4.11:** Theoretically calculated thermal time constant of the MHP vs. thickness of the Si<sub>3</sub>N<sub>4</sub> membrane at an operating temperature of 700°C

#### 4.2.6 Heat losses to Si substrate layer

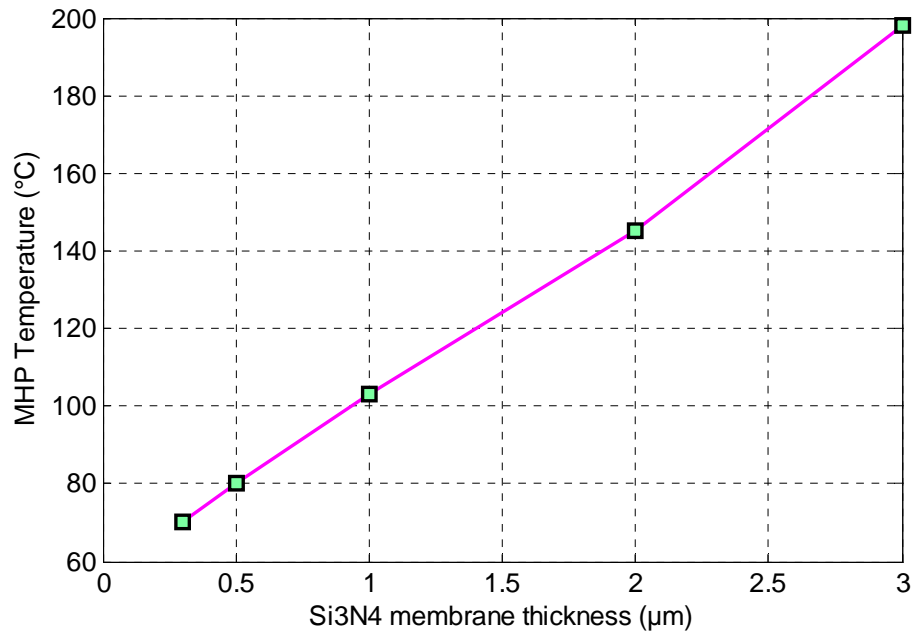
It is expected theoretically that when the thickness of the Si<sub>3</sub>N<sub>4</sub> membrane layer is increased from 0.3 μm to 3 μm, the heat losses to the Si substrate layer via conduction through the microbridges should correspondingly increase. This is because the cross-sectional area of the microbridges increases with increasing thickness of the Si<sub>3</sub>N<sub>4</sub> membrane layer.

Fig. 4.12 shows the heat transfer to the silicon substrate for selected Si<sub>3</sub>N<sub>4</sub> membrane thicknesses of (a) 0.3 μm, (b) 1 μm, (c) 2 μm and (d) 3 μm at the nominal MHP operating temperature of 700°C. A significant increase in heat dissipation to the Si substrate layer is clearly demonstrated as the thickness of the membrane is increased.



**Figure 4.12:** Heat dissipation to the Si substrate for  $\text{Si}_3\text{N}_4$  membrane thickness of (a)  $0.3 \mu\text{m}$ , (b)  $1 \mu\text{m}$ , (c)  $2 \mu\text{m}$  and (d)  $3 \mu\text{m}$  at the MHP operating temperature of  $700^\circ\text{C}$

Fig. 4.13 shows a plot of the maximum temperature on the Si substrate as a function of the  $\text{Si}_3\text{N}_4$  membrane thickness which indicates linear relationship. From the graph, it can be concluded that to design MHP with the minimum heat transfer to the Si substrate the thickness of the  $\text{Si}_3\text{N}_4$  membrane should be less than  $0.5 \mu\text{m}$ .



**Figure 4.13:** Maximum temperature on the Si substrate as a function of the Si<sub>3</sub>N<sub>4</sub> membrane thickness

### 4.3 Effect of Pt heater thickness on MHP characteristics

The effect of variation of the Pt heater thickness from 0.3 µm to 3 µm on the operating temperature, mechanical deflection, power dissipation, current density, mises stress and applied voltage of the MHP is investigated in this section. All the simulations in this section are carried out at a fixed applied voltage of 0.7V.

#### 4.3.1 Temperature and displacement

When a constant voltage of 0.7 V is applied to the Pt heater, the temperature is observed to increase from 600°C to 2300°C as function of the thickness which is varied from 0.3 µm to 3 µm as shown in fig.4.14, while the mechanical displacement of the MHP increases from 4.5 µm to 14 µm as shown in fig.4.15. Fig.4.16 shows a constant current density of about  $6.0 \times 10^9$  pA/µm<sup>2</sup> when the thickness of the microheater is varied from 0.3 µm to 3 µm. Fig.4.17 shows that the mises stress increases linearly from 890 MPa to 2300 MPa as microheater thickness is increased

from 0.3  $\mu\text{m}$  to 2  $\mu\text{m}$  and thereafter remains practically constant between 2300 MPa and 2400 MPa.

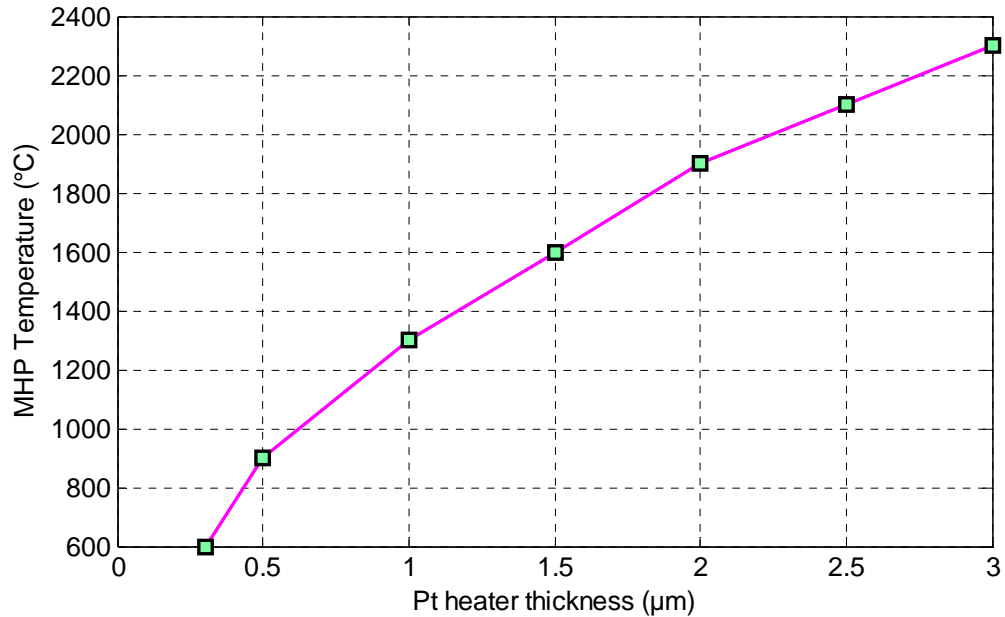


**Figure 4.14:** MHP operating temperature vs. thickness of the heater at an applied voltage of 0.7 V

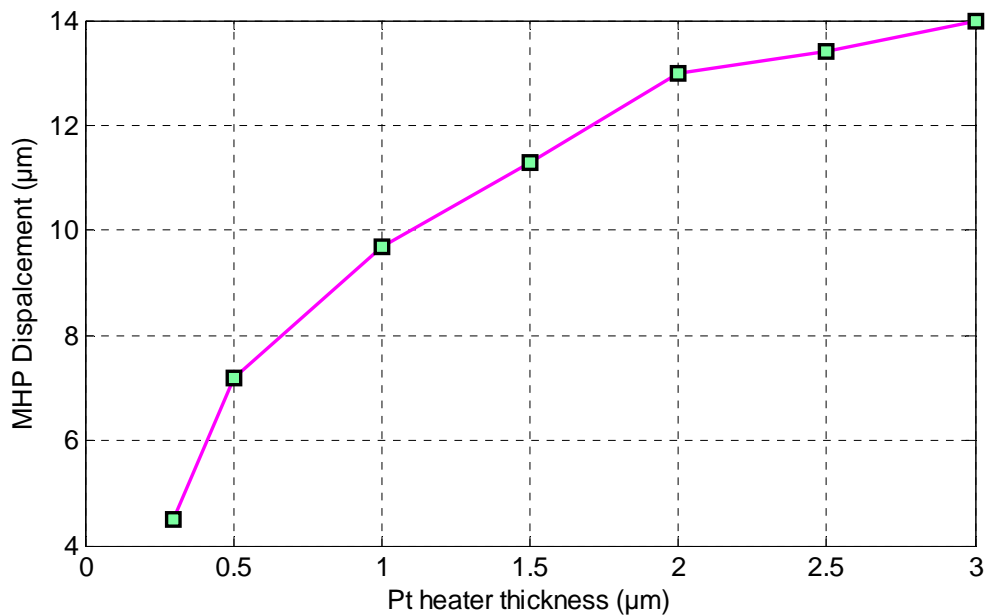


**Figure 4.15:** Maximum displacement on MHP vs. thickness of the heater at an applied voltage of 0.7 V

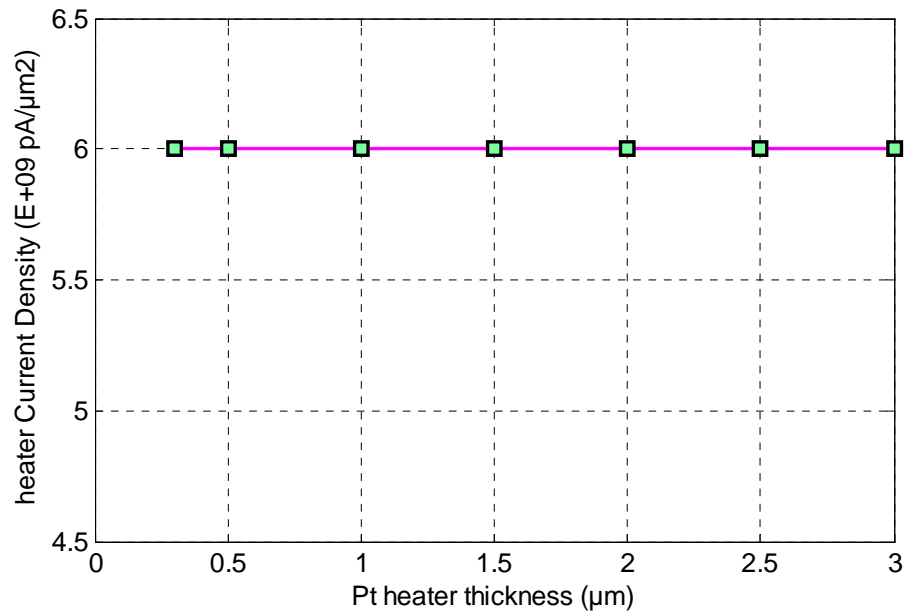


**Figure 4.16:** Current Density on the MHP vs. thickness of the heater at an applied voltage of 0.7 V

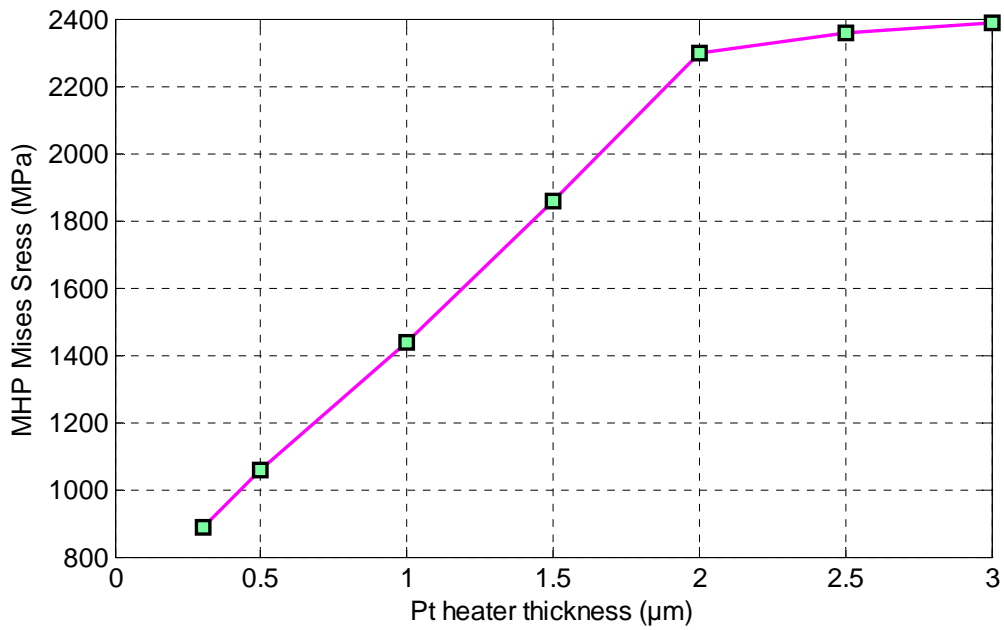


**Figure 4.17:** Misses Stress on the MHP vs. thickness of the heater at 0.7 V

### 4.3.2 Applied voltage, displacement, current density and mises stress

In order to maintain the operating temperature at the nominal value of  $700^{\circ}\text{C}$ , the applied voltage had to be decreases from 0.77 V to 0.41 V while the thickness of the heater is increased from  $0.3\ \mu\text{m}$  to  $3\ \mu\text{m}$ . Fig. 4.18 shows the decrease in voltage as a function of the heater thickness. This observed relation is expected since increase in the thickness of the heating element implies increase in the cross-sectional area of the heater which leads to a lower resistance value. The input power, however, increases from 7.1 mW to 20 mW. Fig. 4.19 shows decrease in the displacement of the MHP from  $5.7\ \mu\text{m}$  to  $4.8\ \mu\text{m}$  as the heater thickness is increased. This result indicates that the heater thickness can be used to stabilize the MHP by reducing its mechanical displacement. Fig. 4.20 shows decrease in current density from  $6.87 \times 10^9\ \text{pA}/\mu\text{m}^2$  to  $3.48 \times 10^9\ \text{pA}/\mu\text{m}^2$  as a function of the heater thickness. The implication here is that the heater dimensions can be used to tune the current density to a required value. Fig. 4.21 shows the mises stress of the MHP as a function of heater thickness. It is observed that the mises stress is independent of the heater thickness at a value of about 995 MPa.

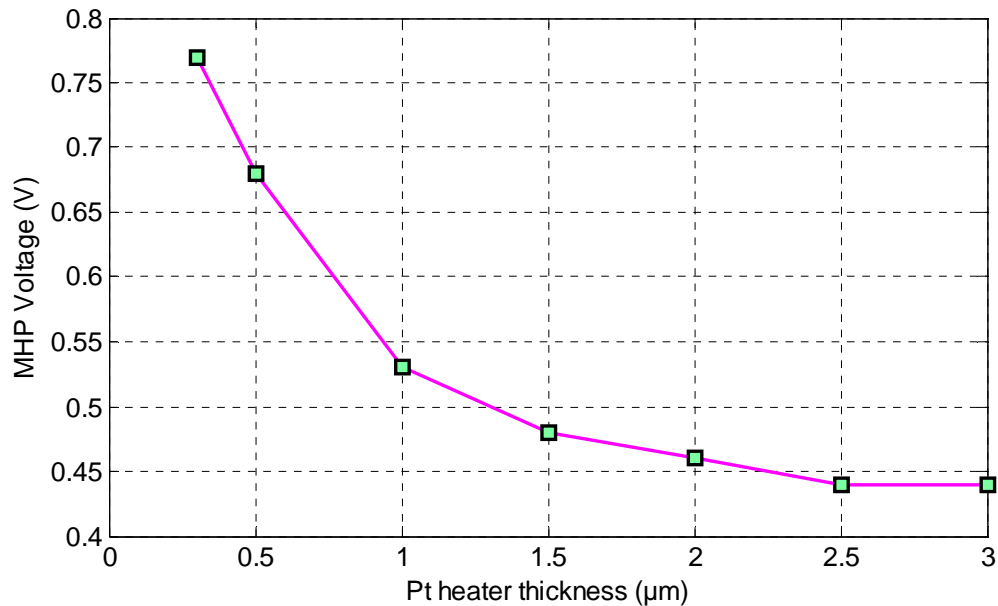


**Figure 4.18:** Voltage of the MHP vs. thickness of the heater at a constant membrane temperature of  $700^{\circ}\text{C}$

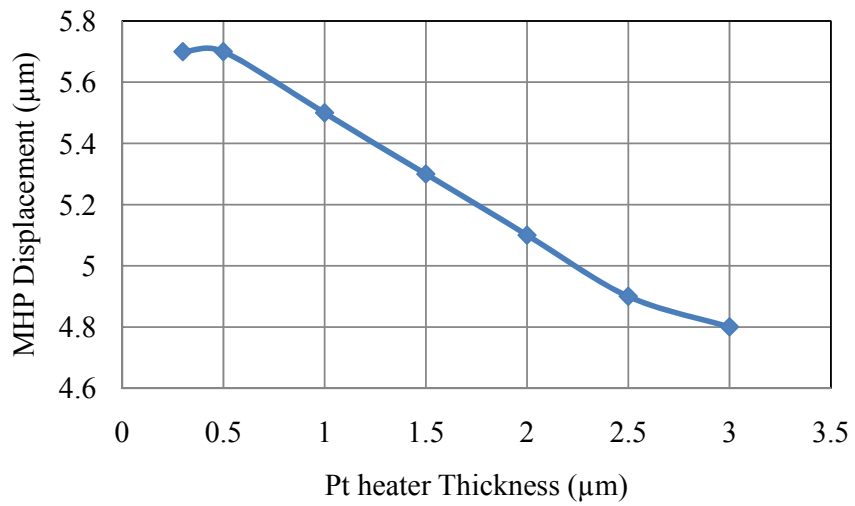


**Figure 4.19:** Displacement of the MHP vs. thickness of the heater at a constant membrane temperature of 700°C

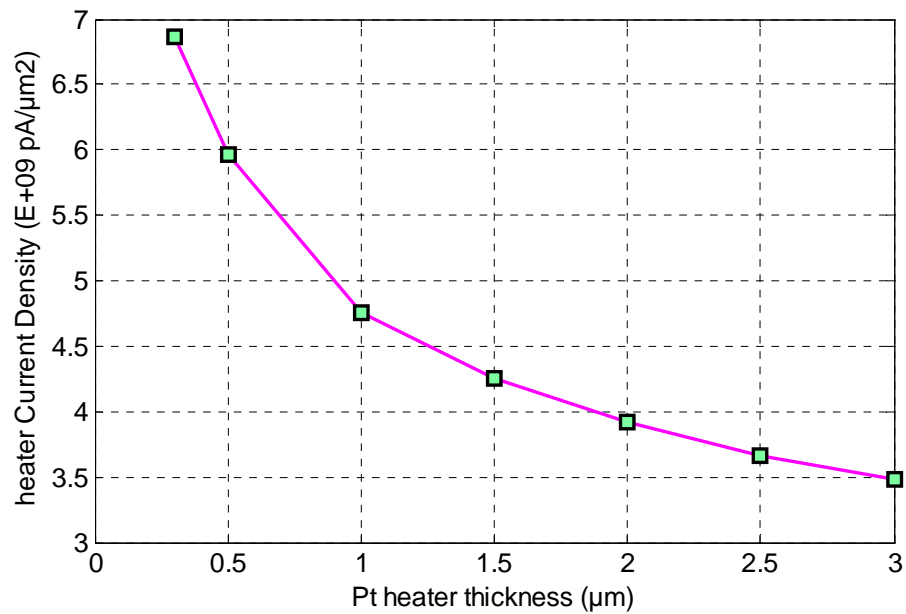


**Figure 4.20:** Current density of the MHP vs. thickness of the heater at an operating temperature of 700°C

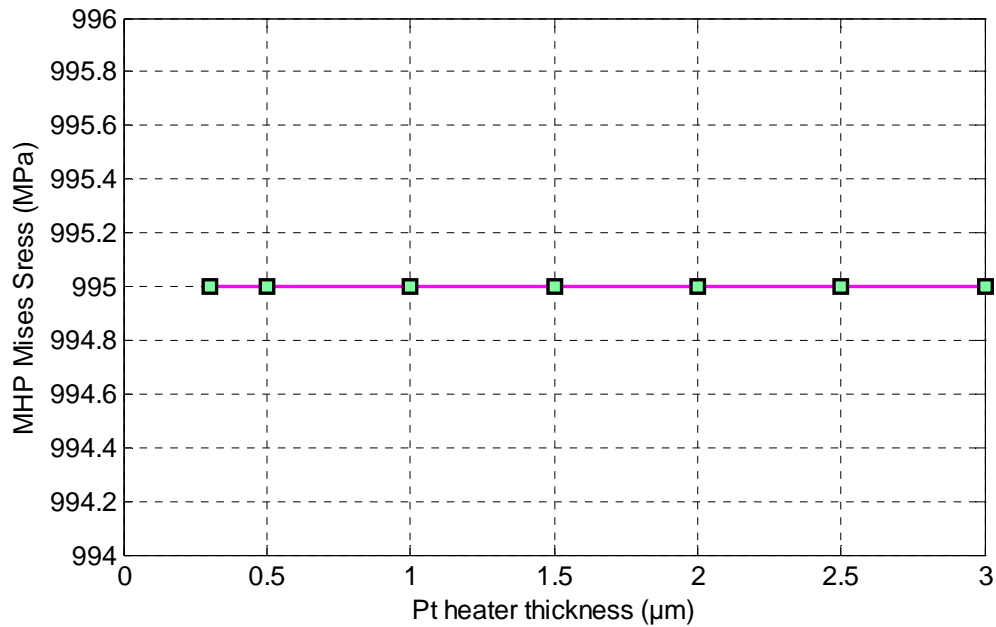


**Figure 4.21:** Mises Stress of the MHP vs. thickness of the heater at an operating temperature of 700°C

#### 4.4 Effect of the thickness of the SiC heat distributor layer on the MHP characteristics

The effect of variation of the thickness of the SiC heat distributor layer from 0.3  $\mu\text{m}$  to 5  $\mu\text{m}$  on the operating temperature, mechanical deflection, power dissipation, current density, mises stress and most importantly on the heat distribution on the MHP surface is investigated in this section. All the simulations in this section are carried out at an applied voltage of 0.7 V and an operating temperature on the MHP of 700°C.

##### 4.4.1 Heat distribution on the MHP surface

When using the MHP as a platform for gas detection, it is imperative to ensure that the temperature is uniformly distributed on the area where the sensing material is going to be deposited. Fig. 4.22 shows the heat distribution on the MHP surface

without heat distributor and with heat distributing layer (SiC plate). The thickness of SiC was varied from 0.3  $\mu\text{m}$  to 5  $\mu\text{m}$ . The temperature values are indicated at intervals from the centre of the MHP to the corners at a distance of 50  $\mu\text{m}$  on each side from the centre (indicated as  $\pm 50 \mu\text{m}$ ). It is observed that without the SiC layer the temperature difference between the centre of the MHP and a point on the membrane at 50  $\mu\text{m}$  from the centre is about  $0.34^\circ\text{C}/\mu\text{m}$ , while with SiC layer the temperature difference decreases from  $0.09^\circ\text{C}/\mu\text{m}$  for a SiC layer thickness of 0.3  $\mu\text{m}$  to  $0.005^\circ\text{C}/\mu\text{m}$  for a layer thickness of 2 to 5  $\mu\text{m}$ . This is a considerable improvement in the uniformity of the heat distribution on the MHP when SiC layer is added. Fig. 4.23 shows the temperature gradient on the MHP (difference in temperature from the centre of the MHP to a point 50  $\mu\text{m}$  from the centre as a function of the thickness of the SiC heat distributor layer). It is observed that the temperature gradient reaches to the minimum value at the heater distributor thickness of about 2  $\mu\text{m}$ . However, before determining that this is the optimum SiC thickness for uniform heat distribution on the MHP thickness, there is need to analyze the effect of the change in the SiC heat distributor layer on the other parameters of the MHP such as power consumption and mechanical displacement.

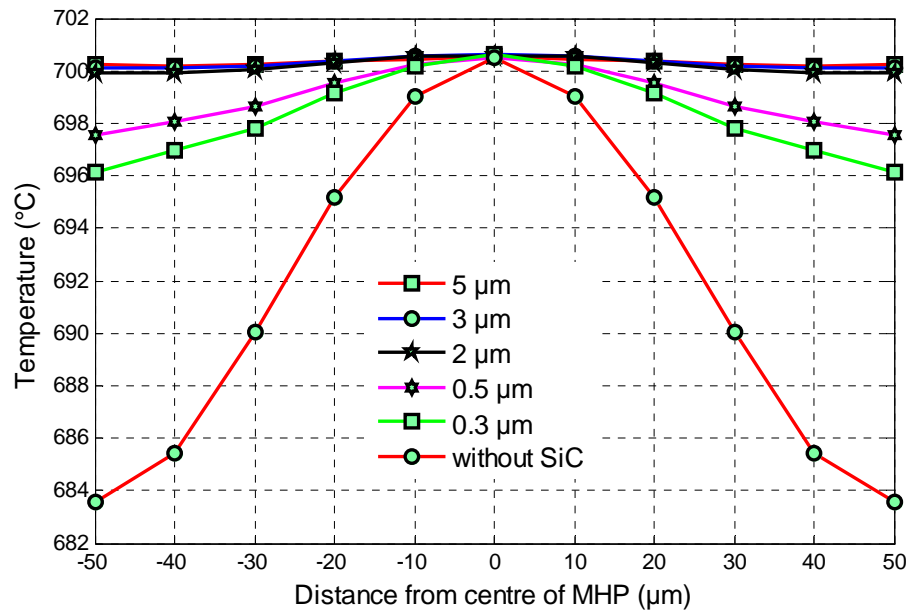


**Figure 4.22:** Heat distribution on the MHP surface with SiC layer of various thicknesses at an operating temperature of 700°C

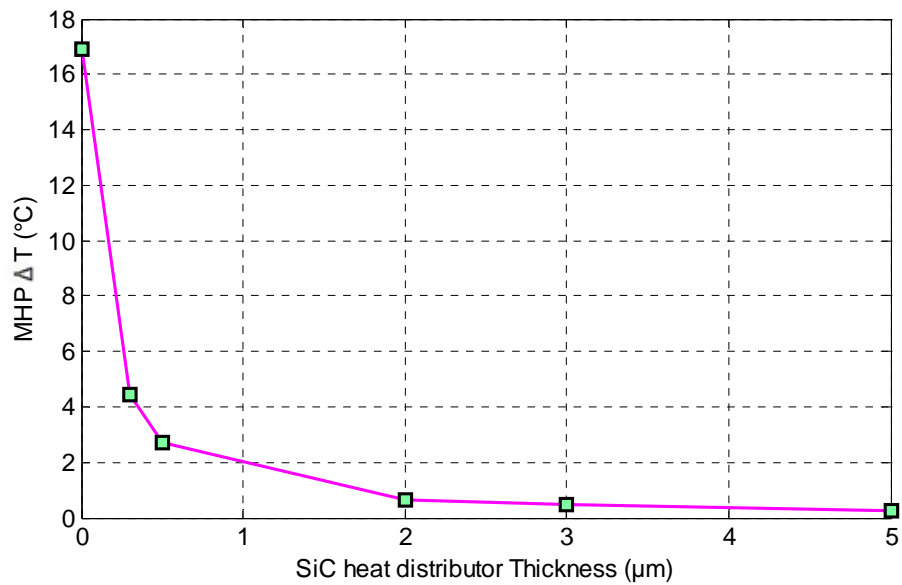


**Figure 4.23:** Temperature gradient on the MHP surface vs. thickness of SiC heat distributor layer at an operating temperature of 700°C

#### 4.4.2 Temperature and displacement

When a constant voltage of 0.7 V is applied to the terminals of the platinum heater, increasing the thickness of the SiC heat distributor layer from 0.3  $\mu\text{m}$  to 3  $\mu\text{m}$  results in a decrease of the temperature of the MHP from 700°C to 550°C as shown in fig.4.24 while its the mechanical displacement is reduced from 5.8  $\mu\text{m}$  to 2.8  $\mu\text{m}$  as shown in fig.4.25. The reduction in the mechanical deflection of the MHP is quite significant indicating that it is preferable to use a thickness of 2  $\mu\text{m}$  and above to improve both the uniformity of heat distribution while at the same time reducing the mechanical deflection. It is observed from fig. 4.24 that the decrease in the temperature on the MHP surface is not that steep and therefore the increase in the power consumption will not be that significant.

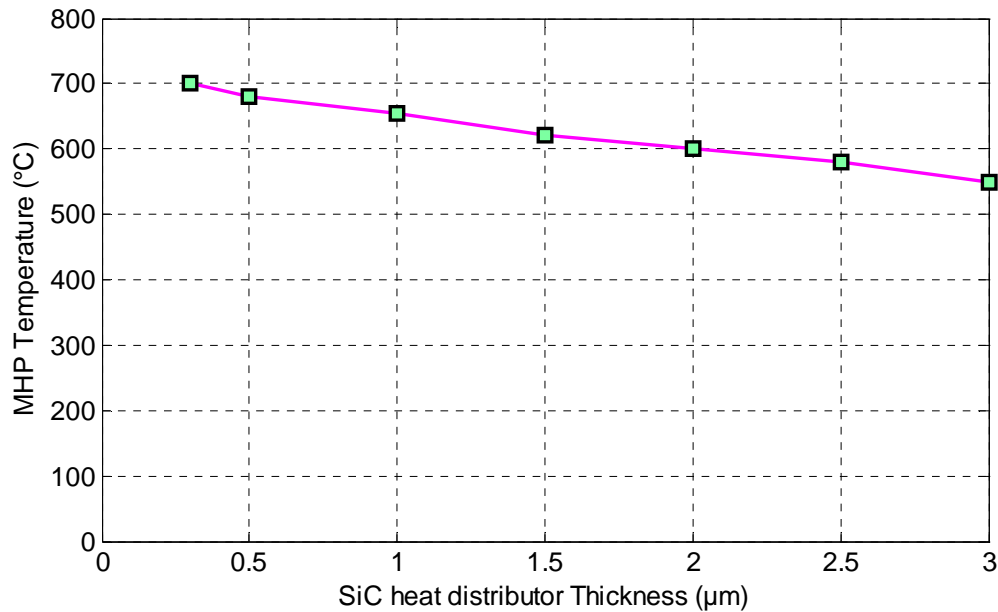


**Figure 4.24:** Maximum temperature on the MHP surface vs. thickness of the SiC heat distributor layer at the applied voltage of 0.7 V

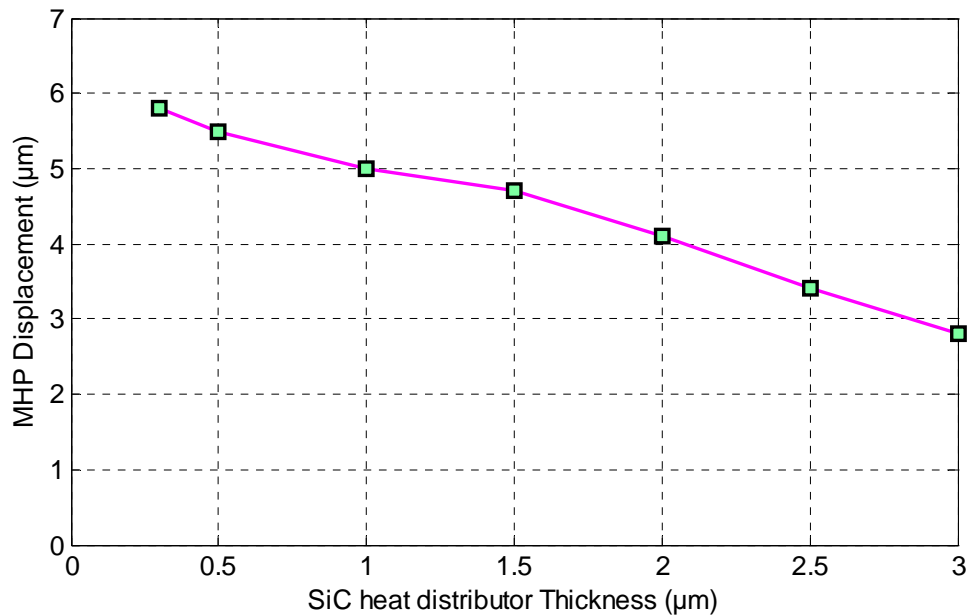


**Figure 4.25:** Maximum displacement of the MHP vs. thickness of the SiC heat distributor at an applied voltage 0.7 V

#### 4.4.3 Power dissipation and displacement

In order to maintain the operating temperature of the MHP at the nominal value of 700°C, the applied voltage had to be increased from 0.75 V to 0.78 V while the thickness is increased from 0.3 μm to 3 μm. This required increase in applied voltage to maintain a constant operating temperature of 700°C implies an increase in the power input to the MHP from 11.25 mW to about 12.17 mW as the thickness of the SiC heat distributor layer is increased from 0.3 μm to 3 μm as shown in fig. 4.26. It is observed that the power dissipation of the MHP becomes constant at and above a SiC thickness of 1.5 μm. It is also observed as shown in fig. 4.27 that the mechanical displacement of the MHP decreases from 5.6 μm to 2.8 μm as the thickness of the SiC heat distributor layer is increased from 0.3 μm to 3 μm. This is an added advantage as the reduction in the mechanical deflection is realized for an increase in the thickness of the SiC heat distributor layer, improving the stability of the MHP, while at the same time improving the uniformity of heat distribution.

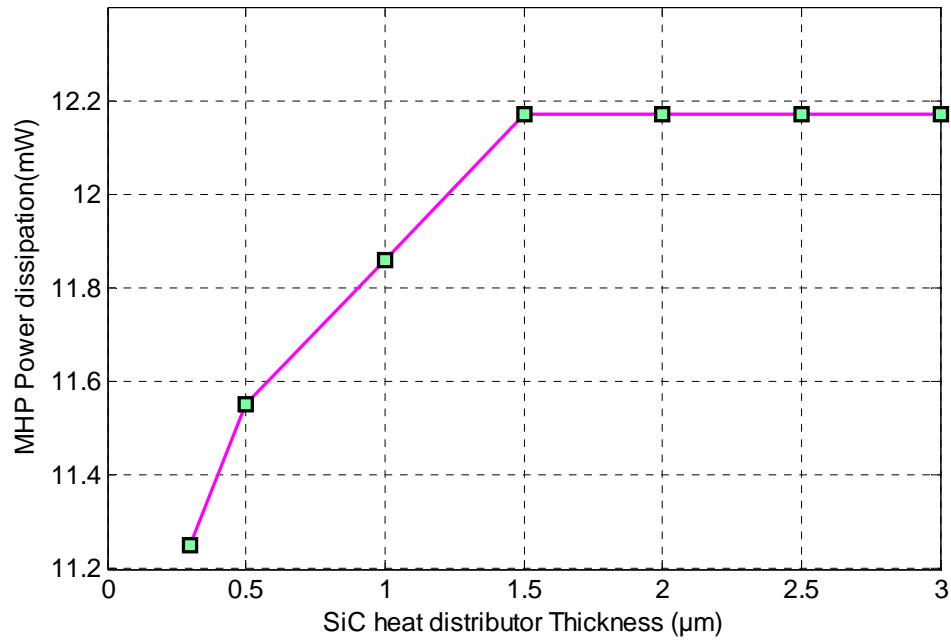


**Figure 4.26:** Power dissipation of the MHP vs. thickness of the SiC heat distributor layer at an operating temperature of 700°C

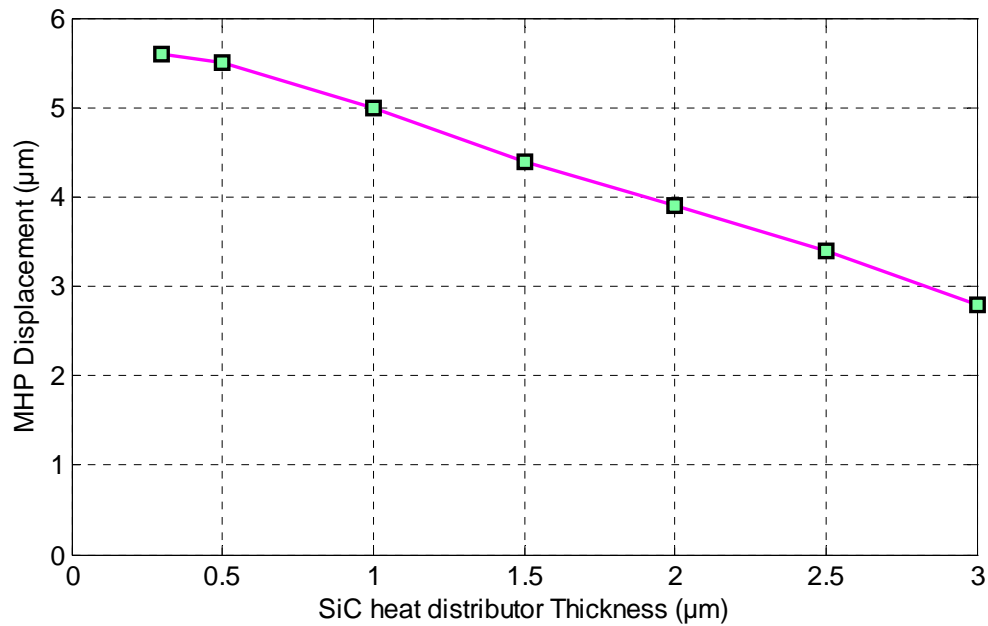


**Figure 4.27:** Maximum displacement of the MHP vs. thickness of the SiC heat distributor at an operating temperature of 700°C

#### 4.4.4 Comparison between simulated and calculated values of power dissipation

Fig. 4.28 shows simulated and calculated results of the power dissipated by the MHP when the SiC heat distributor thickness was varied from 0.3  $\mu\text{m}$  to 3  $\mu\text{m}$ . The graph indicates a good agreement between simulations and calculation results for SiC thickness above 1.5  $\mu\text{m}$ .

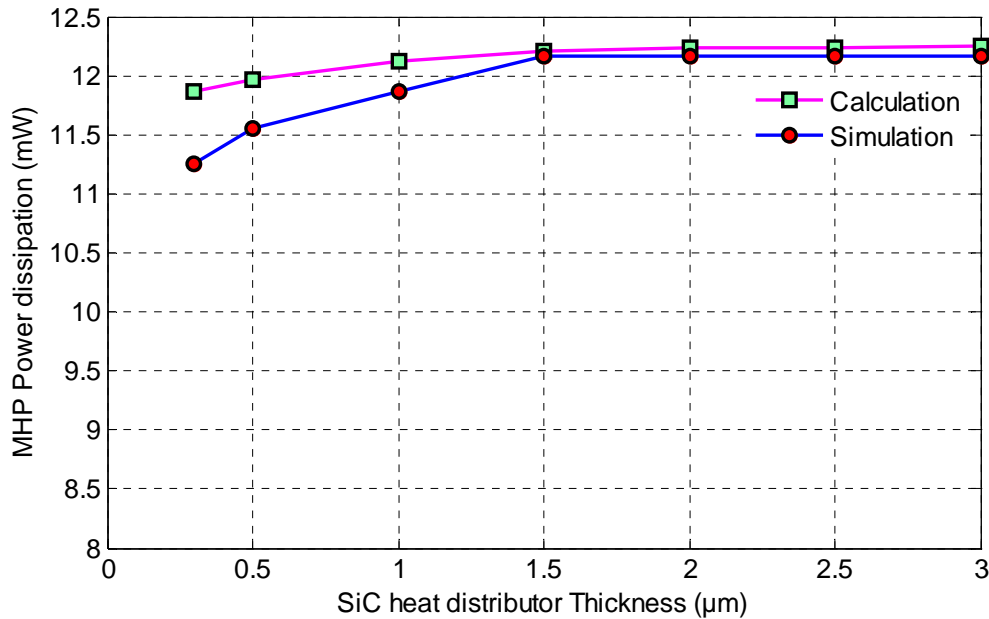


**Figure 4.28:** Simulated and calculated MHP Power dissipation vs. thickness of the SiC heat distributor layer at an operating temperature of 700°C

#### 4.5 Effect of SnO<sub>2</sub> sensing film thickness on the MHP characteristics

The effect of variation of the thickness of the SnO<sub>2</sub> sensing film layer from 0.5  $\mu\text{m}$  to 20  $\mu\text{m}$  on the operating temperature, mechanical deflection, power consumption, current density, mises stress on the MHP surface is investigated in this section. All the simulations in this section are carried out for a fixed applied voltage of 0.7 V and an operating temperature of the MHP of 700°C.

### 4.5.1 Displacement and mises stress

Fig. 4.29 shows that when the operating temperature of the MHP is maintained at the nominal value of 700°C, increasing the thickness of the Sensing film layer from 0.5  $\mu\text{m}$  to 20  $\mu\text{m}$  decrease the displacement of the MHP from 6.2  $\mu\text{m}$  to 1.3  $\mu\text{m}$ , while the mises stress increased from about 96 MPa to reach a maximum value of 277 MPa at a thickness of 3.5  $\mu\text{m}$  and then decreases to a minimum value of 104 MPa as shown in fig. 4.30.

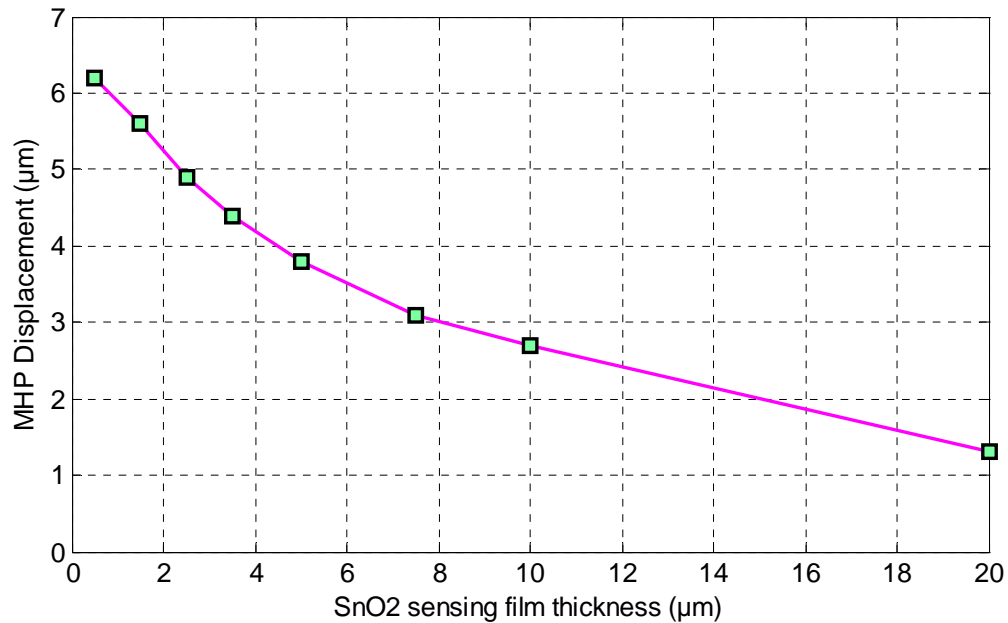


**Figure 4.29:** Displacement on the MHP vs. thickness of the SnO<sub>2</sub> sensing film at an operating temperature of 700°C

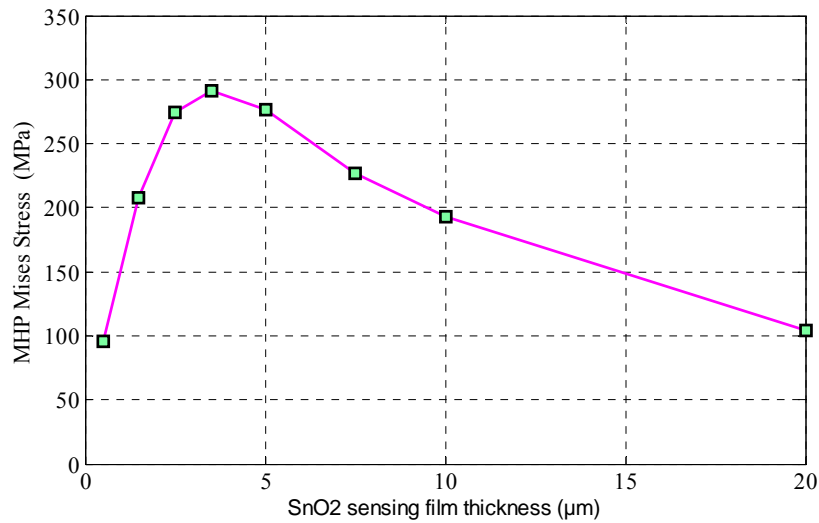


**Figure 4.30:** Mises stress vs. thickness of the SnO<sub>2</sub> at the operating temperature of 700°C

#### 4.5.2 Applied voltage and temperature

When the voltage applied to the Pt heater was varied from 0.5 V to 0.78 V, while maintaining the SnO<sub>2</sub> Sensing film layer at a thickness 0.5 μm, the temperature of the MHP increased approximately linearly from 117°C to 740°C as shown in fig. 4.31

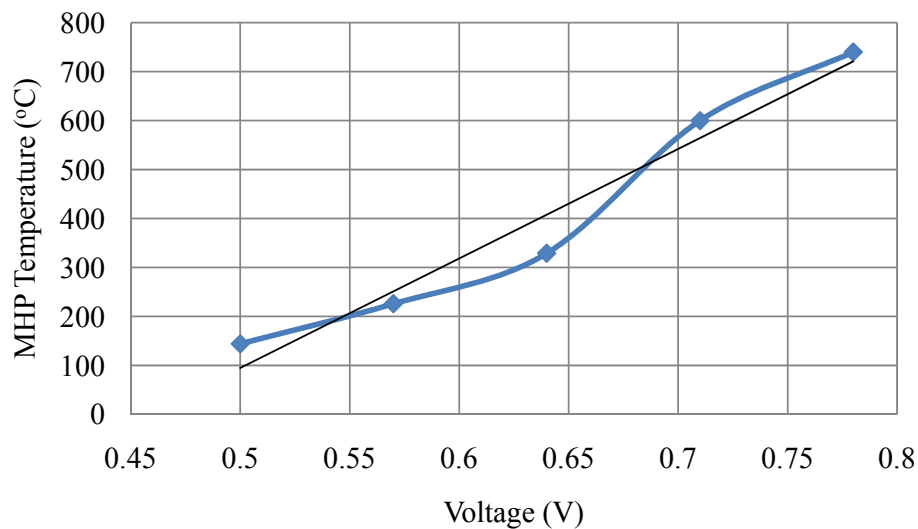


**Figure 4.31:** Temperature on MHP surface vs. applied voltage at a constant SnO<sub>2</sub> sensing film thickness of 0.5 μm

### 4.5.3 Applied voltage, displacement and misses stress

It is also observed that as the voltage on the MHP is increased from 0.5 V to 0.78 V, the displacement increases from 0.5  $\mu\text{m}$  to 3.8  $\mu\text{m}$  as shown in fig. 4.32 while the mises stress increases from 54 MPa to 277 MPa as shown in fig. 4.33.

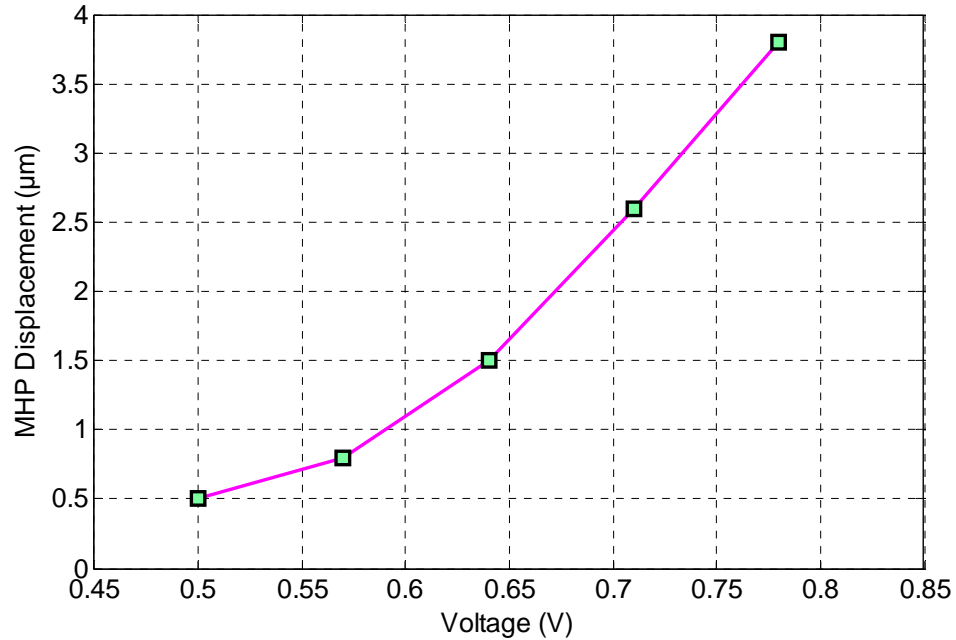


**Figure 4.32:** Mechanical displacement of the MHP vs. applied voltage at a constant  $\text{SnO}_2$  sensing film thickness of 0.5  $\mu\text{m}$

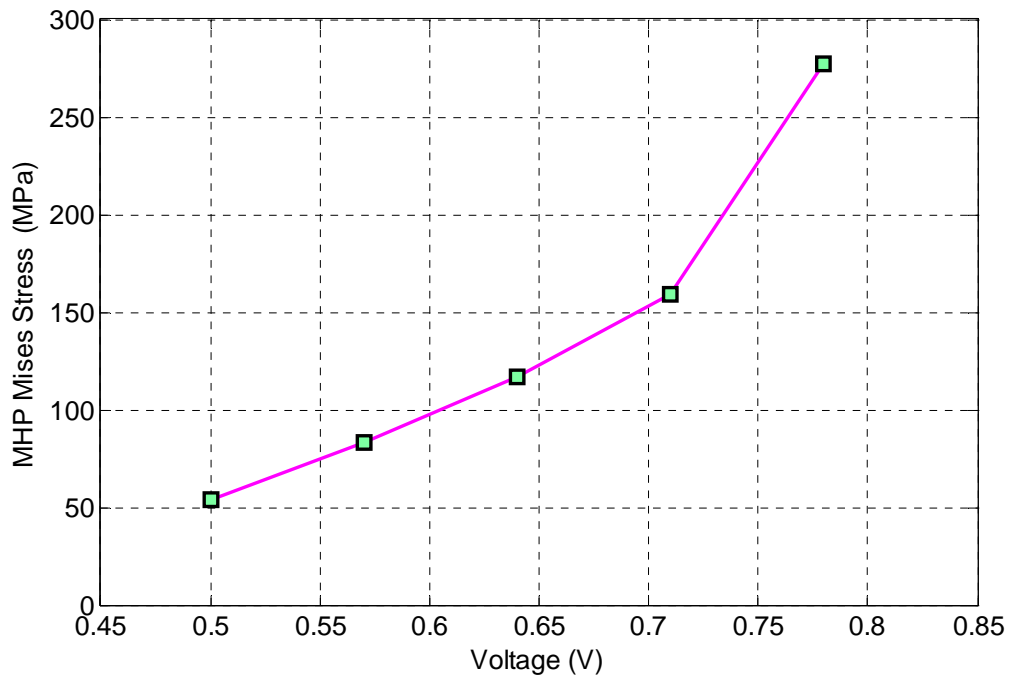


**Figure 4.33:** Mises stress on the MHP vs. applied voltage at a constant SnO<sub>2</sub> sensing film thickness of 0.5 μm

#### 4.5.4 Comparison between simulated and calculated values of power dissipation

Fig. 4.34 shows a comparison of the power dissipation on the MHP obtained from simulation and derived by calculation as a function of the thickness of the SnO<sub>2</sub> sensing film at an operating temperature of 700°C. It is observed that the power dissipation remains practically constant at about 11.8 mW as the SnO<sub>2</sub> sensing film thickness is varied from 0.3 to 3 μm with a close agreement between simulated and calculated values.

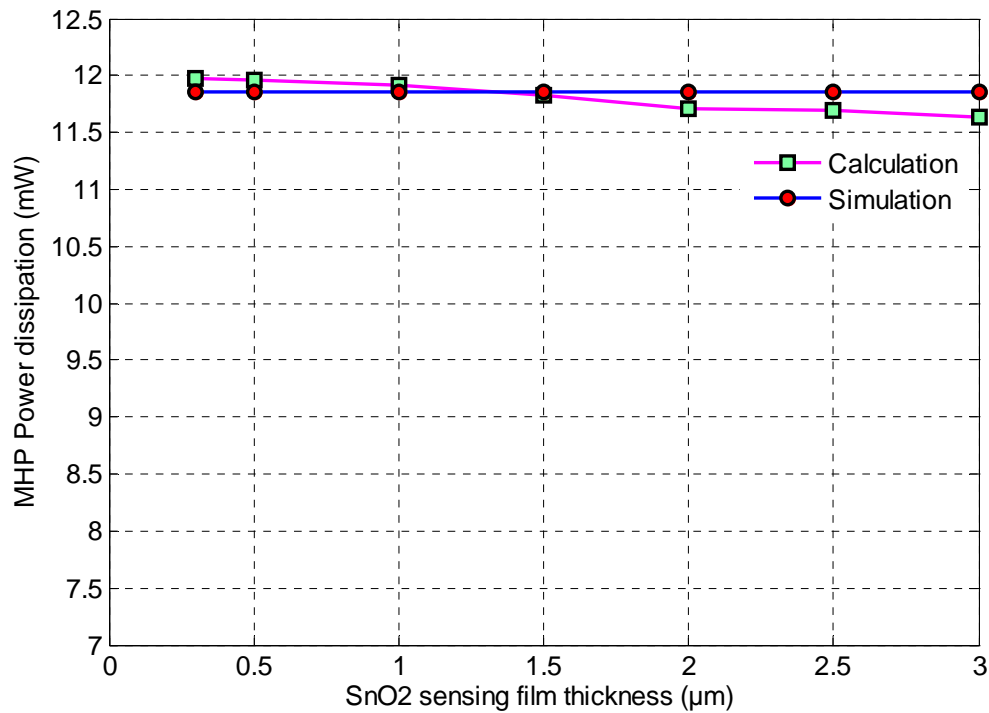


**Figure 4.34:** Simulated and calculated power dissipation on the MHP vs. thickness of the SnO<sub>2</sub> sensing film at an operating temperature of 700°C

#### 4.6 Final design and simulation of a MHP with selected parameters for optimum operation at the elevated temperature of 700°C

After observations of all the relevant parameters that affect the characteristics of the MHP with a high operating temperature of 700°C, a device that is optimized in terms of minimum power consumption, uniform temperature distribution, minimum mechanical displacement and stress is proposed, designed and simulated in this section. The optimum thickness of the various layers for an optimum performance of the MHP at the elevated temperature of 700°C are selected and incorporated into this final design and simulation. These include the thickness of the Si<sub>3</sub>N<sub>4</sub> membrane, Pt heater, SiC temperature distributor layer, and SnO<sub>2</sub> sensing film. The values for the thicknesses of the various MHP layers selected for the final design are shown in table 4.1.

**Table 4.1:** The values for the thicknesses of the various MHP layers

Layers Materials	Thickness ( $\mu\text{m}$ )
Membrane ( $\text{Si}_3\text{N}_4$ )	0.3
Insulators ( $\text{SiO}_2$ )	0.5
Heater (Pt)	0.5
Heat Distributor (SiC)	2
Temperature sensor (Pt)	0.3
Electrode (Au)	0.3
Sensing film ( $\text{SnO}_2$ )	0.3

Fig. 4.35 shows (a) the applied voltage of 0.68 V with the interdigitated electrodes and temperature sensor clearly visible in the foreground and (b) temperature and profile, of the optimized MHP, while fig. 4.35 (c) and (d) show the mechanical displacement and current density, respectively, at the same applied voltage. The mises stress was determined to be 875 MPa. The maximum temperature of  $700^\circ\text{C}$  achieved with an applied voltage of 0.68 V corresponds to a power input of 9.25 mW. The maximum displacement at the operating temperature of  $700^\circ\text{C}$  is found to be very low with a value of  $1.2 \mu\text{m}$ . This low value is desirable for the stability of the MHP over time at elevated temperatures. The current density is found to be  $6.5 \times 10^9 \text{ pA}/\mu\text{m}^2$  and the calculated power dissipation is 10.45mW.

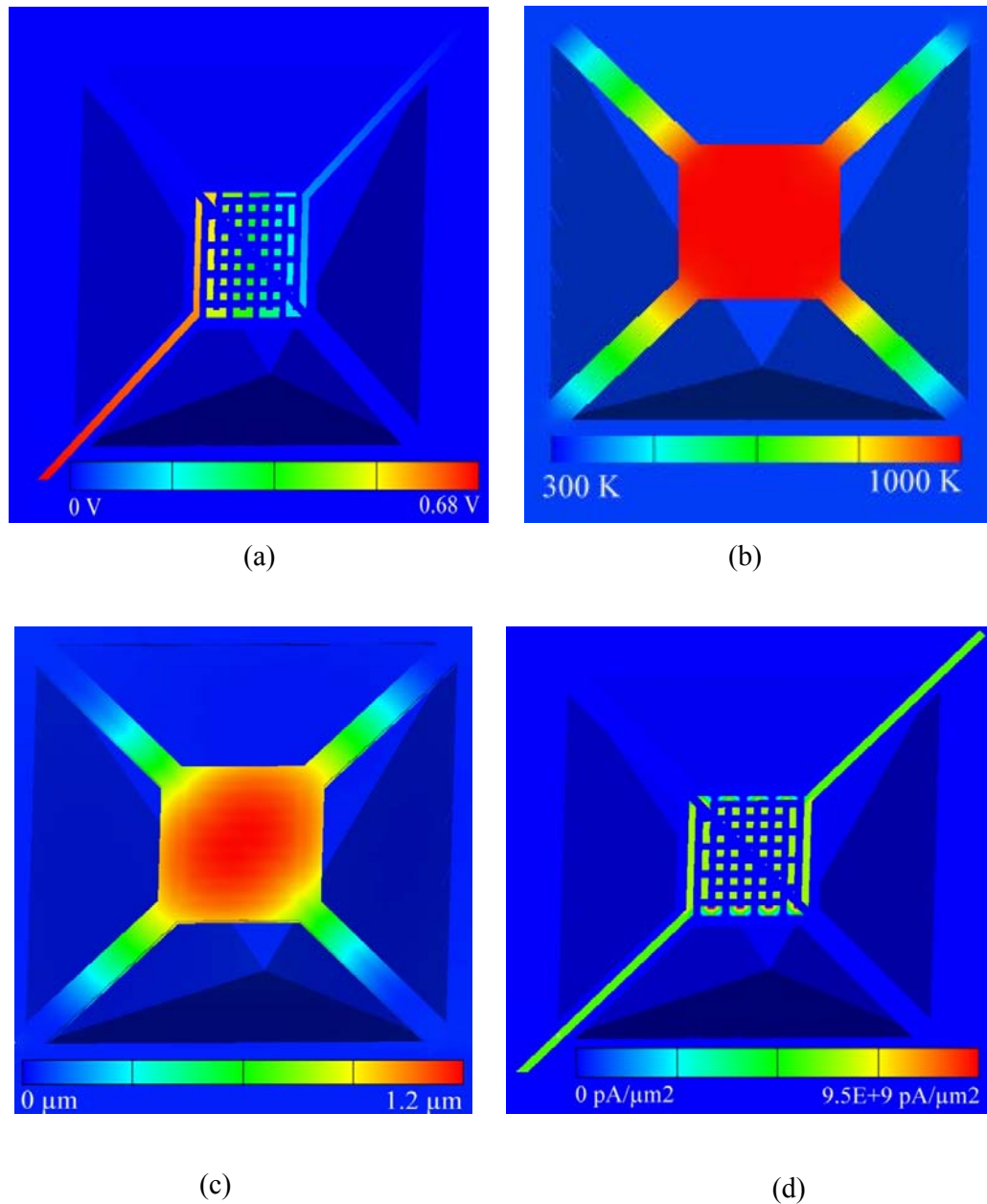


**Figure 4.35:** (a) applied voltage to the heater element, (b) temperature profile on the MHP, (c) mechanical displacement of the MHP and (d) current density in the Pt heating element

#### **4.7 Summary**

In this chapter, the effect of the thickness of the various layers (membrane, heat distributor and sensing film) of the MHP on its characteristics at high operating temperatures of up to 700°C has been presented. At the fixed operation temperature of 700°C, it is shown that as membrane thickness increases, power dissipation, current density, time constant and heat transfer to the silicon substrate increase, while mechanical displacement of the membrane does not change. When the SiC heat distributor thickness increases, a small increase in power dissipation is observed while the displacement decreases. The temperature gradient on the MHP is found to decrease with increasing thickness of the SiC and is a minimum (0.005°C/μm) for thickness of 2 μm and above. An optimized MHP device at 700°C was found to have low power dissipation of about 9.25 mW, maximum mechanical displacement of 1.2 μm, a temperature gradient of 0.005°C/μm and a short time constant of 0.17 ms.

## CHAPTER 5

### CONCLUSION AND RECOMMENDATION

#### 5.1 Conclusion

MEMS MHP consisting of a suspended  $\text{Si}_3\text{N}_4$  membrane that can withstand high temperatures for application in trace gas detection has been designed and simulated using CoventorWare software. All materials selected for the design of the MHP are capable of operating at high temperatures (500°C to 800°C). The MHP was designed on single side p-type [100] silicon wafer. The basic technological steps for the design of the devices start with the selection of Si substrate with a thickness of 300 $\mu\text{m}$  and an area of 400  $\mu\text{m} \times 400 \mu\text{m}$ . In the simulation and modeling, the effect of thickness of the various layers such as the membrane layer, Pt heating element, heat distributor and sensing film on temperature, mechanical deflection, power dissipation, mises stress, current density and time response of the MHP are evaluated.

At the fixed operation temperature of 700°C, it is shown that as membrane thickness increases, power dissipation, current density, time constant and heat transfer to the silicon substrate increase, while mechanical displacement of the membrane does not change. Changing the thickness of the platinum heater at the same temperature (700°C) resulted in the decrease of the voltage and current density while the mises stress does not change. When the SiC heat distributor thickness increases, a small increase in power dissipation is observed while the displacement decreases. The temperature gradient on the MHP is found to decrease with increasing thickness of the SiC and is a minimum (0.005°C/ $\mu\text{m}$ ) for thickness of 2  $\mu\text{m}$  and above. An optimized MHP device at 700°C was found to have low power dissipation of about 9.25 mW, maximum mechanical displacement of 1.2  $\mu\text{m}$ , a temperature gradient of 0.005°C/ $\mu\text{m}$  and a short time constant of 0.17 ms.

In this research the heat distributor on the MHP was improved by an order of magnitude compare to pervious work, the mechanical displacement and power dissipation has been drastically reduced as compare with previous studies.

## **5.2 Recommendation**

The following are recommended possible future extension of the work:

- i. Design, simulation and fabrication of an integrated MHP based gas sensor with sensor support circuits on a single chip (monolithic design).
- ii. Design of the electronic circuit for the heater power control and for constant current to drive the temperature sensor.
- iii. Development of an array of gas sensor element with different sensing film and controlling heater power and temperature sensor.
- iv. Design of analog / digital MHP Microsystems.

## LIST OF PUBLICATION

- [1] Abdelaziz Yousif Ahmed, Member, IEEE, John Ojur Dennis, Mohamad Naufal Mohamad Saad, "Design and Simulation of a High Temperature MEMS Micro-hotplate for Application in Trace Gas Detection", 2008, *ICSE, IEEE International Conference on Semiconductor Electronics, PP 153-157, Malaysia (Johor Bahru) 25-27 Nov, 2008.*
- [2] Abdelaziz Yousif Ahmed, Member, IEEE, John Ojur Dennis, Mohamad Naufal Mohamad Saad, "Simulation Studies on the Effect of High Temperature Operation on the Mechanical Properties of SnO<sub>2</sub> Deposited on a Micro-hotplate", RSCSST2008, Regional Conference on Solid State Science and Technology, Physics Department, Faculty of Science, UPM Malaysia Solid State Science & Technology Society, Tiara Beach Resort, Port Dickson, Negeri Sembilan, Malaysia, Dec 2008.
- [3] Abdelaziz Yousif Ahmed, Member, IEEE, John Ojur Dennis, Mohamad Naufal Mohamad Saad, "Modeling and Simulation of the Effect of Layer Thickness on Power Dissipation and Temperature Distribution of a Microhotplate" International Conference on Electronic Material and Packaging (EMAP 2009) Penang Malaysia, (Under Review)
- [4] A. Y Ahmed, J. O Dennis, M. N Mohamad Saad, "Design, Simulation and Modeling of a Micromachined High Temperature Microhotplate for Application in Trace Gas Detection", *IEEE Sensors Journal* 2009, (Under Review)

## REFERENCES

- [1] G. Sberveglieri, W. Hoellmich, and G. Muller,” Silicon hotplates for metal oxide gas sensor elements”, *Microsystems Technologies* 1997: p. 183-190.
- [2] I. Simon, N. Barasn, M. Bauer, and U. Weimar,” Micromachined metal oxide gas sensors opportunities to improve sensor performance”, *Sensors and Actuators* 2001, **B37**: p. 1-26.
- [3] R. P. Manginell, J. H. Smith, and A. J. Ricco,” An overview of micromachined platforms for thermal sensing and gas detection”, in *Proceeding of the SPIE 3046* 1997.
- [4] Hille, P. and H. Strack., “A heated membrane for a capacitive gas sensor”, *Sensors and Actuators*, 1992. **A 32**: p. 321-325.
- [5] R. Aigner, M. Dietl, R. Katterloher and V. Klee, “Si planar pellistors designs for temperature modulated operation”, *Sensors and Actuators*, 1996, **B33**: p. 151-155.
- [6] P. P. Tsai, I.C.Chen, and C. J. Ho,” Ultralow power carbon monoxide micro sensor by micromachining techniques”, *Sensors and Actuators* 2001, **B76**: p. 380-387.
- [7] Briand, B.van der .Schoot, N. F. de Rooij, H. Sundgren, and I. Lundstrom,” A low power micromachined MOSFET gas sensor”, *Journal of Microelectromechanical Systems MEMS*, 2000: p. 303-308.
- [8] D. Briand, H. Sundgren, B. van der Schoot, I. Lundstrom, and N. F. de Rooij, “Thermally isolated MOSFET for gas sending application”, *IEEE Electron Device Letters* 2001(22): p. 11-13.

- [9] I. Simon and M. Arndt, "Thermal and gas sensing properties of a micromachined thermal conductivity sensor for the detection of hydrogen in automotive applications", *Sensors and Actuators*, 2002, **A 97-98** p. 104-108.
- [10] V. Demarne, and A. Grisel, "An integrated low-power thin-film CO gas sensor on silicon", *Sensors and Actuators*, 1988, **13**: p. 301-313.
- [11] U. Dibbern, "A substrate for thin-film gas sensors in microelectronic technology", *Sensors and Actuators*, 1990. **B33**: p. 63-70.
- [12] S. Wessel, M. Parameswaran, S.R. Morrison and R.F. Frindt, "A CMOS thermally isolated heater structure as a substrate for semiconductor gas sensor", *Journal of Microelectromechanical Systems MEMS*, 1992, **23**: p. 451-456.
- [13] J.S. Suehle, R.E. Cavicchi, M. Gaitan and S. Semancik, "Tin oxide gas sensor fabricated using CMOS micro-hotplates and in-situ processing", *IEEE Electron Device Letters* 1993, **14**(3): p. 118-120.
- [14] R.E. Cavicchi, J. S. Suehle, K.G. Kreider, M. Gaitan and P. Chaparala, "Optimized temperature-pulse sequences for the enhancement of chemically specific response patterns from micro-hotplates gas sensors", *Sensors and Actuators*, 1996, **B33**: p. 142-146.
- [15] J.W. Gardner, A. Pike, N.F. de Rooij, M. Koudelka-Hep, P. A. Clerc, A. Hierlemann and W. Göpel, "Integrated array sensor for detecting organic solvents", *Sensors and Actuators*, 1995. **B 26-27** p, 135-139.
- [16] A. Heilig, N. Barsan., U. Weimar, M. Schweizer-Berberich, J.W. Gardner and W. Göpel, "Gas identification by modulating temperatures of SnO<sub>2</sub> based thick film sensors", *Sensors and Actuators*, 1997. **B43**: p. 45-51.

- [17] I. Singh and S. Mohan, "3D Simulations and Electro-Thermal Analysis of Micro hotplate Designs Using CoventorWare for Gas Sensor Applications", in International Conference on Smart Materials Structures and Systems, 2005.
- [18] A. Heilig, N. Barsan, U. Weimar and W. Göpel, "Selectivity enhancement of SnO<sub>2</sub> gas sensors: simultaneous monitoring of resistances and temperatures", in Conference Proceeding of Eurosensors XII. September 13-16 1998. Southampton (UK).
- [19] D. Briand, A. Krauss, B. van der Schoot, U. Weimar, N. Barsan, W. Göpel and N.F. de Rooij, "Design and fabrication of high-temperature micro-hotplates for drop-coated gas sensors", *Sensors and Actuators*, 2000. **B 68**: p. 223-233.
- [20] M.C. Horrillo, I. Sayago, L. Ares, J. Rodrigo, J. Gutiérrez, A. Götz, I. Garcia, L. Fontseca, C. Cané and E. Lora-Tamayo, "Detection of low NO<sub>2</sub> concentrations with low power micromachined tin oxide gas sensors", *Sensors and Actuators*, 1999. **B 58**: p. 325-329.
- [21] M. Graf, S. Taschini, D. Barrettino, P. Kaeser, J. Cerdà, Hierlemann and H. Baltes, "Smart single-chip CMOS microhotplate array for metal-oxide-based gas sensors", in Proceedings of the IEEE Transducers Boston. 2003. MA, USA.
- [22] S. Semancik, R.E. Cavicchi., M.C. Wheeler, J.E. Tiffany, G.E. Poirier, R.M. Walton, J.S. Suehle, B. Panchapakesan and D.L. DeVoe, "Microhotplate platforms for chemical sensor research", *Sensors and Actuators* 2001. **B 77**: p. 579-591.
- [23] F. Solzbacher, C. Imawan, H. Steffes, E. Obermeier and H. Möller, "A modular system of SiC-based microhotplates for the application in metal oxide gas sensors", *Sensors and Actuators*, 2000, **B 64** p, 95-101.

- [24] D.S. Lee, C.H.S., J.W. Lim, J. S. Huh, D.D. Lee and Y. Tae Kim, Micro sensor array with porous tin oxide thin films and microhotplate dangled by wires in air”, *Sensors and Actuators* 2002. **83**: p. 250-255.
- [25] J. C. Belmonte, et al, “High-temperature low-power performing micromachined suspended micro-hotplate for gas sensing applications”, *Sensors and Actuators B* 114, 2006, 826–835.
- [26] S. Moller, J. Lin, E. Obermeier, “Material and design considerations for low-power microheater modules for gas-sensor applications”, *Sensors and Actuators*, 1995, **B 24-25**: p. 343-346.
- [27] Danick Briand, Stephan Heimgartner, Marc-Alexis Grétilat, Bart van der Schoot and Nicolaas F de Rooij, “Thermal optimization of micro-hotplates that have a silicon island”, *Journal of Micromechanics and Microengineering*, 2002. **12**: p. 971-978.
- [28] M. Graf, R. Jurischka, D. Barrettino, and A. Hierlemann, “3D nonlinear modeling of microhotplates in CMOS technology for use as metal-oxide-based gas sensors”, *Journal of Micromechanics and Microengineering*, 2005, **15**: p. 190-200.
- [29] M. Graf, D. Barrettino, H. P. Baltes, A. Hierlemann, “CMOS Hotplate Chemical Microsensors”, 2007: Springer.
- [30] Tuller L. Tuller, Richard Mlcak, “Advanced sensor Technology Based on Oxide Thins Film-MEMS Integration”, *Journal of Electronics*, June 2000. **4(2)**: p. 415-425.
- [31] [www.coventor.com/coventorware](http://www.coventor.com/coventorware).

- [32] Andrew Pike and Julian W. Gardner, "Thermal modeling and characterization of micropower chemoresistive silicon sensors", *Sensors and Actuators*, 1997, **B 45**: p. 19-26.
- [33] L. Sheng, Z. Tang, J. Wu, P.C.H: Chan, and J.K.O. Sin, "A low-power CMOS compatible integrated gas sensor using maskless tin oxide sputtering", *Sensors and Actuators*, 1998. **B 49**: p. 81-87.
- [34] S. Astié, A.M.Gue., E. Scheid, and J.P. Guillemet, "Design of a low power SnO<sub>2</sub> gas sensor integrated on silicon oxynitride membrane", *Sensors and Actuators*, 2000. **B 67**: p. 84-88.
- [35] F. Solzbacher, C. Imawan, H. Steffes, E. Obermeier, and M. Eickhoff, "A new SiC/HfB<sub>2</sub> based low power gas sensor", *Sensors and Actuators* 2001. **B 77**: p. 111-115.
- [36] Yaowu Mo, Yuze. Okawa, Koji Inoue, and Kazuki Natukawa, "Low-voltage and low-power optimization of micro-heater and its on-chip drive circuitry for gas array", *Sensors and Actuators* 2002, **a 100**: p. 94-101.
- [37] C. Tsamis, A. G. Nassiopoulou, A. Tserepi, "Thermal properties of suspended porous silicon micro-hotplate for sensor application", *Sensors and Actuators*, 2003, **B 95**: p. 78-82.
- [38] Jean Laconte, Cedric. Dupont, Denis Flandre, and Jean-Pierre Raskin, "SOI CMOS Compatible Low-Power Microheater Optimization for the Fabrication of Smart Gas Sensors", *IEEE SENSORS JOURNAL*, 2004, **4(5)**
- [39] T Iwaki, J A Covington, F Udrea, S Z Ali, P K Guha and J W Gardner, "Design and simulation of resistive SOI CMOS micro-heaters for high temperature gas sensors", *Institute of Physics Publishing Journal of Physics: Conference Series*, 2005. **15**: p. 27-32.

- [40] A. Wisitsoraat, A. Tuantranont, and T. Lomas, "Design and Simulation of Electro-fabricated MEMS Microhotplate for Gas Sensor Applications", *Journal of Physics*, 2006(34): p. 643-649.
- [41] J. Cerd, Belmonte, J. Puigcorb'e, J. Arbiol, A. Vil'a, J.R. Morante, N. Sabat'e, I. Gr'acia, C. Can'e, "High-temperature low-power performing micromachined suspended micro-hotplate for gas sensing applications", *Sensors and Actuators*, 2006, **B 114**: p. 826-835.
- [42] Bin Guo, Amine Bermak, Philip C. H. Chan, and Gui-Zhen Yan, "An Integrated Surface Micromachined Convex Microhotplate Structure for Tin Oxide Gas Sensor Array", *IEEE Sensors Journal*, December 2007, **7**(12).
- [43] A. Hierlemann, "Integrated Chemical Microsensors Systems in CMOS Technology", 2005: Springer.
- [44] J. Laconte, D. Flandre, and J-P, Raskin, "Micromachined Thin-Film Sensors for SOI-CMOS Co-Integrated", 2006: Springer.
- [45] F. Udrea and J. Gardner, "SOI CMOS gas sensors", in *Proceeding of the first IEEE Sensors conference*, 2002, USA.
- [46] D.L. Kendall, "On etching very narrow grooves in silicon", *Applied Physics Letters*: Vol. 26. 1975.
- [47] Gregory T. A. Kovacs, Nadim I. Maluf, and Kurt E. Petersen, "Bulk Micromachining of Silicon", in *Proceedings of the IEEE*. AUGUST 1998.
- [48] Florian Solzbacher, PhD Thesis, "A new SiC/HfB<sub>2</sub> based micro hotplate for metal oxide gas sensors". 2003.

- [49] Jianwei Gong, PhD Thesis, “Non-Siliconmicrofabricated Nanostructured Chemical Sensors for Electric nose Application”. 2005.
- [50] Jan G. Korvink, and Oliver Paul, “MEMS a practical guide to design, analysis and applications”. 2006: Springer.
- [51] G. Advani and A. Jordan, “Thin films of SnO<sub>2</sub> as solid-state gas sensor”, *Journal of Electronic Mater*, 1990, **9**: p. 29-49.
- [52] Samuel K.H. Fung, Zhenan Tang, Philip C.H. Chan, Johnny K.O. Sin, and Peter.W Cheung, “Thermal analysis and design of a micro-hotplate for integrated gas-sensor applications”, *Sensors and Actuators*, 1996, **A54**: p. 482-487.
- [53] A. Götz, I. Gràcia, C. Cané, and E. Lora-Tamayo, “Thermal and mechanical aspects for designing micromachined low power gas sensors”, *Journal of Micromechanics and Microengineering*, 1997, **7**: p. 247-249.
- [54] Danick, B, PhD Thesis, “Thermally Isolated Microelectronic Devices for Gas Sensing Applications”, 2001.
- [55] Carlos A. Smith and Armando B. Corripio, “Principles and Practice of Automatic Process Control”, 2006: John Wiley & Sons Inc.

## APPENDIX A

In this appendix, we explain, briefly, the calculation of the power dissipation, current density and thermal constant time. As already mentioned in the methodology (chapter three) the conduction losses appear through the supporting micro bridges of the membrane ( $\text{Si}_3\text{N}_4$ ) as well and through the surrounding air, the heat transfer by convection is neglected because there is no fluid motion and assumed that there is no significant contribution of convective fluid motion because of the small size of the heated structures and heat losses by radiation.

When we using  $\Delta T = 700^\circ\text{C}$ , all the thickness of the layers of the MHP  $0.5 \mu\text{m}$  and thermal conductivity of the mentioned layers are taken from table 1.1 (chapter one). To power dissipation ( $P_{\text{disp}}$ ) can be obtained previous equation (3.10).

$$P_{\text{disp}} = P_{\text{conduction bridges}} + P_{\text{conduction air}} + P_{\text{radiation}} \quad (3.10)$$

Conduction through the membrane can be obtained by (3.1)

$$P_{\text{conduction}} = 4kA \frac{\Delta T}{\Delta x} \quad (3.1)$$

And the thermal conductivity can be calculated by equation (3.2)

$$k = (4d_{\text{SiO}_2} k_{\text{SiO}_2} + d_{\text{Si}_3\text{N}_4} k_{\text{Si}_3\text{N}_4} + 2d_{\text{Pt}} k_{\text{Pt}} + d_{\text{SiC}} k_{\text{SiC}} + d_{\text{Au}} k_{\text{Au}} + d_{\text{SnO}_2} k_{\text{SnO}_2}) / b \times c \quad (3.2)$$

Where  $d$  is the thickness of each layer,  $b$  and  $c$  are factors that are determined as follows:

$$b = (4d_{\text{SiO}_2} + d_{\text{Si}_3\text{N}_4} + 2d_{\text{Pt}} + d_{\text{SiC}} + d_{\text{Au}} + d_{\text{SnO}_2}) \quad (3.3)$$

$$c = \frac{(4d_{\text{SiO}_2} + d_{\text{Si}_3\text{N}_4} + 2d_{\text{Pt}} + d_{\text{SiC}} + d_{\text{Au}} + d_{\text{SnO}_2})}{(d_{\text{SiO}_2} + d_{\text{SnO}_2})} \quad (3.4)$$

We obtained the total thermal conductivity for the membrane about 7.81 W/mK and for the other layer are listed in table (A.1), area of the micro bridge about  $10 \mu\text{m}^2$  length = 113  $\mu\text{m}$ . we found the power conduction 1.94 mW.

The conduction through the surrounding air can be obtained by

$$P = 4\pi Kr_o(T_{hot} - T_{amb}) \quad (3.8)$$

Where  $K$  air thermal conductivity about 0.026 W/mK and  $r_o$  is radius of the heater equal 43.6  $\mu\text{m}$  and  $(T_{hot} - T_{amb}) = 700$  we obtained the power about 9.97mW.

Power losses by radiation can be obtained by Stefan-Boltzmann Law

$$P = \sigma \varepsilon A(T_{hot}^4 - T_{amb}^4) \quad (3.12)$$

Where  $\sigma$  (*Stefan Boltzmann constant*) =  $5.67 \times 10^{-8} \text{ Wm}^{-2}\text{K}^{-4}$ ,  $\varepsilon = 0.1$ , the area of the membrane =  $10^{-8} \text{ m}^2$ ,  $T_{hot} = 1000$  and  $T_{amb} = 300$  we obtained the power about 0.056 mW, the total power dissipation equal  $1.94 + 9.97 + 0.056 = 11.97 \text{ mW}$ .

In order to operate the heater it is necessary to know the voltage required to increase the temperature until the desired value. The voltage can be calculated by this equation

$$V = \sqrt{P_{in} \times R} \quad (3.14)$$

Where  $V$  is the voltage,  $R$  is the resistance and  $P$  in is the power supplied.

The resistance for the heater is calculated using Equation

$$R = \frac{\rho \times L}{A} \quad (3.15)$$

Where  $R$  is the resistance,  $\rho$  is the resistivity =  $105 \times 10^{-9}$ ,  $L$  is the length =  $1195 \mu\text{m}$  and  $A$  is the cross sectional area =  $2.5 \times 10^{-12} \text{ m}^2$ . We found the resistance about 50 ohms and the voltage applied equal 0.77V, the current through the sensor can be calculated using Ohms law

$$J = \frac{V/R}{d \times W} \quad (3.16)$$

Where  $J$  is the current density,  $V$  is the applied voltage = 0.77V,  $R$  is the resistance of the heater = 50 ohms,  $d$  and  $W$  are the thickness and the width of the Pt heater layer  $0.5 \mu\text{m}$  and  $5 \mu\text{m}$ , respectively we obtained the current density =  $6.2 \text{ pA}/\mu\text{m}^2$ .

The thermal time constant,  $t$ , can be obtained by this equation:

$$\tau = \frac{U}{P} = \frac{\rho v c (T_{hot} - T_{amb})}{P} \quad (3.20)$$

Where  $U$  the energy required for heating the active area of the MHP,  $\rho$  density =  $2.9 \times 10^3 \text{ kg}/\text{m}^3$ ,  $v$  the volume =  $5 \times 10^{-15} \text{ m}^3$  and  $c$  the specific heat =  $170 \text{ Ws}/\text{kg K}$  we obtained the thermal time constant equal 0.14 ms.

**Table A 1:** Thermal conductivity calculation of membrane, heater, plate and sensing film layers used in the MEMS microhotplate

Thickness ( $\mu\text{m}$ )	Thermal conductivity (W/mK)			
	Membrane	Heater	Plate	Sensing Film
0.3	8.29	7.9	7.43	7.89
0.5	7.81	7.81	7.81	7.81
1	6.82	7.65	8.44	7.6
1.5	6.04	7.43	8.8	7.29
2	5.4	7.18	8.88	6.8
2.5	4.88	6.93	8.88	6.72
3	4.45	6.7	8.81	6.5

**Table A 2:** Summary of results for membrane characterization

	Thickness ( $\mu\text{m}$ )						
	0.3	0.5	1	1.5	2	2.5	3
$P_{\text{condu}}$ through bridges (mW)	1.234	1.934	3.384	4.494	5.324	6.044	6.614
$P_{\text{condu}}$ through air (mW)	9.97	9.97	9.97	9.97	9.97	9.97	9.97
$P_{\text{radi}}$ (mW)	0.056	0.056	0.056	0.056	0.056	0.056	0.056
Total Power Dissipation (mW)	11.26	11.96	13.41	14.52	15.38	16.07	16.64
Voltage (V)	0.75	0.773	0.819	0.852	0.877	0.896	0.912
Current density ( $\text{pA}/\mu\text{m}^2$ )	6.00E+9	6.18E+9	6.55E+9	6.82E+9	7.02E+9	7.17E+9	7.3E+9
Time Constant (ms)	0.1	0.14	0.26	0.36	0.44	0.54	0.62